ERROR PROPAGATION IN CARBON ESTIMATION USING THE COMBINATION OF AIRBORNE LiDAR DATA AND VERY HIGH RESOLUTION GEO-EYE SATELLITE IMAGERY IN LUDHIKHOLA WATERSHED, GORKHA, NEPAL

DANG ANH NGUYET
February, 2012

SUPERVISORS:
Dr. M.J.C. Weir
Dr. Y.A. Hussin

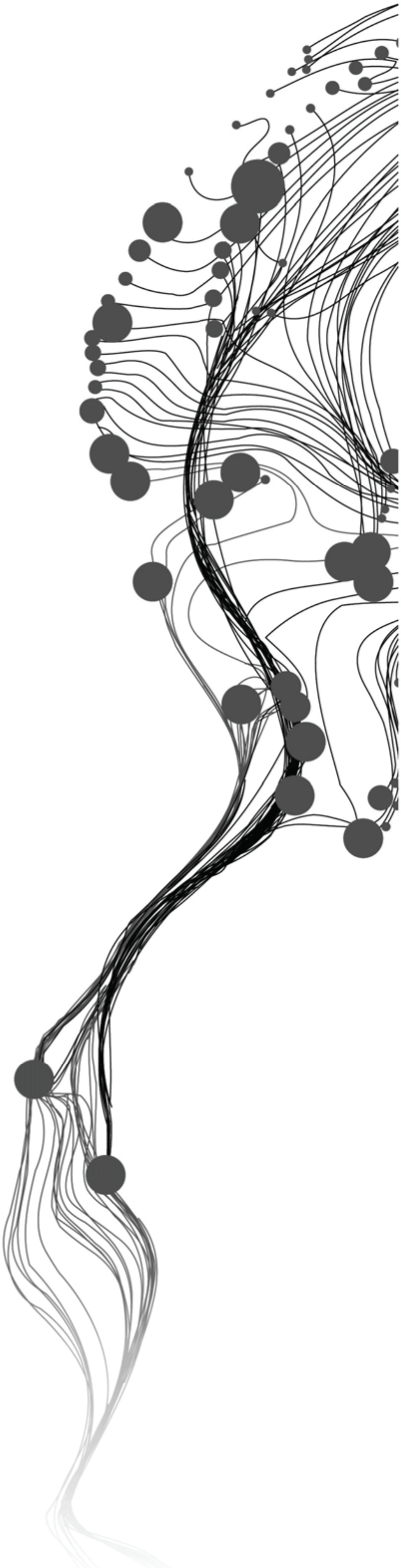

ERROR PROPAGATION IN CARBON ESTIMATION USING THE COMBINATION OF AIRBORNE LiDAR DATA AND VERY HIGH RESOLUTION GEO-EYE SATELLITE IMAGERY IN LUDHIKHOLA WATERSHED, GORKHA, NEPAL

DANG ANH NGUYET
Enschede, The Netherlands, February, 2012

Thesis submitted to the Faculty of Geo-Information Science and Earth Observation of the University of Twente in partial fulfilment of the requirements for the degree of Master of Science in Geo-information Science and Earth Observation.
Specialization: Natural Resources Management

SUPERVISORS:
Dr. M.J.C. Weir
Dr. Y.A. Hussin

THESIS ASSESSMENT BOARD:
Dr. A. Voinov (Chair)
Dr. T. Kauranne - Arbonaut Oy Ltd. and Dept of Mathematics and Physics - Lappeenranta University of Technology, Finland (External examiner)

ABSTRACT

Carbon dioxide (CO_2) is believed the main anthropogenic greenhouse gas which causes global climate change. In the carbon cycle, forest plays an important role both as a carbon source and a carbon sink. Therefore, forest carbon inventories and emission reduction programs, in particular REDD, are one of the main efforts to combat climate change. REDD provides opportunities for Nepal and other developing countries to take part in the international carbon market and to promote sustainable forest management. Forest inventories and programs for emission reduction require robust methods to quantify carbon sequestration in forests. The combination of LiDAR data and high resolution satellite imagery is one of potential approach for assessing forest carbon sequestration. The application of LiDAR data and high resolution satellite imagery in carbon estimation are mostly based on the strong relationship between tree parameters, crown projection area (CPA) and height, with carbon stock of individual trees. A Canopy Height Model (CHM) is created from Airborne LiDAR data in order to derive the tree height information. The crown projection area is delineated from a very high resolution Geo-Eye satellite imageey with Region growing algorithm. Field-based carbon stock of individual tree (obtained through an allometric equation) is then related to CPA and height obtained from remote sensing data through multiple linear regression modelling.

The crown delineated with Region growing resulted in 71.9% accuracy, LiDAR derived height fitted well with the measured height with the coefficient of determination R^2 =0.72. The object based image classification is applied to classify *Shorea robusta* and *Other species* with reasonable accuracy of 81% overall. Modelling the relationship between CPA and LiDAR derived height with carbon stock of *Shorea robusta* and *Other species* results in R^2 values of 0.76 and 0.68 respectively.

In order to complete the carbon stock accounting and monitoring process, uncertainty estimates are required as an essential element of the process. Uncertainty estimates can help to reduce the uncertainty of inventories in the future, and guide decision on the choice of method. The combination of data requires more complex data processing and analysis techniques than using high resolution image or LiDAR data alone. As a result, the risk of error propagation through carbon estimation process is higher. The main sources of error are associated with ground-based sampling, LiDAR data processing, image processing and data integration processing. Most studies have used the standard error of regression equation as a measure of uncertainty but the uncertainty maybe two to three times the standard error. Accordingly, error propagation assessment needs to be evaluated to make correct inference about forest carbon stock.

The trees used as the input for multiple linear regression analysis mostly affect the result of carbon estimation process. For the purpose of error propagation analysis, Monte Carlo Simulation is applied to generate a number of input datasets, which then were used to develop different *regression predictive models of carbon*. The input datasets were created by adding the random error to individual tree's parameters (CPA, height, field-based carbon). Carbon stock then calculated based on simulated carbon predictive model. The results of different iterations were compared to see the effect of error propagation.

Key words: LiDAR, canopy height model, very high resolution image, object based image analysis, region growing, above ground biomass, forest carbon,

ACKNOWLEDGEMENTS

Words cannot express my grateful to my first supervisor, Dr. Michael Weir, for his support and patience during the thesis period. Thank you for your guidance and your encouragement when you listened to my complicated ideas about error propagation.
I would like to thank also my second supervisors Dr. Yousif Hussin for his support, advice and critical comment on my thesis work. I also want to say the big "thank you" to Mr. Willem Nieuwenhuis for helping me when I was trapped in the programming process.
I would like to express my sincere gratitude and appreciation to Dr. Alexey Voinov for his comments and suggestions during my proposal and mid-term defence.
I am grateful to ICMOD staff in Nepal for organizing the fieldwork in Nepal and for helping us to obtain the needed data sooner than expected. I am also grateful to my friends Pema Wangda and Sajana Marhajan who were always beside me and who encouraged me during the hard fieldwork. And Purna "dai", the guide for our field work, thank you for giving me a hand when I fell down many times in the field.
Thanks to Fatimeh Hatami and Vinord Kumar for sharing your knowledge and experience of using LiDAR data with me. I also appreciate the encouragement and support of all my NRM colleagues.
I would like to acknowledge to Huygen Scholarship and the Netherlands organization for international cooperation in higher education (NUFFIC) for granting me a scholarship to study in the Netherlands.
Last but not least, my sincere and deepest gratitude goes to my family for their love and their words to cheer me up!

TABLE OF CONTENTS

LIST OF FIGURES

LIST OF TABLES

LIST OF APPENDICES

LIST OF ACRONYMS

AGB	Above ground biomass
C	Carbon
CF	Community Forest
CFUGs	Community forest user groups
CHM	Canopy height model
CO_2	Carbon dioxide
CPA	Crown projection area
DBH	Diameter at breast height
DN	Digital Nummer
DSM	Digital Surface Model
DTM	Digital Terrain Model
FAO	Food and Agricultural Organization of the United Nations
GCP	Ground control point
GHGs	Greenhouse Gases
GPS	Global Positioning System
ICIMOD	International Centre for Integrated Mountain Development
IPCC	International Panel on Climate Change
LiDAR	Light Detection and Ranging
MOFSC	Ministry of Forest and Soil Conservation
OBIA	Object based image analysis
REDD	Reducing Emission from Deforestation and Degradation
RMSE	Root Mean Square Error
UNFCCC	United Nations Framework Convention on Climate Change
VHR	Very High Resolution

1. INTRODUCTION

1.1. Background of the study

Carbon dioxide (CO_2) is believed to be the major greenhouse gas which causes global climate change (IPCC, 2001). In the carbon cycle, forest plays an important role both as a carbon source and a carbon sink (Watson, 2009). About 60% of the terrestrial vegetation carbon and about 50% of soil carbon are stored in the forest (Dong *et al.*, 2003). When forest is cleared or degraded, its stored carbon is released into the atmosphere as CO_2. Consequently, forest turns into the carbon source which enhances climate change. Therefore, forest carbon inventories and emission reduction programs are crucial for combating climate change.

At the Bali Climate Change Conference in 2007, REDD, which stands for Reduced Emissions from Deforestation and Forest Degradation, was adopted by the parties of the United Nations Framework Convention on Climate Change (UNFCCC). It opened new opportunities for developing countries to participate in forest carbon financing (MOFSC, 2009). Within the concepts of REDD, countries that demonstrate forest carbon reserves and emission reductions are able to sell carbon credits on the international carbon market (UNFCCC, 2005). Similar to other forest carbon inventories and emission reduction programs, estimates of forest carbon stock are required to generate baseline information for REDD application.

The main carbon pools in the forest are biomass (above-ground and below-ground biomass), dead organic matter (dead wood and litter) and soil organic matter (IPCC, 2006a). Among these, above ground biomass (AGB) governs the potential carbon emission that could be released to the atmosphere due to deforestation (Gibbs *et al.*, 2007). Estimation of AGB, therefore, is the most critical step in quantifying carbon stocks from the forest (Gibbs et al., 2007). According to the IPCC definition, AGB is all living biomass above the soil including stem, stump, branches, bark, seeds, and foliage; the carbon makes up approximately 47% of AGB (IPCC, 2003). In other words, carbon stock is obtained from AGB by multiplying AGB with the rate of 0.47. Because of difficulties in collecting field data of below-ground biomass, most previous research focused on AGB (Lu, 2006) and this present study also focuses on the carbon stock contained in AGB.

As with most forest measurement, field methods can be employed for AGB estimation with high accuracy but this approach is generally time consuming, labour intensive, and difficult to implement in remote areas (Lu, 2006). Meanwhile, remote sensing methods can be combined with field measurements to estimate AGB at a wide range of scales with relatively low cost (Popescu, 2007). As a result, remote sensing methods have been increasingly applied and become the primary source of data for AGB or carbon estimation (García *et al.*, 2010; Lu, 2006).

A variety of satellite data are used for AGB or forest carbon estimation. These data are broadly classed into optical sensor data, radar data and light detection and ranging data (LiDAR). Each type of data has its own characteristics, both advantages and disadvantages. Hence, the integration of different sources of remotely sensed data may enhance the information extraction process and overcome the drawbacks of using one type of data alone (Sohn *et al.*, 2007). In the light of this, the combination of LiDAR data and high resolution satellite image is also one of potential approaches to individual tree-based carbon estimation (Kim *et al.*, 2010).

The application of LiDAR data and high resolution satellite imagery in carbon estimation are mostly base on the strong relationship between tree parameters, for instance crown properties and height properties, with the AGB or carbon stock of individual trees. The crown properties (crown projection area, crow width) were used to predict the diameter at breast height (DBH) or AGB of tree in a number of previous researches (Popescu, 2007; Soares *et al.*, 2005). The DBH comes to the forefront since AGB is often estimated from the allometric equation on DBH (Muukkonen *et al.*, 2007). Tree height derived from LiDAR data is also closely related to AGB of the tree (Jochem *et al.*, 2011; Ni-Meister *et al.*, 2010). Hence, the approach to model forest carbon stock based on both crown properties and tree height is expected to increase the accuracy of carbon stock estimation.

1.2. Problem statement

Measurement of AGB, or carbon sequestration, in trees is crucial for REDD signatory parties such as Nepal. However, estimating AGB is still a challenging task because of the practical or methodological limitations, especially for tropical and sub-tropical areas which have complex stand structure and abundant variety in species composition (Foody *et al.*, 2001).

Although LiDAR data has been widely available, it is still too costly to be used over large areas (Gibbs et al., 2007). At present, one way of reducing the cost of acquiring LiDAR data for large areas is to increase flight altitude (Yu *et al.*, 2004). If other scan properties (pulse repetition frequency and the scan angle) are not changed, the laser-sampling density is, therefore, reduced. According to previous researches, use of low-density LiDAR data (point density is less than 5 point/m^2) might result in less accurate individual tree detection and crown property measurements (Takahashi *et al.*, 2010). Thus, the combination with high resolution imagery is essential in order to successfully use low density LiDAR for carbon estimation over large areas (Jochem *et al.*, 2009).

The choice of remote sensing system will influence the levels of uncertainty in the estimates of forest carbon (Gonzalez *et al.*, 2010). Combination of data sources requires more complex data processing and analysis techniques than using high resolution image or LiDAR data alone. As a result, the risk of error propagation through the carbon estimation process is higher. The main sources of error are associated with LiDAR data processing, image processing, data integration processing, ground-based allometry, ground-based sampling and regression modelling. Previous researches on carbon estimation in Nepal emphasized the importance of error propagation. However they just defined the sources of error and did not assess the actual error propagation (Shah, 2011; Tsendbazar, 2011).

In order to complete the carbon stock accounting and monitoring process, the uncertainty estimates are required as an essential element of the process (Brown, 2002). Therefore, it is significant to indicate the effect of error sources on the final result in our research. The uncertainty analysis is expected to be useful to make correct inference about forest carbon stock.

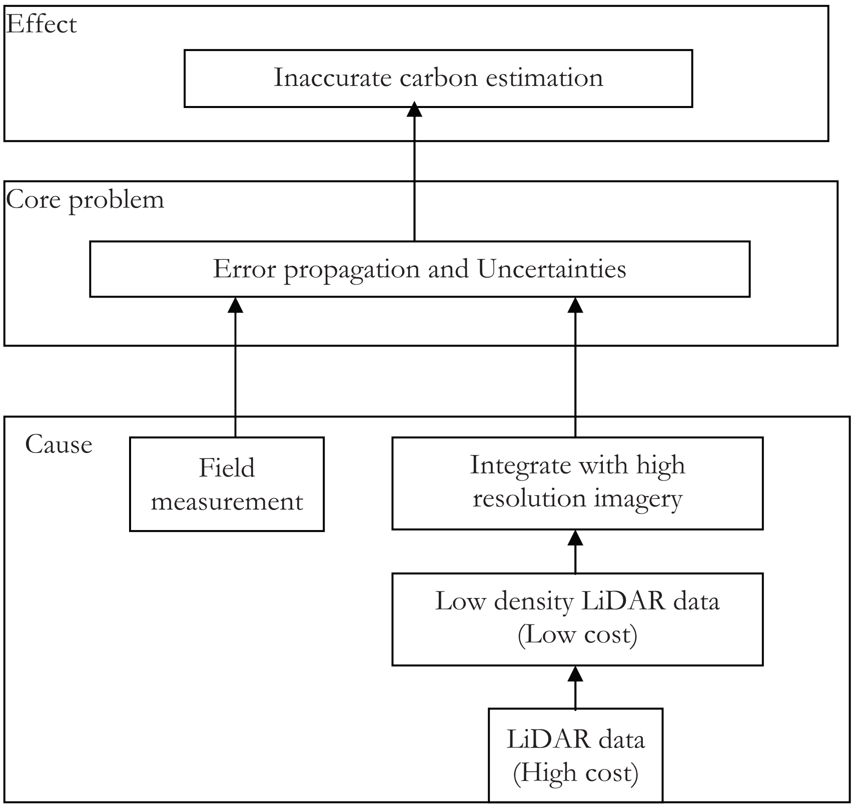

Figure 1: Problem tree

1.3. Objective

The main objective of this study is to assess error propagation in the estimation of carbon from the combination of LiDAR data and high resolution satellite Geo-Eye imagery. The specific objectives are:

1. Develop a predictive model of carbon using tree height derived from airborne LiDAR data and crown projection area (CPA) derived from high resolution satellite imagery.
2. Analyse the sources of error causing the uncertainties in the carbon estimation process and assess the accuracy of each parameter, which takes part in the predictive model of carbon (LiDAR derived height, CPA and field based-carbon estimate).
3. Develop a method for assessing the propagation of error in carbon estimation.
4. Estimate carbon stock in the study area and analyse the impact of error propagation in this carbon stock estimation.

Table 1: Research objectives, research questions and hypothesis

Objective	Research Question	Hypothesis
Develop a predictive model of carbon using tree height derived from airborne LiDAR data and crown projection area (CPA) derived from high resolution satellite imagery	1a. What is the relationship between CPA and carbon?	Ho: There is no significant relationship between CPA and carbon. H1: There is a significant relationship between CPA and carbon.
	1b. What is the relationship between tree height and carbon?	Ho: There is no significant relationship between tree height and carbon. H1: There is a significant relationship between tree height and carbon.

Objective	Research Question	Hypothesis
	1c. What is the relationship between tree height, CPA and carbon?	Ho: There is no significant relationship between tree height, CPA and carbon. H1: There is a significant relationship between tree height, CPA and carbon.
Analyse the sources of error causing the uncertainties in the carbon estimation process and assess the accuracy of each parameter, which takes part in the predictive model of carbon (LiDAR derived height, CPA and field based-carbon estimate)	$2a_1$. What are the error sources of LiDAR derived height? $2a_2$. What is the accuracy of LiDAR derived height?	Ho: The accuracy of LiDAR derived tree height is not acceptable (error is ± 5m or more) H1: The accuracy of LiDAR derived tree height is acceptable (error is less than ± 5m)
	$2b_1$. What are the error sources of image segmentation? $2b_2$. What is the accuracy of image segmentation?	Ho: Image segmentation accuracy is not acceptable (error is 30% or more) H1: Image segmentation accuracy is acceptable (error is less than 30%)
	$2c_1$. What are the error sources of image classification? $2c_2$. What is the accuracy of image classification?	Ho: Image classification accuracy is not acceptable (error is 30% or more) H1: Image classification accuracy is acceptable (error is less than 30%)
	$2d_1$. What are the error sources of field based carbon? $2d_2$. What is the amount of field based carbon estimation?	Ho: The accuracy of field based carbon is not acceptable. (error is 5 kg or more for individual tree) H1: The accuracy of field based carbon is acceptable. (error is less than 5 kg for individual tree)
Develop a method for assessing the propagation of error in carbon estimation	3. How to link various error sources to final carbon estimation?	Ho: The trees selected and used to develop the predictive model of carbon have no impact on carbon stock estimation process H1: The trees selected and used to develop the predictive model of carbon have most impact on carbon stock estimation.
Estimate carbon stock in the study area and analyse the impact of error propagation in this carbon stock estimation	4a. What is the amount of carbon in the study area? 4b. What is the range of carbon stock variation due to error propagation?	Ho: The range of carbon stock variation is not acceptable (error is 10 ton/ha or more) H1: The range of carbon stock variation is reasonable (error is less than 10 ton/ha)

2. LITERATURE REVIEW

2.1. Remote sensing approaches for Above-ground biomass estimation

An overview of the various types of satellite data used for AGB or carbon stock estimation is presented in this section.

Moderate optical remote sensing imagery

Many studies have been conducted using moderate spectral or spatial resolutions optical remote sensing imagery such as Landsat, ASTER and MODIS to assess their usefulness for estimating AGB e.g. Foody *et al.*(2003); Muukkonen *et al.* (2007); Blackard *et al.*(2008) and Chopping *et al.* (2010). The relationship between biomass and spectral signatures or vegetation indices, primarily the Normalized Difference Vegetation Index (NDVI), is created to estimate AGB (Foody *et al.*, 2003; Muukkonen *et al.*, 2007). Using vegetation indices is possible to reduce the impacts on reflectance caused by viewing conditions (due to variation in sensor view angle or solar elevation) and shadows, especially in those sites with complex vegetation stand structures (Lu *et al.*, 2004). Nevertheless, the sensitivity of vegetation indices to biomass varies among environments and can limit the ability of the index to represent accurately AGB (Foody *et al.*, 2001).

High spatial resolution imagery

High spatial resolution imagery such as QuickBird, IKONOS, WorldView, and Geo-Eye are used widely for AGB estimation (Wulder *et al.*, 2010). Different approaches have been applied to extract biophysical parameters from high spatial-resolution data, including photo interpretation, threshold-based spatial clustering, object oriented analysis, etc. (Lu, 2006). Among these, object oriented analysis is a promising technique to improve AGB estimation. This technique can overcome the drawbacks of pixel-base image analysis (Lamonaca *et al.*, 2008). The relationships between tree biophysical characteristics and tree crown area is established to estimate forest AGB or carbon stocks with high certainty (Gonzalez *et al.*, 2010). However, high spectral variation and shadows caused by canopy and topography or cloud may create difficulty in developing AGB estimation models using high resolution imagery, especially in tropical forest (Gibbs et al., 2007; Patenaude *et al.*, 2005).

Radar data

Beside optical sensors, data from active sensors - in particular radar - can be used as the appropriate data sources to estimate AGB (Ranson *et al.*, 1997). The backscatter of the illumination generated from radar is proportional to the amount and organization of forest biomass (Lefsky *et al.*, 2001). Thus, the relationship between radar backscatter and forest stand parameters (diameter at breast height, tree height, basal area and stand diversity) has been investigated to determine ABG (Saatchi *et al.*, 2010). The radar systems are able to overcome the limitation of optical data by collecting earth feature data irrespective of weather or light conditions (Lu, 2006). On the other hand, it has been shown that radar backscatter will saturate for high biomass values (Morsdorf *et al.*, 2009; Nguyen, 2010).

Light detection and ranging data (LiDAR)

Light detection and ranging (LiDAR) can avoid the saturation problem and has great potential to acquire direct three-dimensional measurements of the forest canopy (García *et al.*, 2010). Unlike passive remote sensing systems, LiDAR uses active laser pulses to capture the vertical structure of forest canopies that are useful for estimating a variety of forest inventory parameters (tree height, volume, and biomass) (Næsset, 2002; Wulder *et al.*, 2010; Zhao *et al.*, 2009). Lefsky, et al. (2001) indicated that LiDAR has produced more accurate estimates of forest biomass than both Landsat, high spectral resolution sensors and synthetic aperture radar (SAR). For example, using LiDAR, Næsset and Goabakken (2008) were able to explain 88% and 85% of the variability in aboveground and belowground biomass, respectively, in the coniferous boreal zone of Norway. Nevertheless, LiDAR data are limited currently to the local or regional scales (Popescu *et al.*, 2011).

2.2. Research conceptual framework

2.2.1. Airborne LiDAR data

In recent years, the use of Airborne LiDAR technology to measure forest biophysical characteristics has been rapidly increasing (Popescu *et al.*, 2003). Airborne LiDAR system includes (i) a Laser scanner unit transmitting short and collimated pulses towards the Earth surface and recording both travel time of the laser beam and the energy (intensity) , (ii) a Global Positioning System (GPS), which is used to record the aircraft position, and (iii) Inertial Measurement Unit (IMU) that measures the angular attitude of the aircraft (roll, pitch and heading) (Jochem et al., 2011). The figure 2 shows the fundamentals of airborne LiDAR for forest purposes.

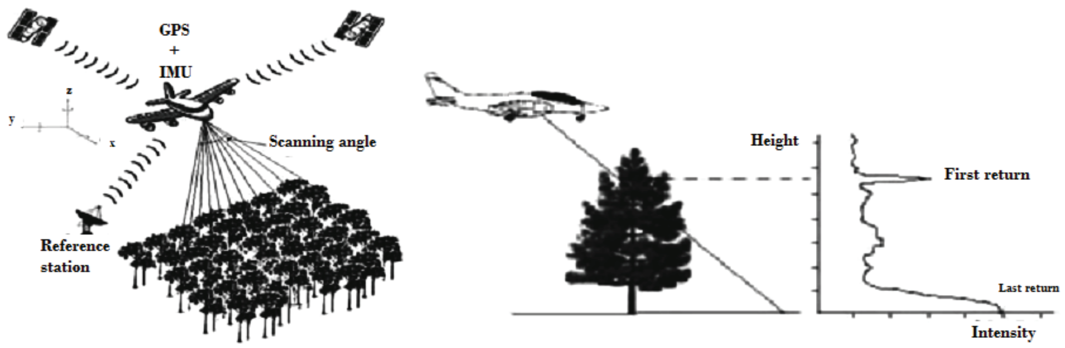

Figure 2: The fundamental of airborne LiDAR (García *et al.*, 2007)

The data collected consist of a three-dimensional cloud of irregularly spaced points near the Earth's surface (James *et al.*, 2007). Each point has x, y, z information, in which x is the latitude, y is longitude and z is the elevation. The retrieval of tree parameters from LiDAR data has focused largely on utilizing the Canopy Height Model (CHM) (Rahman *et al.*, 2008). In order to create this canopy height model (CHM), the point data is filtered as first returns and last returns (or ground returns). The ground returns are interpolated to produce Digital Terrain Model (DTM) and the first returns are interpolated to produce Digital Surface Model (DSM). Subtraction of the DTM from the DSM produces a CHM (Popescu *et al.*, 2002).

2.2.2. Individual tree based approach with LiDAR data

There are two approaches for utilizing LiDAR data for AGB assessment: i) the area-based approaches and ii) the individual tree based approaches (Dalponte *et al.*, 2011). In the first approach, distributional metrics, such as the mean canopy height or the standard deviation of the canopy height, are taken from CHM and then used in conjunction with regression equations to predict forest properties (Lim *et al.*, 2004; Means et al., 2000). In terms of individual tree based approach, it is mostly based on regression models focusing on a relationship between LiDAR derived individual tree parameters (e.g. tree height, crown dimensions) and field based estimates of AGB.

Previous research highlighted that the individual tree based approach has several advantages over the area-based approach (Parker *et al.*, 2009; Yu *et al.*, 2010). Firstly, the use of individual tree approach increase the accuracy for deriving biomass estimates remotely and this approach offers the means of better understanding the sources of uncertainty (Popescu, 2007). Secondly, biomass or carbon estimation calculated based on individual tree can avoid the impact of non-forested land which may contaminate the measurements, causing the retrieved biomass predictions to be inaccurate (Riitters *et al.*, 2000). In addition, using an individual tree-based approach permits the estimation of parameters at the tree level rather than the plot or stands level. This will allow detailed evaluation of silvicultural techniques, including those designed to boost carbon storage, and may permit individual tree-based management in the future (Bortolot *et al.*, 2005).

Both horizontal and vertical vegetation structure information of individual tree (tree height or crown properties) can be provided at the desired accuracy with Airborne LiDAR techniques (Zimble *et al.*, 2003). The tree height is defined as the distance from the ground to the tree top or to the living crown (Erik *et al.*, 2002). Tree height can be derived from CHM by employing local maxima technique. The local maxima technique operates on the assumption that high laser values in a spatial neighbourhood represent the top of a tree crown (Zhao et al., 2009). The horizontal tree parameters, like crown properties, are then extracted from CHM through crown delineation algorithm. Popescu *et al.* (2003) introduced the method to estimate the crown diameter from a LiDAR derived CHM.

The single tree based approaches require LiDAR data with high point densities (>5 points/m²). However, Næsset *et al.*(2004) have reported generally good results with LiDAR measurement of height, volume, stocking, and basal area in coniferous areas with LIDAR point densities ranging from low density of 0.1 to higher density of 10 points/m². Therefore, such individual tree based approach can used for lower point densities (<5 points/m²) but require an extensive set of reference data (Jochem *et al.*, 2009).

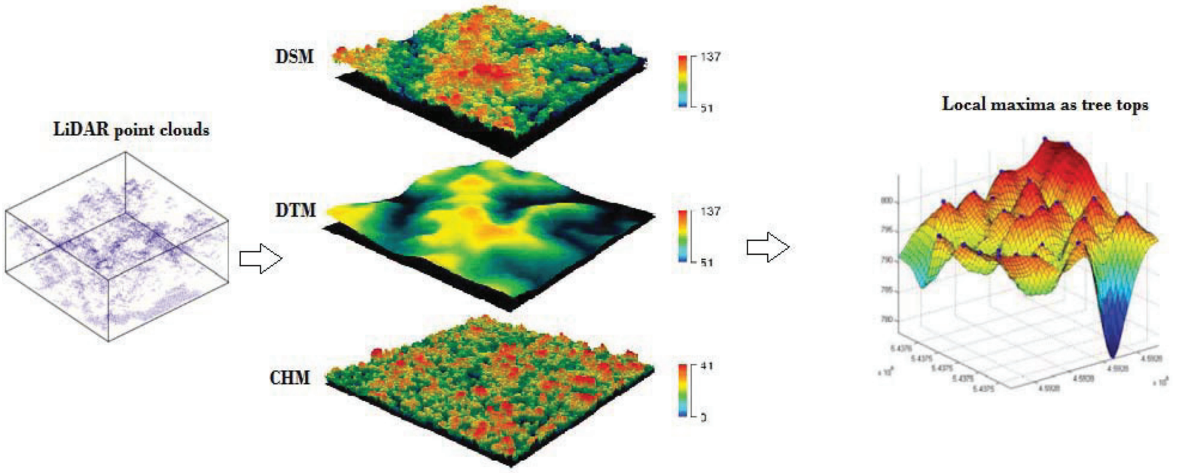

Figure 3: Outline of the process to obtain the Canopy Height Model (CHM) and extract tree height from local maxima [The diagram was created by combining the graphic objects from the research of Kellner *et al.* (2009); Reitberger *et al.* (2007) and Zhao *et al.* (2009)]

2.2.3. Object based image analysis

Object based image analysis (OBIA) and image segmentation technique have been used in very high resolution imagery as an option to overcome the drawbacks of pixel-base image analysis. With high resolution imageries, objects on the earth surface having similar reflectance properties would be hardly separable for forestry applications (Burnett *et al.*, 2003). Meanwhile, image objects can be delineated by image segmentation based on the relationships between spectrally delineated image segments and observed spatial heterogeneity in forest structure, including gaps in the outer canopy (Lamonaca *et al.*, 2008).

Three main steps of object-based classification are: 1) creation of image objects using an image segmentation algorithm, 2) extraction of object-based metrics, and 3) classification using the object-based metrics (Ke *et al.*, 2010). Various researches have attempted to estimate AGB using OBIA with different image segmentation techniques for individual tree crown delineation, such as Maker – controlled Watershed segmentation (Kim *et al.*, 2010); Region growing algorithm or Chessboard algorithm (Soares *et al.*, 2005) and multi-resolution segmentation. The object-based metric which is widely used in carbon estimation studies is crown projection area (CPA)(Shimano, 1997). Crown area or crown projection area is defined as the proportion of the forest floor that is covered by the vertical projection of the tree crowns (Jennings *et al.*, 1999) as shown in Figure 4. CPA is calculated from the maximum crown diameter assuming a circular crown projection (Timo, 1991).

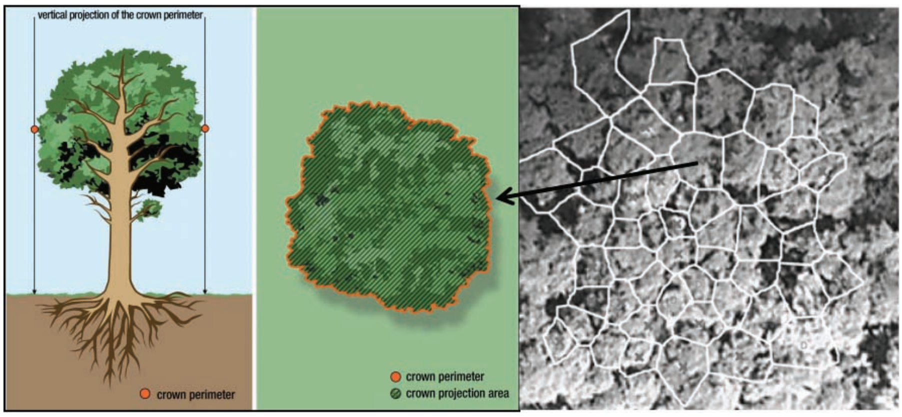

Figure 4: Crown projection area and segmented crowns from high resolution image [The figure was created by combining the graphic object from the research of Gschwantner *et al.* (2009) and Kim *et al.* (2010)]

2.2.4. Integrate low density LiDAR data and high resolution imagery

The integration of optical sensor data with LiDAR is believed to hold great promise for improving the accuracy of forest inventory and ecological modelling (Anderson *et al.*, 2008; Kim et al., 2010; Leckie, 2003; Sohn *et al.*, 2007). In the light of this, using a combination of high resolution imagery with low density LiDAR data for assessing carbon storage is also a potential approach. The first reason for the combination is to obtain more information about tree parameters. LiDAR data can directly provide three-dimensional information, such as tree height and crown based height, at an individual tree and stand level, which is difficult to obtain using high resolution imagery (Kim et al., 2010). Conversely, high resolution imagery can provide spectral and horizontal information for the individual tree, like crown width or crown area, which would hardly be delineated from low positing density LiDAR data (Ke et al., 2010). In addition, these two sources of data can compensate the disadvantages of each other. The laser measurements do not distribute homogeneously and usually have gaps in between (Suárez *et al.*, 2005). Sequentially, it causes the challenge to validate results for individual trees, when an correspondence needs to be established between field- and LiDAR-measured individual trees (Popescu, 2007). In this case, visual interpretation of high resolution imagery is used to assist LiDAR data to identify each individual tree (Næsset, 2004). The integration of high spatial resolution imagery and LiDAR data can produce more effective and efficient forest classification (Ke et al., 2010). By combining variables derived from both high resolution imagery and LiDAR, species-wise carbon estimations at tree level can be obtained (Packalén *et al.*, 2006) which is not able to be done by using low density LiDAR data alone.

2.2.5. Semi-empirical AGB/carbon model

Both empirical and semi-empirical models, which are primarily based on linear or non-linear regression analysis, are widely used for biomass or forest carbon estimation (Næsset, 2004; Popescu, 2007). The empirical model or allometric equation is developed on the basic of the relationship between sparse measurements from destructive sampling (oven-dry biomass per tree) and the more easily collected biophysical properties of trees, such as diameter at breast height (DBH) and commercial bole height (CBH) (Basuki *et al.*, 2009). Although the allometric equation is the most accurate method for ABG estimation, it requires destructive sampling by cutting of trees and weighing of their parts, which is invasive and costly. Additionally, the allometric equation is not able to be applied for carbon estimation and carbon mapping over large areas. Meanwhile, the semi - empirical model relates the reflectance of the canopy recorded at the sensor to biomass estimates based on allometric equations obtained from field measurement then extrapolate these estimates to entire forest ecosystems (Gibbs et al., 2007; IPCC, 2007). With the support of remote sensing, semi - empirical models can be used to estimate AGB and carbon stock over large areas. The result of allometric equation with high accuracy is often used to validate the predicted AGB/carbon from less invasive and costly semi-empirical methods.

Table 2: Example of Empirical model and Semi-empirical model for individual - tree AGB/C estimation

	AGB/Carbon predictive model (kg/tree)	**Independent variables**	**Dependent variables**	**Reference**
Empirical Model	*Tropical moist hardwoods:* AGB = exp[–2.289 + 2.649*ln (DBH) - 0.021*(ln(DBH))^2]	DBH: diameter at breast height	AGB	IPCC (2007)
Semi-empirical Model	*Pine tree:* AGB = Exp[-2.5356 + 2.4349*ln(-0.16+CD+1.22*H)	CD: crown diameter H: height	AGB	Popescu (2007)
	Pinux roxburghii: C = -9.31496 + 11.932*CPA	CPA: crown projection area	C	Tsendbazar (2011)

2.2.6. Error and error propagation approach

The error should be seen, first and foremost, as a means to help prioritise national efforts to reduce the uncertainty of inventories in the future, and guide decision on methodological choice (IPCC, 2006b). Almost all related researches concentrated in assessing the accuracy of each steps in carbon estimation process and rarely considered carefully the error propagation in the final result (Chave *et al.*, 2004). Accordingly, error propagation assessment needs to be evaluated to make correct inference about forest carbon stock.

In simple terms, the word *error* is used to convey that something is wrong (Weir, 1999). Heuvelink *et al.* (1998) defines error as the difference between reality and our representation of reality. Measurements of errors are generally described in terms of *accuracy*. The accuracy of single measurement is *the closeness* of *observations, computations or estimates* to *the true value or the values perceived to be true* (Weir, 1999). However, the "truth" can never be known; it is instead acceptable that the truth could be obtained using the best available field survey (Harrell *et al.*, 1997; Persson *et al.*, 2002; Shi *et al.*, 2002). In this study, the field measurements or human visualization and interpretation is also considered the truth.

Carbon monitoring in forests with high spatial variation of tree density and species composition poses major challenges (Gonzalez et al., 2010). Potentially, many sources of error may affect the final carbon estimate, for example tree inventory errors; errors in the allometric equations; data processing errors. Therefore, it is important to evaluate the degree of uncertainty of the result. Most studies use the standard error of regression equation as a measure of uncertainty but the uncertainty maybe two to three times the standard error (Harrell et al., 1997). The reason is that system performance of uncertainties is not considered; error will add up and propagate in the final estimate. Hence, error propagation analysis is required to assess the propagation of the uncertainty from multiple sources in carbon estimates (Lo, 2005; Sherrill *et al.*, 2006).

Error propagation analysis has been applied researches on forest inventory, e.g. Sherrill *et al.* (2006); Larocque *et al.* (2008); Gonzalez *et al.* (2010). One simple example is the error propagation in calculating total timber volume given by equation $T = \sum v^* a$, in which v is the mean volume per unit area and a is the area of an individual stand (Weir, 2002). Because the mean stand volume is obtained from a sample, it has a standard error SE_v, area also has an error SE_a, v and a are determined independently, there is no covariance and the standard error of the total volume is:

$$SE_T^2 = SE_v^2 * a^2 + SE_a^2 * v^2$$

2.2.7. Main sources of error when combine LiDAR data and VHR satellite imagery

Error sources of CHM generation

The height of the tree extracted from the LiDAR -CHM is defined as the pixel having the highest value in a pixel cluster corresponding to a crown. However, this "top pixel" is normally situated near the center of the crown and sometime be found away from the center of the crown (St-Onge *et al.*, 2001). A local maximum filter algorithm was introduced to detect tree tops. The main problem encountered when using local maxima to detect tree tops is that non-treetop local maxima are incorrectly classified as treetops (Huang *et al.*, 2009). Zimble *et al.* (2003) indicated that trees often occur as clumps and therefore the peak of tree may have been missed altogether. In some case, two tree peaks are identified in the canopy of one tree. For all these reasons, tree height variance due to the distribution of LiDAR point. The extracted height from CHM may inaccurate in the following scenarios (Suárez et al., 2005):

- Small trees close to bigger ones are ignored
- Laser returns do not hit true top of tree
- One of hits is intercepted at a lower height and model produces two tree tops
- In a situation of sparse density of returns, some trees can be ignored completely.

In addition, some information in the original laser points is lost in the DTM and DSM interpolation process (Popescu et al., 2002). The residual of interpolation process is also one source of errors.

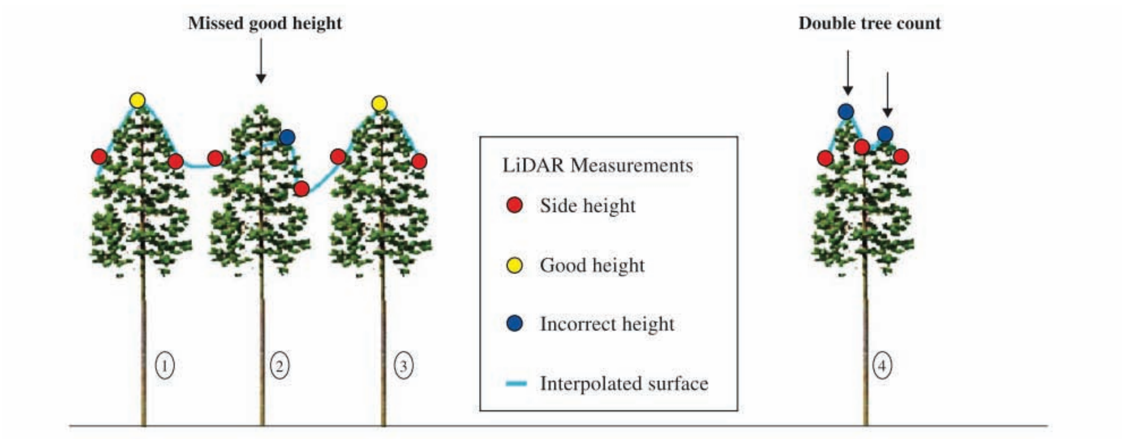

Figure 5: The example of misplace LiDAR point leading to inaccurate estimates height (Suárez et al., 2005)

Error source of crown delineation

With regard to VHR imagery, the sources of error such as sensor view angle, sun elevation and topography may affect the extracted value of crown properties and then affect the regression analysis to estimate AGB or carbon. (Darius *et al.*, 2002) suggested that real geometric and radiometric properties of tree crown can be detected best with small off nadir view angles (less than 15 degrees) and higher solar zenith angles. (Erikson *et al.*, 2005) found out that low elevation angle resulted in a shaded side of the tree crown which makes it difficult to distinguish it on remotely sensed imagery. As for view angle, view angle during image collection also influences the apparent shape of tree crowns on the image and the quality of delineation (Leckie *et al.*, 2005). View angle nearer to the nadir result in circular crown shape on the image when the solar elevation angle is high, whereas, tree crown displays a crescent shape in off-nadir images.

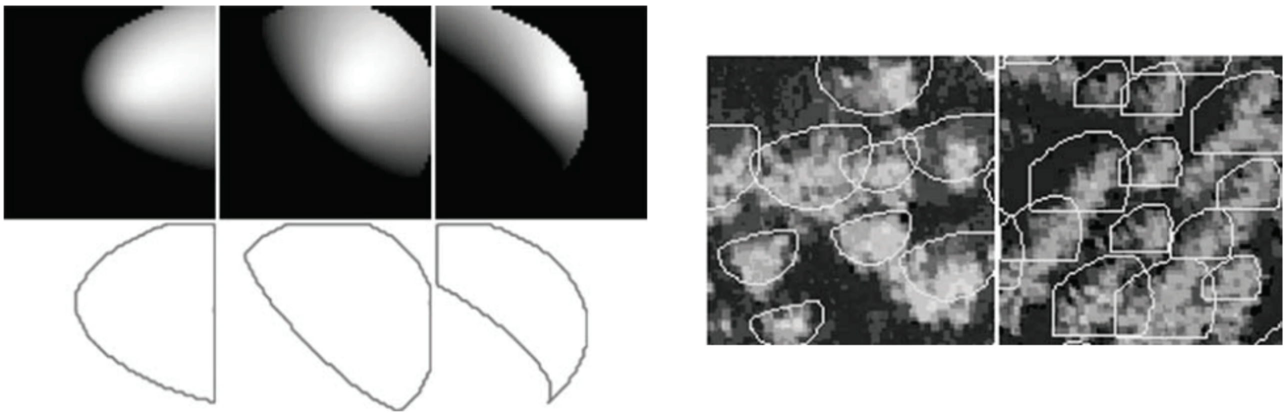

(a) (b)

Figure 6: (a) Templates and the corresponding polygons delineating the sun-lit areas of the template, (b) Aerial images with template hits shown as polygons. Left: near nadir viewing angle. Right: oblique viewing angle (Erikson et al., 2005)

3. STUDY AREA

3.1. Study area selection

3.1.1. Nepal and forest carbon estimation approach

Enhancing the effective contribution of mountain people to climate change mitigation through programmes to encourage carbon sequestration has become an important priority (Nogués-Bravo *et al.*, 2006). Over the past several decades, the shift in forest management authority from state to local communities in the Himalayan region, including Nepal, has been successful in reducing deforestation and increasing biomass on common lands (Banskota, 2007). According to FAO (1998), community forest is National forest that has been handed over to a community forest user group (CFCG) for its development, conservation and utilization. Until April 2009, one-third of Nepal's population was practising community forestry and directly managed over one-fourth of Nepal's forest area (Baral, 2011). REDD provides opportunities for Nepal to take part in the international carbon market and to promote sustainable forest management. It helps to consolidate local actions and raise concerns of communities about receiving benefits through programmes for forest conservation and protection (ICIMOD, 2010). Community-based forest management is a sustainable management regime which contributes to stabilizing atmospheric CO_2 concentrations by maintaining a carbon pool in the terrestrial ecosystem. Therefore, in Nepal and other developing countries participated in REDD, it has become important to determine the national scenarios of deforestation and forest degradation as well as estimate carbon stock of community forests (MOFSC, 2009).

3.1.2. Criteria to select the study area

The Ludhikhola watershed was selected for this study based on three main criteria: i) ecological zones, ii) interest of the local people and iii) accessibility. These criteria are also considered in the site selection procedures of the REDD project in Nepal (ICIMOD, 2010). Firstly, the watershed is representative for hilly areas which in the sub-tropical ecological zone of Nepal. The specific species for this ecological zone are *Shorea robusta*, *Schima Wallichi* and *Castanopsis indica*. The interest of local people is important to any forest management and conservation programmes. Involving local communities help to increase the local people's awareness of the benefits that they receive when deforestation and forest degradation is reduced. Local people, therefore, are ready to support and assist the research. Last but not least, the accessibility is should be considered because of the limitation of time for field work as well as specific terrain in Nepal. The study area meets this requirement because it has good road access.

3.2. Study area description

3.2.1. Location

The Gorkha district is in the Western development region of Nepal and has an area of 3,610 km^2. The Ludhikhola watershed area is located in the southern part of Gorkha district between 27^{o}55'02" to 27^{o}59'43"N and 84^{o}33'23" to 84^{o}40'41"E and covers an area of 5750 ha.

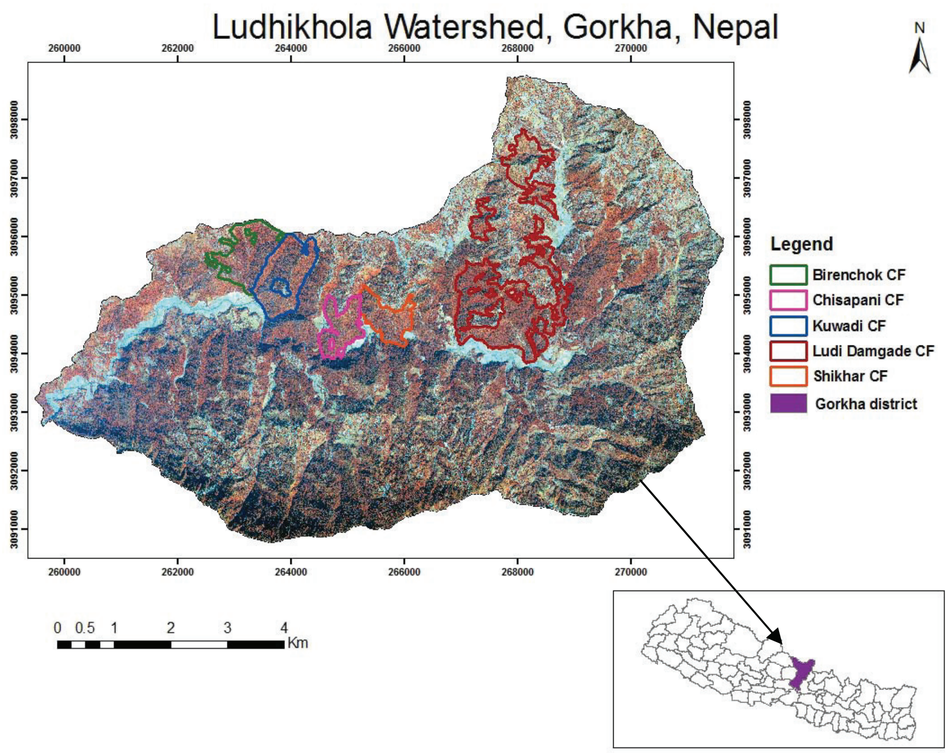

Figure 7: The Ludikhola watershed

3.2.2. Topography

The Ludhikhola watershed lies in Nepal's Middle Mountain Ecological Zone. Generally, the area is mountainous with an altitude ranging from 318 m to 1714m. 61% of the land is steep sloping (slope range of 30-60%) and the remaining land has less than 30% slope. The watershed has four major rivers that run within and along it, namely Chepe, Daraudi, Marsyangdi and Budhi Gandaki.

3.2.3. Climate

The climate of the area varies from subtropical at lower altitudes to temperate at higher altitudes. The temperature in Ludhikola watershed has an average daily temperature of 23.1^{o}C. The minimum temperature is 5^{o}C and the maximum is 33^{o}C, the hottest and driest days are in March, April and May. The rain season commences in June and ends in August with an average annual rainfall of 1972 to 2000m.

3.2.4. Settlement

The population in Ludhikhola watershed is 23,197 with 3800 households (ICIMOD, 2010). The main ethnic groups are Magar, Gurung, Tamang, Dalit and few Brahmin, Chhetri.

3.2.5. Forest

Forest type

Table 3: Land cover in Ludhikhola watershed (ICIMOD, 2010)

Land cover type	Area (ha)	Percentage (%)
Closed to open broadleaved (dense) forest	3873	67.34
Open broadleaved (sparse) forest	996	17.31
Natural water bodies	9	0.17
Bare Soil	241	4.19
Agriculture land and built up areas	632	10.99
Total	5750	100

Table 3 reveals that forest forms major land use in all the watersheds. Within these forest categories, the dense forest area occupies the largest proportion in the watershed. The forests are mostly young forest which is characterised by upper tropical to sub-tropical lower forests. The forests are mixed forest and species vary with the change of altitude and aspects. *Shorea robusta* (Sal) is the dominant species most commonly found in the southern aspects and lower altitudes of northern aspects. In the upper parts of northern aspects *Schima wallichii* (Schima) and *Castanopsis indica* (Chestnut) are the dominant species. In addition, there are a small number of *Mangifera indica* (Mango), *Ficus racemosa* (Fig), *Terminalia bellirica* (Belliric Myrobalan), *Syzygium cumini* (Black plum), *Rhus wallichii* (Ceasar weed), *Bombax ceiba* (Cotton), *Lyonia ovalifolia* (Oval leaved Lyonia), *Lagerstromia parviflora* (Myrtle), *Garuga pinnata* (Balsam).

Forest management

The main forest management regimes in Ludhikhola watershed are community forest and government managed forest. Private forest occupies only a very small area. There are 31 community forests (CFUGs) covering a total of 1880 hectares of forest area, and the remainder of the forest is classified as government and private forests. Community managed forest management is the new type of management which is recommended in the government's Master Plan for the Forestry Sector in1988. Community forest is autonomous and perpetual and provides institutions with rights to mobilize all types of resources to ensure the wellbeing of communities (Baral, 2011). Commercial timbers such as *Shorea robusta* and *Terminalia* are generally auctioned by the government for revenue generation. The forests where these valuable stocks predominated were rarely handed over to local communities until the early 2000s (Bhattarai *et al.*, 1999). Community forestry has become the most important program to conserve, manage and utilize forest resources in Nepal (Maskey *et al.*, 2006). Recently, community forest has been involved in different types of community development works including REDD program.

The forested areas under government control have virtually complete open access. This is because the district forestry staffs are mostly engaged in community forestry activities after the implementation of community forestry programs and therefore do not control access to the forest. The relatively high loss of forest area under state control can be explained by this condition of open access.(Krishna, 2011).

4. MATERIALS AND METHODS

4.1. Material

The main materials used for this research are the remote sensing data and the software which supports the analysis of these remote sensing data, software for statistical analysis and for the composition of the thesis.

4.1.1. Very high resolution satellite Geo –Eye imagery

The Geo-Eye imagery used for this research are Geo-Eye panchromatic 0.50 cm and Geo-Eye multispectral 2m images recorded on 2 September 2009 (Source: ICIMOD, Nepal). The Geo-Eye multispectral image consisted of four bands: blue (450-510 nm), green (510-580 nm), red (655-690 nm) and near infrared (IR) (780-920 nm). The obtained images were already ortho-rectified and geo-referenced to the UTM WGS 84 coordinate system by the ICIMOD project in Nepal.

4.1.2. Low density LiDAR data

The Airborne LiDAR data used for this research was recording using a Leica ALS50-II LiDAR-scanner consisting of a laser scanner, a geodetic-quality GPS receiver and an inertial measurement unit (IMU), which provide information about scan angle and the aircraft coordinates. The data was collected from 16 March to 2 April 2011 in UTM WGS 84 coordinate system (Source: FRA, Nepal). The average point density of the LiDAR data is 0.8 points per m^2. The LiDAR scanning process was at an absolute altitude of 2200m and recorded with a scan frequency of 52.9 kHz.

4.1.3. Other reference dataset

- Topographic maps at 1:25000 scale, published by the Survey Department of the Government of Nepal in 1994.
- Digital Elevation Model (DEM) with 20 m resolution (generated from contour lines of the topographic maps)
- Gorkha geo-database, which consists of the following layers: watershed boundary, land cover, community forest boundary, roads, rivers (Source: ICIMOD and FRA, Nepal)
- Digital camera imagery acquired in March 2011, consists of 3 bands (red, green, blue) and has a resolution of 0.45 m. The imagery was ortho-rectified by FRA in Nepal (Source: FRA, Nepal)

4.1.4. Software

In order to facilitate the research, different software was employed which is shown in the below table. Among these, Lastool was mainly used for LiDAR data processing and the Erdas Imagine 2011 and eCognition Developer 8.7 software was used for object based image analysis.

Table 4: Software used in the research

S.N	Software	Purpose
1	ArcGIS version 10	GIS analysis
2	eCognition Developer 8.7	Object based image analysis
3	Erdas Imagine 2011	Image processing and remote sensing applications
4	LasTool	LiDAR data processing
5	Treevaw	LiDAR data testing
6	SPSS	Statistical analysis
7	Microsoft Excel	Statistical analysis
8	Microsoft PowerPoint	Presentation of research
9	Microsoft Word	Writing thesis

4.2. Workflow of research method

The flow chart showed below in the figure 8 summarizes the procedures of the individual tree-based approach for carbon estimation and uncertainty assessment through error propagation analysis.

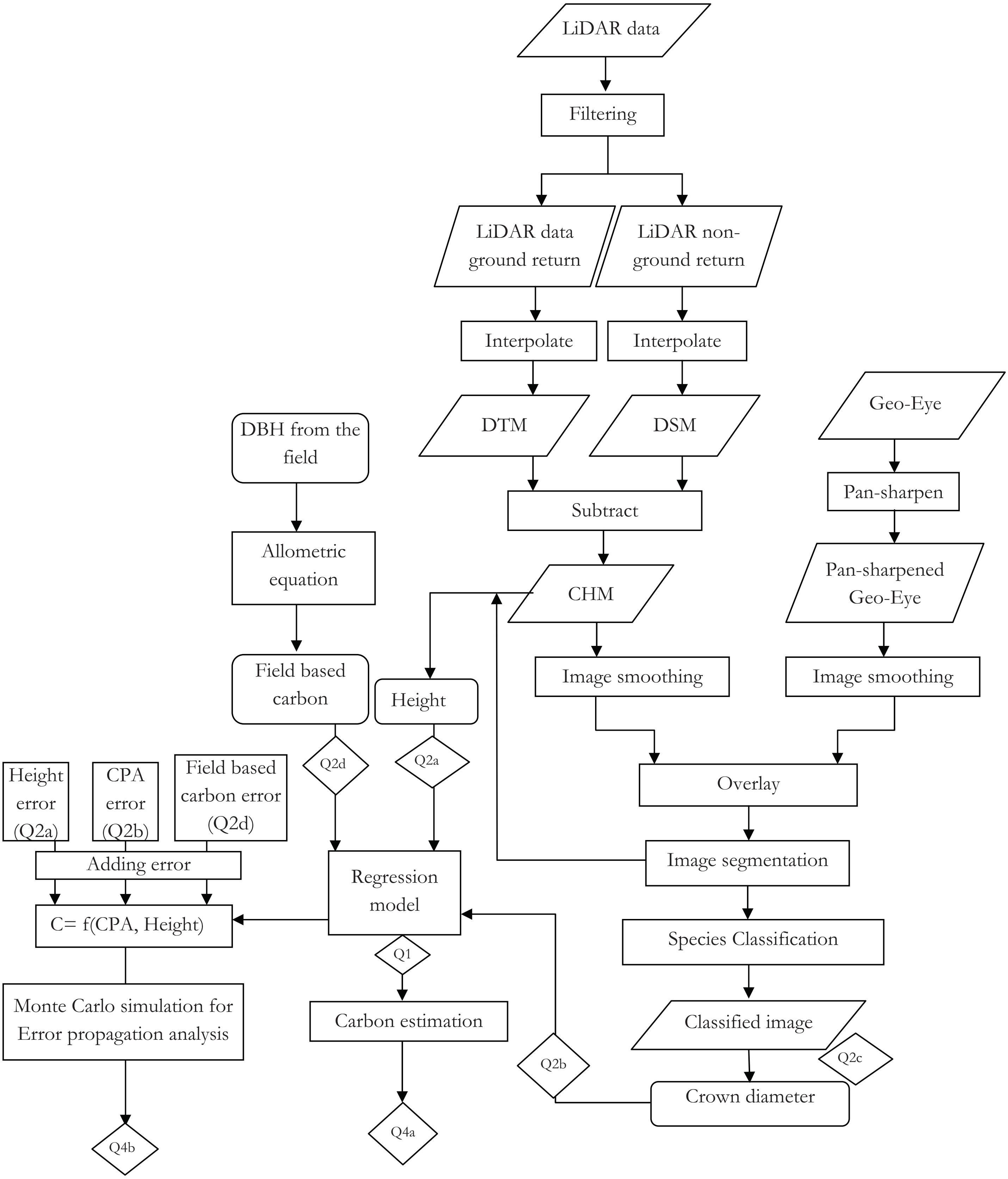

Figure 8: Workflow of the research method

4.3. Image pre-processing

Image pre-processing in the research comprises two processes: image stacking and image fusion.

4.3.1. Image stacking

The Geo-eye imagery was obtained in five separate images (4 multispectral bands and 1 panchromatic band) so the first operation done was to stack the image before images fusion. This task was performed in Erdas Imagine 2011.

4.3.2. Image fusion

Image fusion is the process of merging two or more images to retain the most desirable characteristics of each. A panchromatic (PAN) image was fused with multispectral imagery in order to acquire the image that has the spatial resolution of the panchromatic imagery and the spectral resolution of the multispectral imagery. There are several methods that are commonly used to fuse remotely sensed images, notably IHS (Intensity Hue Saturation); HPF (high pass filter) and wavelet resolution merge.

In this research, Geo-Eye panchromatic imagery was fused with Geo-Eye multispectral imagery using HPF (high pass filter) pan-sharpening method in Erdas Imagine 2011. In HPF resolution merge, small high-pass filter is applied in PAN image, and then this result is combined with the lower resolution multispectral data, pixel to pixel. HPF maintains the spectral properties of the original multispectral image and therefore the fused image has higher spatial resolution with all the bands of original multispectral image (ERDAS, 2011). Therefore, HPF is employed for image fusion in this research.

As a result, a MSS pan-sharpened image with 0.5 resolution has 4 bands which will be useful for tree species classification and identification.

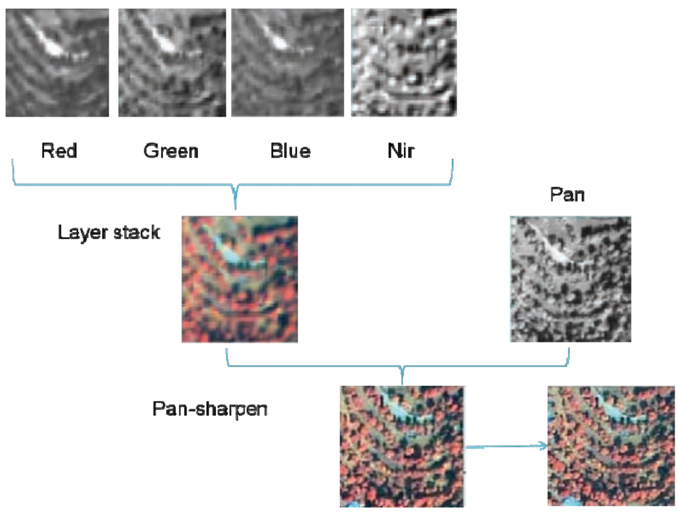

Figure 9: The image processing

4.3.3. Image filtering/Convolution

Image filtering is an image enhancement technique which helps to sharpen the image objects. A moving window/ kernel containing an array of coefficient or weighing factors is established and moved over the original image pixel by pixel and the average of the values within the window is placed the result in the centre pixel (ITC, 2010). The process used to apply filters to an image is known as convolution.

There are three main image filter methods: low pass filtering, high pass filtering and Laplacian filtering .e.g. Low pass filtering is a means for increasing class reparability of a data set consists of multi-pixel objects (1998). In the low pass filter method, an image is smoothed by decreasing the disparity between pixel values by averaging nearby pixels so the image will become blurred or smoothed and noise will be removed. Platt et al (2009) indicated that low pass filtering can reduce the over segmentation. In the segmentation task, we need only detailed outline and shapes of the trees. Hence it is necessary to remove the pattern of gray-level changing per pixel. Different window sized median filters can be used for individual tree crown delineation, for example 3-by-3, 5-by-5, and 7-by-7. In this study, 5-by-5 filter was used because it avoids removal of small peaks in the canopy (small trees) while maximizing the smoothing function (Parker et al., 2009).

4.4. Field work

4.4.1. Sampling design

Sampling design was done in order to indentify the number of plots and the location of plots which direct the field work operation. Stratified random sampling was selected since stratification generally yields more precise estimates for a fixed cost than the other options (MacDicken, 1997). Stratification was based on community forests and random sampling was done in each stratum. The community forest is used as a stratum to ensure that the samples are separated in the whole study area. In addition, the REDD project in Ludhikhola watershed focuses on sequestering carbon through community-based forest management. Therefore research on carbon estimation in community forest in Ludhikhola watershed is needed. The number of plots is calculated through the equation taken from Community forest guideline in Nepal (DOF, 2004):

$$a = I*A/100$$

$$n = a/p$$

Where a is the total study area (the area of sampling); I is the sampling intensity; n is the number of plot; p is the area of one sample plot.

Secondary data of local community forestry areas was used to facilitate the stratification. The number of plots was calculated for each stratum and plots were located randomly in stratum using ArcGIS. A map of the study area showing the individual stratum and all plots as well as images of plots were prepared for field work.

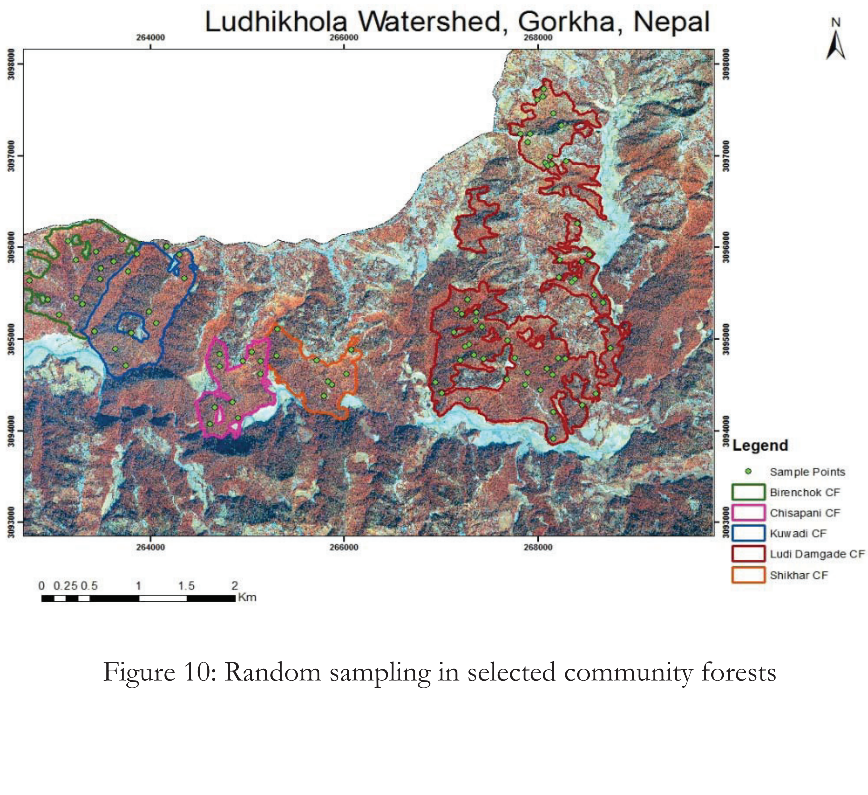

Figure 10: Random sampling in selected community forests

4.4.2. Field equipment

The equipment used during the fieldwork is shown in table 5 below. Geo-Eye imagery, Gorkha geo-database, sampling plot with correct geo-reference were uploaded on iPAQ. The watershed map and plot images were printed for the identification of recognizable trees.

Table 5: The equipment used in the field

Instrument	Purpose
iPAQ and Garmin GPS	Navigation
Diameter tape (5meters)	Tree diameter measurement
Meter tape (30 meters)	Distance measurement
Clinometer	Slope measurement
Plot centre marker	Marking plots
Chalk	Marking trees
Haglof Vertex V4	Tree Height measurement
Suunto compass	Find direction in the field
Data sheet	Taking notes and recording data

4.4.3. Data collection

Circular plots of diameter 12.62 m with an area of 500m^2 (IPCC, 2003) were established in the field. Both IPAQ and GPS Garmin were used to navigate to the plot center. In each plot, individual tree measurements were taken for DBH, tree height and canopy density. Only trees with DBH more than 10 cm were considered because it is generally assumed that the trees with diameter 10 cm or less contribute little to the total biomass carbon of a forest (Brown, 2002). Slope and aspect were record in the field. For the areas with slope greater than 5%, slope correction was applied. (The slope correction table is attached in the appendices-appendix 5).

Data were collected in five community forests: Shikhar, Birenchok, Chisapani, Kuwadi, Ludi Damgade. The community forests were selected based on the accessibility and theie elevation characteristics. Among these, Ludi Damgade is the largest community forest and it is diverse in elevation. A previous study on carbon stock in Nepal also shows that Ludi-Damgade is one of the community forests that has the highest forest carbon stock (ICIMOD, 2010).

4.4.4. Field data analysis

After field work, all the collected data were entered in appropriate format and descriptive analysis was carried out. The trees recognized in image during the fieldwork were recorded using ArcGIS. Afterwards, manual tree delineation was done based on the recognized trees. These delineated trees were later used for the validation of segmentation accuracy as well for validation of the regression model. The tree height measured in the field was used to validate the LiDAR derived height.

The DBH of identified tree was used to calculate the field -based AGB or field-based carbon of that tree through an allometric equation. The field based carbon was then considered as the ground truth data for carbon model validation.

In this research, the allometric equations for *Shore robusta* and *Other species* were selected from the research of Basuki *et al* (2009) in the tropical forest of Indonesia. These allometric equations were used since the mean annual rainfall (2000mm) and temperature (21^0 C to 34^0 C) was similar to that of the study area. It therefore provided the best available allometric equation for use in the study area. In addition, these allometric equations come together with the error of residuals, which is needed for further analysis.

i. TAGB = EXP [-2.193 +2.371*Ln(DBH)] ……………Allometric equation for *Shorea robusta*

ii. TAGB = EXP(-1.201+2.196*Ln(DBH)) ……………Allometric equation for *Other species*

Where, TAGB = Total above ground biomass,
DBH= Diameter at breast height

The total above ground biomass obtained from these equations is converted to carbon stock using a conversion factor (IPCC, 2007)

C=TAGB * CF

Where, C= carbon stock (kg for individual tree and MgC for study area)
TAGB = Total above ground biomass
CF= Carbon fraction of biomass (=0.47)

4.5. Creating the DSM, DTM and CHM from the LiDAR data

DTM and DSM were created directly using LasTools software. Digital surface model values (DSM) were computed for each point by gridding the point to desired pixel size. If a cell contained no laser reflection point, the value of this cell was determined by averaging the height values found in the eight neighboring cells (St-Onge *et al.*, 2008). The DTM is generated using the ground return (last returns) elevation values using an initial triangulated irregular network (TIN). Triangulation with linear interpolation is an exact interpolator that works by creating triangles by drawing lines between data points(Popescu *et al.*, 2002). The interpolated grid cell size for both DTM and DSM was 0.5m which is the spatial resolution of Geo-Eye imagery. The tree height information on the field data collection was used to threshold the laser height values in order to eliminate the effect of shrubs and understory vegetation.

The Canopy height model (CHM) is computed as the difference between DSM and the corresponding DTM values. Hence, the CHM gives the interpolated height of all points in the canopy in the form of a regularly spaced grid with a 0.5 m pixel size.

4.6. Image- to- image coregistration

Image to image co-registration is the process of geometrically aligning Geo-Eye imagery with CHM in order to use the information of individual tree from both sources of data. The dissimilarities between the Geo-Eye imagery and the CHM due to differences in the acquisition process (different sensors, platforms, time of recording) need to be corrected by co-registration procedures. Among these, manual registration remains the most common way to accurately align their imaging data (Zavorin *et al.*, 2005). In this research, manual registration with polynomial transformation was used to co-register Geo-Eye imagery with the Digital camera imagery as reference image instead of using CHM. The reason is that it would hardly to find the control points from CHM. Meanwhile, the ortho-rectified Digital camera imagery was simultaneously acquired with LiDAR data and matches with the LiDAR..

The procedure of image co-registration consists of two stages which can be executed using Erdas Imagine 2011. The first stage is a standard co-registration of images based on a set of corresponding points on the images. This stage is meant to provide the first approximation to a matching of images, and for convenience the co-registration points are chosen by eye. The second stage makes use of a polynomial transformation to fit the conjugate matching points.

Polynomial equations are used to convert source file coordinates to rectified map coordinates. A transformation matrix is computed from the image and ground coordinates of the Ground control points (GCPs). The matrix consists of coefficients that are used in polynomial equations to convert the coordinates. The goal in calculating the coefficients of the transformation matrix is to derive the polynomial equations for which there is the least possible amount of error when they are used to transform the reference coordinates of the GCPs into the source coordinates

Co -registration validation

Root mean square error is used to validate the co-registration result. RMS (Root Mean Square) error is the discrepancy in A, Y and the total between the reference CGPs and the retransformed point. A small RMS error means that the desired output coordinate for a control point and the actual output coordinate for the same point is close. For the registered images, the higher the total RMS error is, the higher the local geometric distortion is.

4.7. Tree crown delineation

4.7.1. Hybrid techniques approach

A pre-requirement for delineation of tree crown is that the crowns should be at least visually recognizable as a distinct object in the remote sensing images and the spatial resolution of the image should be much higher than the size of tree crowns (Zhengrong *et al.*, 2008). Many researchers have explored the use of segmentation technique to delineate tree crown on high spatial resolution imagery (resolution >1.0 m) e.g. Brandtberg *et al.*(1998); Pouliot *et al.*(2002) Ke *et al* (2011). There are primarily four types of segmentation techniques: thresholding, boundary-based, region-based, and hybrid techniques(Jianping *et al.*, 2001).
Among these, hybrid methods tend to combine boundary detection and region growing together to achieve better segmentation (Haddon *et al.*, 1990; Jianping *et al.*, 2001; Pavlidis *et al.*, 1990; Tsendbazar, 2011). This technique makes use of the phenomenon that in high spatial resolution imagery, trees appear as bright objects surrounded by a shaded area and the tree tops typically the brightest spot within the bright object. Local maxima and minima have frequently been used to detect tree tops and define crown boundaries, respectively (Leckie *et al.*, 2005). Local maxima are used as seeds for growing and local minima are used as a restriction for growing region (Darius *et al.*, 2002). Starting at a potential seed pixels, neighboring pixels are examined sequentially and merged to growing region based on the similarity to the seed pixels, which is defined through both the spectral variance and geometry of the object (Definines, 2009). This process continues until a significant boundary is found and then these pixels are considered to belong to the region corresponding to the seed pixel (Ke *et al.*, 2011).

4.7.2. Tree crown delineation using eCognition software

Based on the theories described above, tree crown delineation was done in eCognition Developer 8.7. The steps are as follows:

- **Image segmentation**: apply a top-down segmentation algorithm to the pan-sharpened Geo-Eye imagery in order to cut the image into square objects with the desired size. The selected algorithm is a so-called chessboard with the grid size of 2 pixels (equal to $1m^2$). The grid size selection affects tree top detection. If the grid size is too small, one tree may contain more than one top. If the grid size is too big, the top of tree A may be assigned to the top of tree B.
- **Masking non-tree objects:** non-tree objects are the objects that belong to water bodies, bare soil and shadows. Non-tree objects are separated from trees by selecting the certain threshold for each class. The aim is to avoid mistakes in the tree top detection. It can be observed from the image that bare soil and water have brightness that is greater than that of a tree. If they are not removed, the system would assign tree tops within bare soil or water body. Masking shadow to avoid the situation that the seed (top tree) may grow over shadow area.
- **Finding local maxima and local minima:** The local maxima (tree tops) and local minima are detected based on the brightness of the image.
- **Apply region growing algorithm to the seeds**: The local minima are used to define the crown boundaries. Local minima seeds are grown with respect to neighboring object that have the least mean difference to the local minima. In this way, objects that have the least difference to local minima are merged and grown to create the boundary of the tree crown. The tree top is then used as a seed point which is then expanded under region growing algorithm with the search range of

five objects (to detect smaller tree crown recorded in the field). The neighbouring objects of the tree top are examined and added to the seed if their mean difference to the tree top seed is similar. Region growing continues until significant boundaries of tree crown are found.

- **Refine the shape of crown**: The crown is refined and sharpened by mean of Watershed transformation and Morphology operation. Watershed transformation helps to split the overlapping tree crowns into individual tree crowns based on the splitting threshold. This threshold is given on the basis of expert knowledge on crown width. The Morphology operation is carried out to smooth the border of the segment crowns.

Segmentation validation

One of the methods to validate the segmentation is by means of checking for one to one correspondence (Zhan *et al.*, 2005). One to one correspondence describes the similar aspects between reference objects (manual digitized objects) and segments. The first aspect is the difference in area between reference objects and the segments they intersect. The second is the positional difference between reference objects and segments. The reference objects and segments are considered one to have one matching if the following four criteria are fulfilled (Clinton, 2010):

1. The centroid of the reference object is in segmented object
2. The centroid of the segmented object is in reference object
3. $area(x_i \cap y_j) / area(y_j) > 0.5$ (The area $(x_i \cap y_j)$ = the area of the geographic intersection of reference object x_i and segment y_j)
4. $area(x_i \cap y_j) / area(x_i) > 0.5$ (The area $(x_i \cap y_j)$ = the area of the geographic intersection of reference object x_i and segment y_j)

Clinton *et al.* (2010) proposed a measure which they call the closeness (D) and which considers both the over-segmentation and under-segmentation. D is interpreted as the closeness measure to an ideal segmentation result. It ranges between 0 and 1. With D =0 corresponding to an ideal segmentation.

$$D = \sqrt{\frac{\text{oversegmentation}_{ij}^2 + \text{undersegmentation}_{ij}^2}{2}}$$

$$\text{Oversegmentation}_{ij} = 1 - \frac{\text{area}\,(x_i \cap y_j)}{\text{area}(x_i)}$$

$$\text{Undersegmentation}_{ij} = 1 - \frac{\text{area}\,(x_i \cap y_j)}{\text{area}(x_i)}$$

4.8. LiDAR derived height

The height of a tree is defined as the maximum value of CHM corresponding to the tree crown. The delineated crowns from Geo-Eye imagery were used as the zone to extract the local maximum value from the CHM. Within each crown, the maximum pixel value was extracted from CHM using Zonal statistic tool in ArcGIS 10. Zonal statistic calculates statistics on values of a raster within the zone (the crown). The highest value in each zone is assigned the local maxima of the zone.

LiDAR derived height validation

The LiDAR derived height was compared to corresponding height of the corresponding measured tree. Linear regression is performed between ground-measured heights and LiDAR derived heights yielded a R^2 to validate CHM created (St-Onge, 2000)

4.9. Object-based classification

Once the tree crowns have been delineated, the tree species can be classified by means of the nearest neighborhood algorithm in eCognition Developer 8.7 software. In comparison to pixel based training, the object based approach of nearest neighbor requires fewer training samples. The training samples are image objects which are the result of the segmentation process. The species information of the object was taken from the field sample data. The field sample data was divided into two parts, 2/3 was used for training data and 1/3 was used for classification validation. The feature space was created based on the training samples. The object features that were selected for feature space creation are layer value of each MSS bands, panchromatic band; object geometry and the thematic layer information related to each object. Starting from the selected sample, nearest neighbor classification looks for the closet sample in the feature space for each image object and assigns the class for that object. The descriptive statistic as well as the observation from the field shows that more than 70% of the trees in study area are *Shorea robusta*. Therefore the image was classified in two classes: 1) *Shorea robusta* and 2) *Other species*.

Image classification validation

The accuracy of the classified image is assessed by comparing it to reference (ground truth) data (ITC, 2010). Accuracy assessment is done using the error matrix or confusion matrix which compares the classification result with true world. Accuracy assessment was done in Erdas Imagine 2011.

4.10. Multiple regression for carbon estimation

Regression analysis has been widely applied to spatially extend predictions of total aboveground biomass (TAGB) and other biophysical properties over large forested areas (Frazer *et al.*, 2011). Above ground biomass or the carbon stock derived from it is highly related to other canopy structural parameters such as tree crown area (Gill *et al.*, 2000) and stem height (Fang *et al.*, 2006; Lim *et al.*, 2004; Næsset, 2002). Then, to estimate carbon, the regression model can be established between field based carbon stock and height or between field based carbon stock and tree crown area.

Both simple and multiple regression models can be used for the estimation of AGB (Soares *et al.*, 2005) and ultimately, carbon estimation. Research of Nakai (2009) has indicated that the multiplicative equation offered better results than the ones using tree height or crown area alone. Therefore, multiple regression models relating field-based carbon stock with tree height (from CHM) and crown projection area (CPA) were developed. The significance of these models would be compared and the most significant one selected..

The regression analysis contains three main steps:

- Prior to regression analysis, the detected and delineated trees are automatically linked with the field measured trees to combine the information for each tree. Each tree has the information about tree height (extracted from the CHM), CPA (extracted from the tree crown delineation result) and field-based carbon (calculated using the appropriate allometric equation)
- Using Microsoft Excel to develop regression analysis. The independent variables are height and CPA, the dependent variable is carbon (C). The developed model is called the *regression predictive model of carbon*
- Testing the significance of the model through an analysis of variance (ANOVA)

The trees selected for the development of the model are the trees that are well-delineated (one to one matching) and correctly classified. In addition, the accuracy of predicted height of the tree has to be acceptable. Trees were excluded if a CHM-extracted height was more than 1.5 times the field-measured height (Holmgren *et al.*, 2004). The expected final model has the form as shown in table 6.

Table 6: The expected final carbon predictive model

Field measurement	Parameter extracted from remote sensing data	Expected carbon predictive model established by regression analysis
DBH converted to $C_{field-based}$ by allometric equation	- CPA extracted from image segmentation	C= f(CPA)
DBH converted to $C_{field-based}$ by allometric equation	- LiDAR derived height	C= f(Height)
DBH converted to $C_{field-based}$ by allometric equation	- CPA extracted from image segmentation - LiDAR derived height	C = f(CPA, Height) = a*CPA + b*Height + c

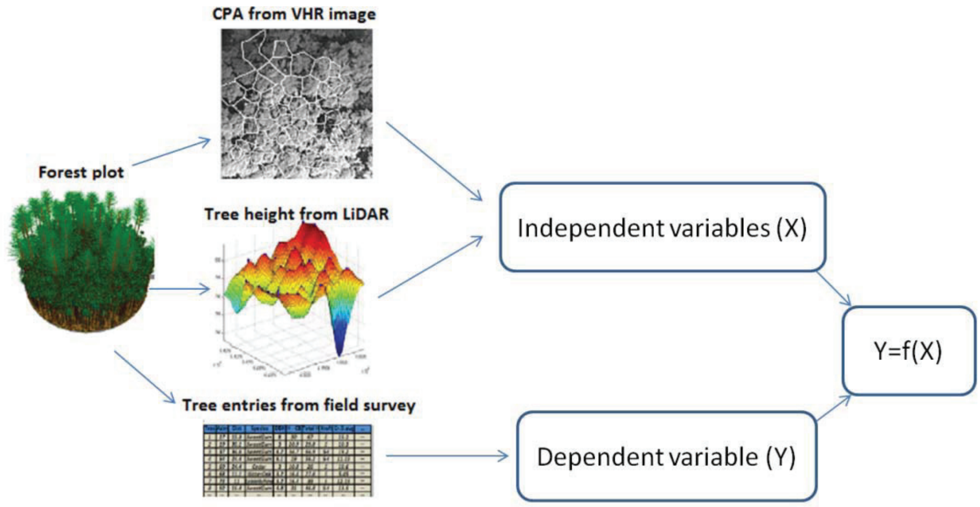

Figure 11: Outline of the multiple regression model development for carbon estimation [The diagram was created by combining the graphic objects from the research of Kim *et al.* (2010)]; Zhao *et al.* (2009)]

Carbon model validation

The model was validated using the test data set obtained from the field. Validation of the model was done by comparing the amount of carbon predicted by the model and amount calculated from the field data. Root mean square error (RMSE) is calculated to check the amount of error in the carbon stock map.

$$RMSE = \sqrt{\sum \frac{(Cp - Co)^2}{N}} \text{................ RMSE}$$

Where, RMSE = Root Mean Square Error,
Cp- Carbon predicted by the model
Co-Carbon calculated
N-Number of observations

4.11. Monte Carlo Simulation

4.11.1. Monte Carlo Simulation introduction

In our study, carbon stock of individual tree is the output of *regression predictive model of carbon*. The uncertainty of this output is affected by uncertainty in the input data. The uncertainty analysis is carried out to answer the question how the output changes with the variation in the input. Both sensitivity analysis and Monte Carlo analysis are used for evaluating output uncertainty based on the input (Jochem *et al.*, 2009; Weir, 2002). However, sensitivity analysis is used to assess the impact of changes in each input parameters on the output but not the effect of error in this parameters (Larocque *et al.*, 2008). Meanwhile, the purpose of uncertainty assessment carried out using Monte Carlo simulation is to combine uncertainties in order to analysis the changes in the output (Monni *et al.*, 2007).

To quantify uncertainty of forest carbon estimates, the IPCC recommends Monte Carlo analysis (Gonzalez *et al.*, 2010; IPCC, 2006b). Lo (2005) recommended that Monte Carlo Simulation is especially useful for studies that involve step by step calculations where measurements taken at a smaller temporal or spatial scale are used to estimate a value at larger scales. Monte Carlo simulation is based on the repetition of many individual model realizations with each realization using a randomly constructed set of parameters. The model outputs are then aggregated into a probability distribution which shows the variation in the output (Schade *et al.*). In simple words, Monte Carlo simulation is essentially a statistical analysis (Kuo *et al.*, 1983) which relies on repeated random input sets to compute their results. As Monte Carlo analysis is based on simple assumptions and does not require the development of complex algorithms, it constitutes a major advantage when applied to complex models (Larocque *et al.*, 2008). The model can be written as $Y = f(X_1, X_2, ..., X_k)$. The Monte Carlo simulation procedure for error propagation involves four main steps:

(1) Assign a random error for each input factor X_i
(2) Generate randomly N (a number of realizations or iteration) sets of input factors X_i, with l =1, ..., N (a set of input factors is called a sample);
(3) Evaluate the model and compute the corresponding model output Y_i
(4) Analyse the resulting output values Y_i , with l = 1, ..., N.

To give a simple example, if a tree has the measured height of 15m and the error of LiDAR predicted height is ± 2m, so the Monte Carlo simulation to analyse error propagation of predicted height of that tree consists of the flowing steps:

(1) Assign a random error for LiDAR predicted height, for example: E_1= 1m, E_2= 1.2m, E_2= -0.5m…
(2) Adding the random error to the measured height of the tree. For each realization, new value of tree height is generated:
   - Realization 1: $H_1' = 15 + 1= 16$; Realization 2: $H_2' = 15 + 1.2 = 16.2$; Realization 3: $H_3' = 15 – 0.5 = 14.5$ ….Realization N
(3) From N realization, the frequency of height error can be obtained for this tree

Many runs (N) are required to provide statistically reliable information about the predicted mean and the total variance. There is no formula for determining an acceptable number of iteration to use (Haness *et al.*, 1991), the choice of number of iterations to include in the simulation therefore depends on the purposes of the model. As a result, each researcher has their own reason for the selected number of repetition. In the research of James (1983), 30 Monte Carlo runs were required to define the mean variance of a simple model. Meanwhile, Haness *et al.* (1991) conducted at 1000, 10 000, 100 000 iterations and explored that there was no significant differences the 10 000 and 100 000 iteration runs. The selection of suitable value for N is therefore a matter of balancing the requirements for statistical confidence level against the computational load (Weir, 1999).

4.11.2. Monte Carlo Simulation for carbon estimation

Models used for Monte Carlo Simulation

In this study, uncertainty impacts of different input parameters were combined to analyse the variation of the output using Monte Carlo simulation. The Monte Carlo Simulation is applied separately for 2 classes: *Shorea robusta* and *Other species*. Each class employs two models in the carbon estimation procedure. The first model is the *allometric equation* used to estimate field-based carbon, which is used as the input for establishing the second model called *regression predictive model of carbon*. *Regression predictive model of carbon* describe the relationship between field-based carbon and parameter extracted from remote sensing data (The expected *Regression predictive model of carbon* was shown in table 6).

The Monte Carlo Simulation starts with the task of identifying the error sources which propagate in the two models (different for classes). The error sources are showed in the following diagram:

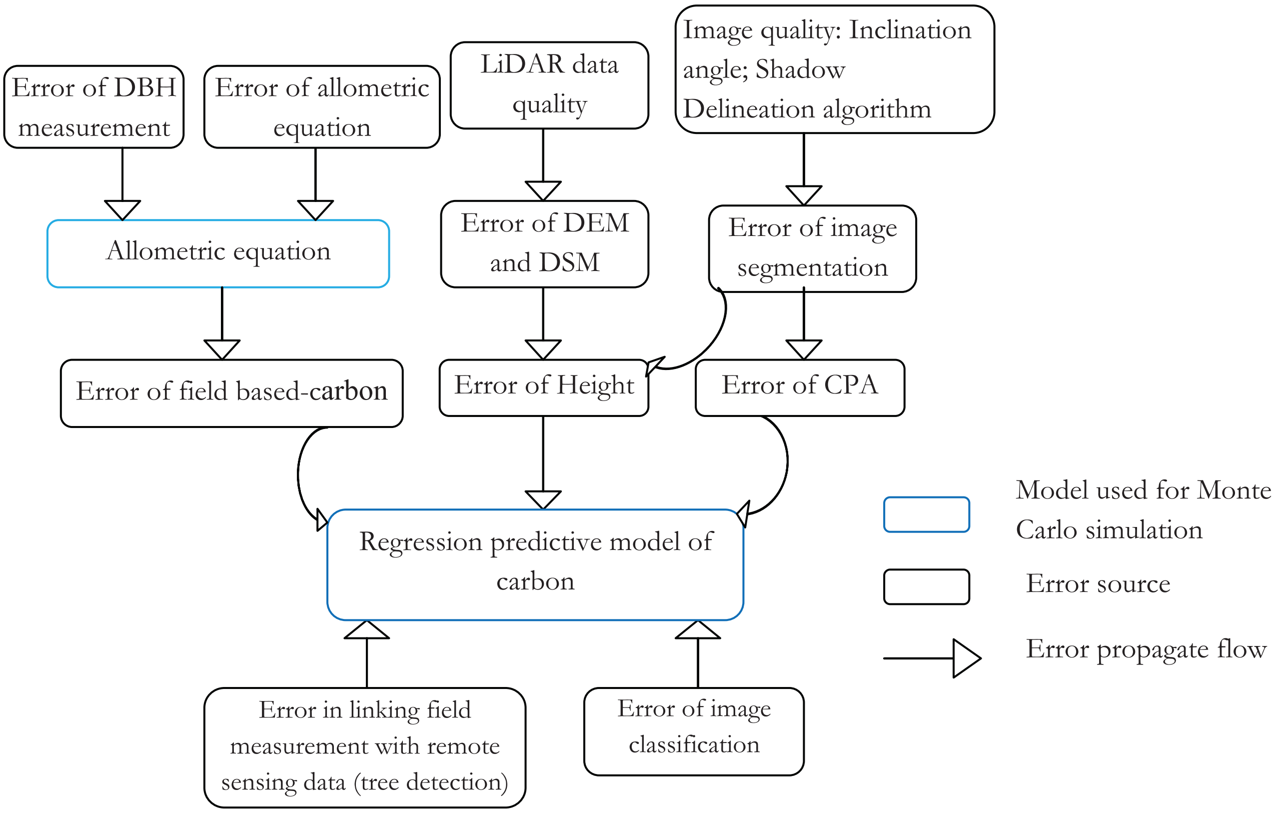

Figure 12: The error sources and the propagation of error

Unit of Monte Carlo Simulation

The Monte Carlo Simulation is applied to each individual tree because the individual tree is the research subject or the sample unit. Specifically, we focus on the trees selected for building the *regression predictive model of carbon*, which are considered one to one matching between field measurement and remote sensing data. For Monte Carlo analysis, we assumed that we have n' *Shorea robusta* trees and n" *Other species* trees.

Input variables for Monte Carlo Simulation

The accuracy of the output depends on the accuracy of both dependent and independent variables used to create the *regression predictive model of carbon*. The coefficients of the *regression predictive model of carbon* may change due to the change of input data including: field based carbon, LiDAR derived height and CPA extracted from the Geo-Eye imagery segmentation. Hence, the input data sets for Monte Carlo Simulation contain three main variables: field-based carbon ($C_{field\text{-}based}$); Height and CPA of each tree.

The sources of error causing the uncertainties of $C_{field\text{-}based}$; Height and CPA were explained in the Figure 12. In the created input data sets, each tree will have the simulated values of $C_{field\text{-}based}$; Height and CPA. These new value are used to develop regression models. The variance of the carbon stock of individual tree calculated based on different models is studied for uncertainty analysis.

Random number generation

For the first step of simulation, random number is required to simulate the stochastic nature of the model. Random numbers are generated from input distributions (e.g. thousands of times), and the output distribution is calculated based on each set of random numbers.(Monni *et al.*, 2007). There is some assumption that should be met when performing this estimation procedure. The residual must be distributed normally, independently and with constant variance (Samalca, 2007). Gonzalez *et al.* (2010) generated random number from a normal distribution with mean =0 and standard deviation = 1 for Monte Carlo analyses. This method also selected for generating random number in this research. We called the random number for each variable is $V_{variable}$. $V_{variable}$ is a random number (different for each variable) from a normal distribution with mean = 0 and standard deviation = 1.

4.11.3. Error estimation from the error sources

Field based carbon error ($E_{C\text{-}field\ based}$)

Field based carbon for *Shorea robusta* and *Other species* was obtained from the allometric equations as follows:
$C_{field\text{-}based\ Shorea\ robusta} = 0.47 * EXP\ [-2.193 + 2.371 * Ln\ (DBH_{Shorea\ robusta})]$
$C_{field\text{-}based\ Other\ Species} = 0.47 * EXP[-1.201 + 2.196 * Ln(DBH_{other\ Species})]$

In the analyses of field data, the sources of error are (i) filed measurement errors of tree diameter (DBH) and (ii) statistical uncertainty of allometric equations. We also applied the Monte Carlo approach to quantify the uncertainty in field measurement of carbon stock. We generated N (N=1000) realizations of field- based carbon stock for each tree, adding error terms for (i) and (ii) to the original value of DBH and $C_{field\text{-}base}$ respectively.

$$C_{field\text{-}base} = f(DBH + V_{dbh}E_{dbh}) + V_{allometric}E_{allometric}$$

$V_{variable}$ is random number (different for each variable) from a normal distribution with mean = 0 and standard deviation = 1
E_{dbh}: standard error of DBH measured in the field
$E_{allometric}$: standard error of allometric equation (taken from reference)

The process is as follows:

Step 1: For each tree, generate a random number V_{DBH}, $V_{allometric}$

Step 2: For each tree, generate a random error:

$$\delta\ DBH = V_{dbh}E_{dbh}$$
$$\delta\ allometric = V_{allometric}E_{allometric}$$

Step 3: Adding the error of parameter for each tree:

$$DBH' = DBH + V_{dbh}E_{dbh}$$

Step 4: Repeat step 1, 2and 3… N times for each tree and store the results. Each individual tree has N combination of simulated DBH' and $V_{allometric}E_{allometric}$

Step 5: From each combination, new value of field-based carbon of the tree is calculated

Step 6: Calculate the RMSE between the simulated field-based carbon and initial value obtained from allometric equation (without simulation), store the result.
Step 7: Repeat step 5 and 6… N times
Step 8: Calculate $E_{\text{C-field based}}$

E_{dbh} is expressed as the relative RMSE of the difference between the initial diameter measurement and the repeated measure. Due to the time limitation of the research, E_{dbh} is taken from previous research of field measurement research of DBH. Gonzalez *et al.* (2010) estimated E_{dbh} as the diameter error from repeated measures of a random sample of 169 trees (19 cm<148cm) and E_{dbh} equalled 0.027.
For $E_{allometric}$, we used the standard error of each equation which goes along with the allometric equation taken from the research of Basuki *et al* (2009). For each of the trees chosen for *regression predictive model of carbon*, 1000 realizations were generated. The simulated $\bar{C}_{\text{field-based}}$ for individual tree is calculated based on the equation:

$$\bar{C}_{\text{field-based}} = \frac{1}{1000}\left(\sum^{all\ realizations} C_{field-based}\right)$$

$\bar{C}_{\text{field-based}}$ is the simulated value of field based carbon for individual tree.
The field based carbon error is the RMSE between the simulated field-based carbon value and the initial field-based carbon from original allometric equation:

$$E_{\text{C-field based}} = RMSE = \sqrt{\sum \frac{(\bar{C}_{\text{field-based}} - C_{field-based})^2}{N}}$$

Height extraction error (E_{Height}) and CPA extraction error (E_{CPA}) and the involvement of tree detection error

A visual interpretation was used to link automatically delineated crown segments with trees measured on the ground. For each segment, three different cases can occur: (1) no field tree is within the segment, (2) one field tree is within the segment, and (3) more than one field tree is within the segment. Only the case (2), the field tree was linked to the delineated tree crown (tree detection) for generating the *regression predictive model of carbon*. The wrong link between delineated crown and the tree measured on the ground mostly happend to poor delineated crowns. The segmentation accuracy is acquired in percentage, for example S (%), then the error of segmentation is S' (%) = 100 – S. It means there is S' (%) of delineated crowns might wrongly link to the trees measured on the ground.

The poor-delineated tree has an error magnitude lager than the well-delineated tree. Therefore, the data set was divided into well-delineated trees and poor-delineated trees in order to involve the linking error between field measurement and satellite data in error propagation analysis. The error of CPA extraction contains $E_{\text{CPA-well}}$ and $E_{\text{CPA-poor}}$ in which the $E_{\text{CPA-well}}$ is estimated from the well-delineated crown dataset and $E_{\text{CPA-poor}}$ is obtained from the poor-delineated crown dataset. The error of CPA extraction is caused by the following sources: understory and overlapping crown, shadow in the image, inclination angle, automatic segmentation, shadow. E_{CPA} is the RMSE of estimates height; calculate the difference CPA taken from manual digitization and the CPA taken from segmentation.

$$E_{\text{CPA-well}} = RMSE = \sqrt{\sum \frac{(CPA_{well-delineated\ crown} - CPA_{digitized})^2}{N}}$$

$$E_{\text{CPA-poor}} = RMSE = \sqrt{\sum \frac{(CPA_{poor-delineated\ crown} - CPA_{digitized})^2}{N}}$$

Similarly, the error of LiDAR derived height also contains $E_{\text{Height-well}}$ and $E_{\text{Height-poor}}$ in which the $E_{\text{Height-well}}$ is estimated from the well-delineated crown dataset and $E_{\text{Height-poor}}$ is obtained from the poor-delineated crown dataset. The error of LiDAR derived height is affected by the following sources: LiDAR quality data (point density, seasonal acquired), CHM creation procedure (interpolation algorithm), co-registration error, and image segmentation error. Delineation error leads to the error of CPA. In addition, it is also a problematic to used delineated crown to derive information of tree height. E_{height} is the RMSE of estimates height; calculate the difference between height measurement from the field and height extracted from CHM.

$$E_{\text{Height-well}} = RMSE = \sqrt{\sum \frac{(Height_{LiDAR\ derived\ from\ well-delineated\ crown} - Height_{field-based})^2}{N}}$$

$$E_{\text{Height-poor}} = RMSE = \sqrt{\sum \frac{(Height_{LiDAR\ derived\ from\ poor-delineated\ crown} - Height_{field-based})^2}{N}}$$

The involvement of classification error in Monte Carlo Simulation process

The image classification will be validated by the error matrix, from which the classification accuracy is obtained in percentage. For example, the accuracy of *Shorea robusta* is A% (A≤100%) and the accuracy of *Other species* is B % (B≤100%). In other words, classification error for *Shorea robusta* is A' (%) = 100 – A; and the classification error for *Other species* is B' (%) = 100 – B.

If an individual tree is classified incorrectly (*Shorea robusta* is classified as *Other species* or *Other species* is classified as Shorea robusta), the affected variable is $C_{\text{field-based}}$. The $C_{\text{field-based}}$ of incorrect classified *Shorea robusta* is obtained from the allometric equation for *Other species* and the $C_{\text{field-based}}$ of incorrect classified *Other species* is taken from the allometric equation for *Shorea robusta.* The error of classification therefore affects the regression predictive model of carbon stock. In order to involve the classification error, one more variable should be generated, $C_{\text{field-based-wrong}}$.

Table 7: Allometric equation applied for incorrect classified trees

Class	Allometric equation to calculate $C_{\text{field-based-wrong}}$
Shorea robusta	$C_{\text{field-based-wrong}}$ = 0.47 * EXP(-1.201+2.196*Ln(DBH)) n (the allometric equation of *Other species*)
Other species	$C_{\text{field-based –wrong}}$ = 0.47* EXP [-1201 +2.196*Ln (DBH) (the allometric equation of *Shorea robusta*)

Calculate field-based carbon stock error of incorrect classified tree ($E_{\text{C-field based-wrong}}$)

Similar to $E_{\text{C-field based}}$, $E_{\text{C-field based-wrong}}$ is also obtained from Monte Carlo Simulation. The only difference is that the allometric equation used for simulation is exchanged.

4.11.4. Monte Carlo Simulation process

The Monte Carlo Simulation process is as follow:

Step 1: For each tree, generate random number $V_{variable}$

Step 2: For each tree, generate random error

$$\delta\ C_{field\text{-}based} = V_{C\text{-}field\ based} \cdot E_{C\text{-}field\ based}$$
$$\delta\ C_{field\text{-}based\ –wrong} = V_{C\text{-}field\ based\text{-}wrong} \cdot E_{C\text{-}field\ based\text{-}wrong}$$
$$\delta\ Height_{well} = V_{Height\text{-}well} \cdot E_{Height\text{-}well}$$
$$\delta\ Height_{poor} = V_{Height\text{-}poor} \cdot E_{Height\text{-}poor}$$
$$\delta\ CPA_{well} = V_{CPA\text{-}well} \cdot E_{CPA\text{-}well}$$
$$\delta\ CPA_{poor} = V_{CPA\text{-}poor} \cdot E_{CPA\text{-}poor}$$

Step 3: Adding the error of parameter for each tree:

$$C'_{field\ based} = C_{field\text{-}based} + \delta\ C_{field\text{-}based}$$
$$C'_{field\text{-}based\ –wrong} = C_{field\text{-}based\ \text{-}wrong} + \delta\ C_{field\text{-}based\ \text{-}wrong}$$
$$Height'_{well} = Height + \delta\ Height_{well}$$
$$Height'_{poor} = Height + \delta\ Height_{poor}$$
$$CPA_{well}' = CPA + \delta\ CPA_{well}$$
$$CPA_{poor}' = CPA + \delta\ CPA_{poor}$$

Step 4: Repeat step 1 and 2, 3 N times for each tree and store the results. N sets of selected trees (n' *Shorea robusta* tree and n" *Other species* tree) will be generated, each tree has the combination of $C'_{field\text{-}based}$; $C'_{field\text{-}based\ –wrong}$; $Height'_{well}$; $Height'_{poor}$; CPA'_{well}; CPA'_{poor}

Step 5: In each generated set, randomly select:

- From n' *Shorea robusta* tree":
  (4) Randomly select S' (%), we have a number of n'*S'/100 trees. These trees will be assigned as poor-delineated trees and the parameter Height is taken from $Height'_{poor}$; the parameter CPA is taken from CPA'_{poor}. Store the result
  (5) From previous result, randomly select A' (%), we have a number of n'*A'/100 trees. These trees will be assigned as incorrect classified tree and the field based carbon is taken from $C'_{field\text{-}based\ –wrong}$.
- Similarly, from n" *Other species* tree"
  (6) Randomly select S' (%), we have a number of n"*S'/100 trees. These trees will be assigned as poor-delineated trees and the parameter Height is taken from $Heigh_{poor}'$; the parameter CPA is taken from CPA'_{poor}. Store the result.
  (7) From previous result, randomly select n"*B'/100 trees which are assigned as incorrect classified tree and the field based carbon is taken from $C'_{field\text{-}based\ –wrong}$.

Step 6: Generate the regression model based on the selected combination. This model called simulated regression model.

Step 7: Calculate carbon with the simulated regression model for each tree

Step 8: Calculate the RMSE between the carbon estimated from simulated regression model and initial regression model which was created with the original set of data (without simulation), store the result

Step 9: Repeat step 5, 6, 7 and 8 …N times

Step 10: Analysis the propagated error and the error frequency

As there are many variables and symbols may cause confusion, the variables and symbols table is introduced in the following table:

Table 8: Table explains the variables and signs in Monte Carlo Simulation

Variable	**Meaning**	**Individual simulated error**	**Meaning**	**Estimated Error**	**Meaning**
$C_{field\text{-}based}$	Field-based carbon taken from true allometric equation	$\delta\ C_{field\text{-}based}$	Random error of $C_{field\text{-}based}$	$E_{C\text{-}field\ based}$	Error of $C_{field\text{-}based}$
Height	Tree height extracted from CHM	δ Height	Random error of Height	E_{Height}	Error of Height
CPA	Crown projection area taken from Image segmentation result	δ CPA	Random error of CPA	E_{CPA}	Error of CPA
$C_{field\text{-}based\ –wrong}$	Field-based carbon obtained from the wrong allometric equation (i.e in case of tree is incorrectly classified	$\delta C_{field\text{-}based\ –wrong}$	Random error of $C_{field\text{-}based\ –wrong}$	$E_{C\text{-}field\ based\ wrong}$	Error of $C_{field\text{-}based\ wrong}$
$C'_{field\text{-}based}$	Simulated field-based carbon (= $C_{field\text{-}based} + \delta\ C_{field\text{-}based}$)				
$C'_{field\text{-}based\text{-}wrong}$	Simulated $C'_{field\text{-}based\text{-}\ wrong}$ (= $C_{field\text{-}based\ –wrong} + \delta\ C_{field\text{-}based\ –wrong}$)				
$Height'_{well}$	Simulated Height with the error obtained from well-delineated segments (= Height + $\delta\ Height_{well}$)	$\delta\ Height_{well}$	Random error of extracted Height from well-delineated segments	$E_{Height\text{-}well}$	Error of extracted Height from well-delineated segments
$Height'_{poor}$	Simulated Height with the error obtained from poor-delineated segments (= Height + $\delta\ Height_{poor}$)	$\delta Height_{poor}$	Random error of extracted Height from poor-delineated segments	$E_{Height\text{-}poor}$	Error of extracted Height from poor-delineated segments
CPA'_{well}	Simulated CPA with the error obtained from well-delineated segments (= CPA + $\delta\ CPA_{well}$)	$\delta\ CPA_{well}$	Random error of extracted CPA from well-delineated segments	$E_{CPA\text{-}well}$	Error of extracted CPA from well-delineated segments
CPA'_{poor}	Simulated CPA with the error obtained from poor-delineated segments (= CPA + $\delta\ CPA_{poor}$)	$\delta\ CPA_{poor}$	Random error of extracted CPA from poor-delineated segments	$E_{CPA\text{-}poor}$	Error of extracted CPA from poor-delineated segments
Other Character: N: time generating regression predictive model of carbon; n': number of *Shorea robusta* tree; n": number of *Other species* tree; A: Accuracy of classification (*Shorea robusta*); A': Error of classification (*Shorea robusta);* ; B: Accuracy of classification (*Other species*); B': Error of classification (*Other species);* S: Accuracy of segmentation; S': Error of segmentation					

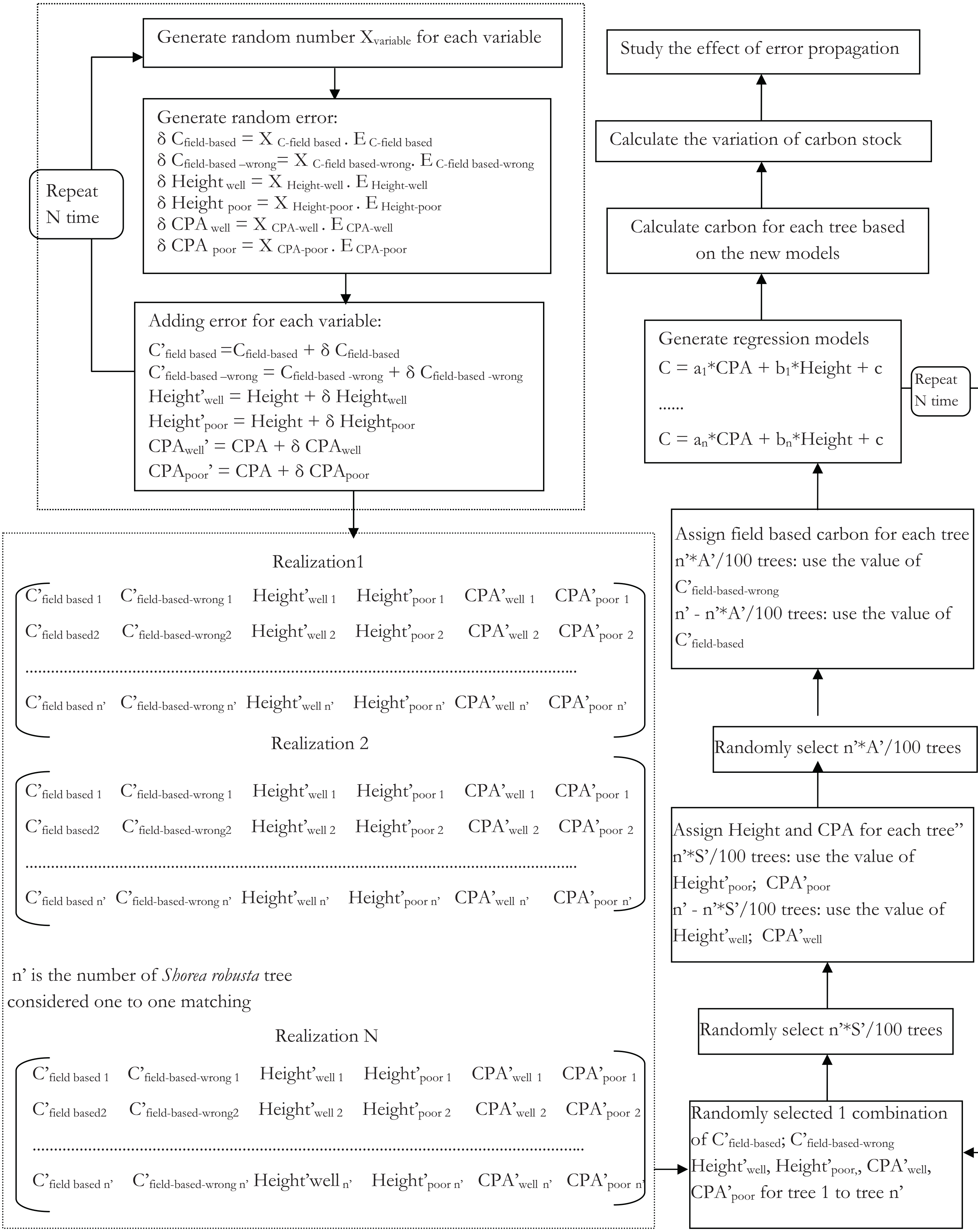

Figure 13: Outline of a Monte Carlo simulation process for each individual *Shorea robusta* tree

4.11.5. Monte Carlo Simulation implementation and validation

The input data was prepared in Excel Microsoft Office. The function NORMSINV(RAND()) was used to generate random number to generate random error for each parameter. Visual Basic Language is applied to generate N time of simulation and the results are stored in the Excel file type.

In practice, the Visual Basic method described above is rather cumbersome in its operation and the computation time is quite long for 1000 realizations. Therefore, a professional programmer rewrote the procedure in IDL programming language, which enables the routines to be significantly speeded up.

5. RESULTS

5.1. Descriptive statistics

In the field work, forest stand parameters data of 2935 trees were collected in 86 plots within five community forests in the Ludikhola watershed, Gorkha, Nepal. Out of these trees, about 265 trees were recorded as understory and lopped trees, 982 trees were detected on the image and 369 trees were digitized as a source of reference data. In total, 28 species were recorded, of which *Shorea robusta* is the dominant species (accounting for 75 % of total) and then followed by *Schima wallichi* (accounting for 13 %). The contribution of other species for example *Rhus wallichi*, *Castanopsis Indica, Terminalia alata* and *Pinus Roxbughii* are less than 3%. There are some species that can be rarely observed in the field, such as *Spondias pinnata* or *Phlogacanthus thyrsiflorus* (only one tree of each species was recorded).

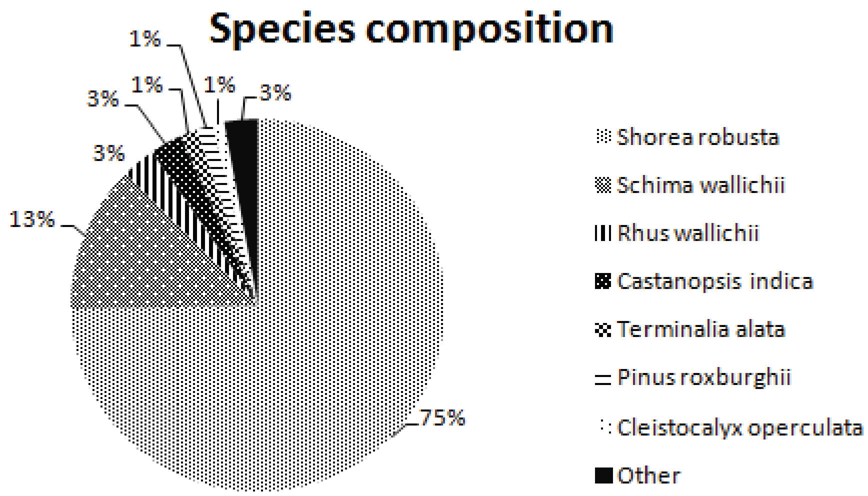

Figure 14: Species composition in the study area

The measured DBH and height of *Shorea robusta* , *Schima wallichi* and other species were analysed and presented in the following box-plots (Fingure 15).

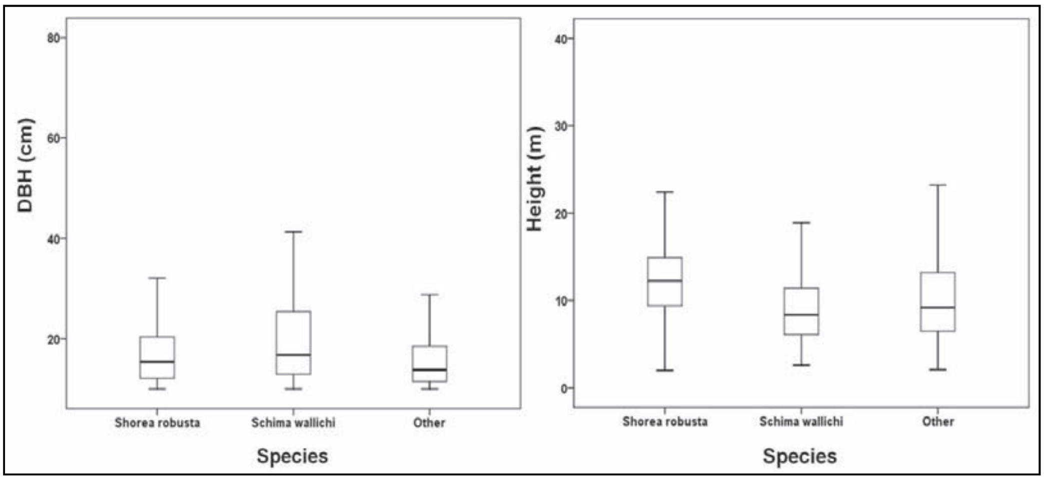

Figure 15: Box-plot of DBH and height of *Shorea robusta*, *Schima wallichi* and other species

The average DBH of *Schima wallichi and Shorea robusta* are more than that of other species. As for height, *Shorea robusta* is the tallest species and *Schima wallichi* has the average height lower than the average height of other species. From the field observation and recorded data, *Schima wallichi* is primarily under the crown of *Shorea robusta* and other species. Therefore, it is difficult to detect *Schima wallichi* on the image.

5.2. Canopy Heght Model

The canopy height model was created by subtracting DSM to DTM. The pixel value of CHM, which represents the height of cover vegetation, was filtered to the range of 0 to 40 (0-40m). The reason to select the range is that the maximum measured height is not in excess of 35 m.

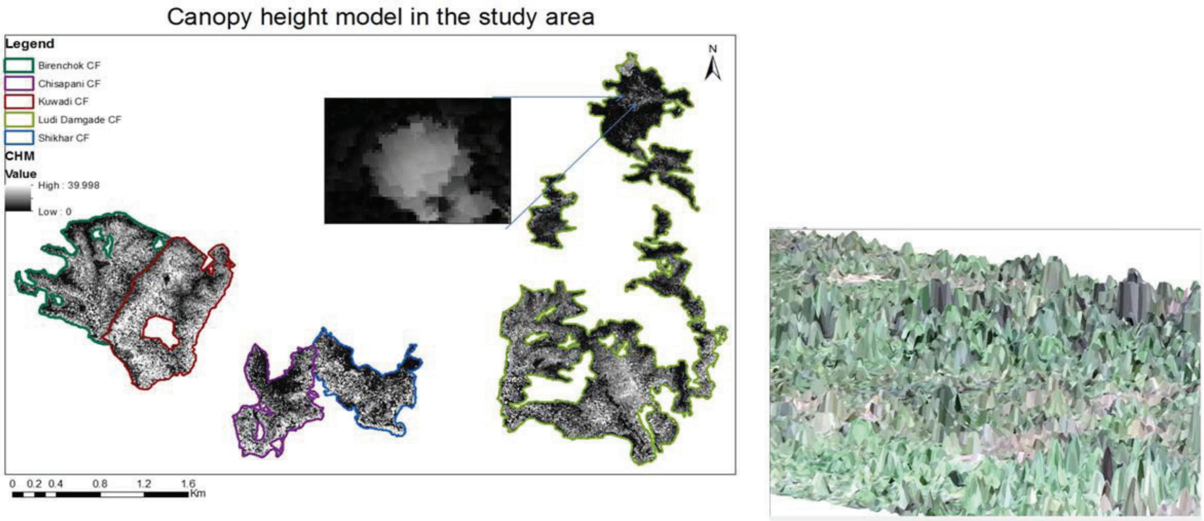

Figure 16: Canopy height model and 3D-view of canopy height model

5.3. Image- to- image coregistration

The root mean squared error (RMSE) obtained from the process of co-registering the Geo-Eye imagery with the ortho-rectified digital camera imagery was 0.39 m. The following image shows an example of the co-registration process.

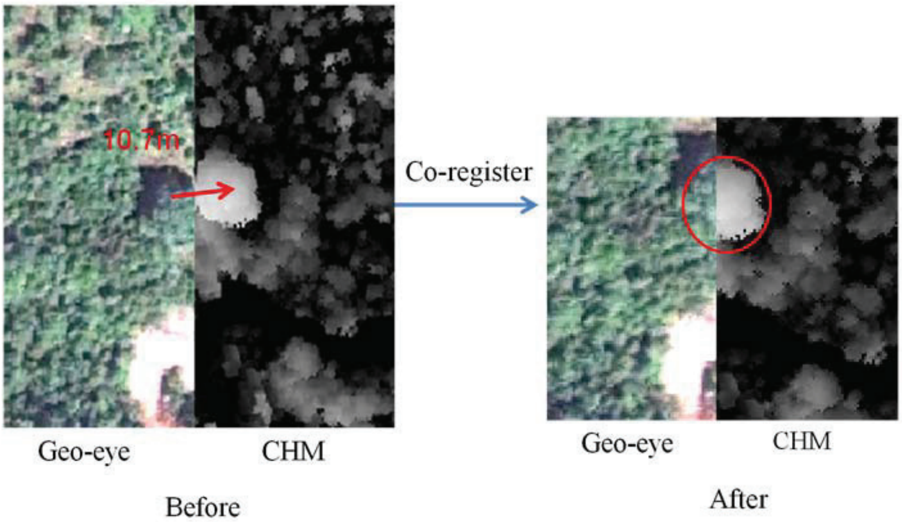

Figure 17: Co-registration result

5.4. Tree crown delineation

Individual tree crown was delineated using Region Growing approach, the result of image segmentation process is shown in figure 20:

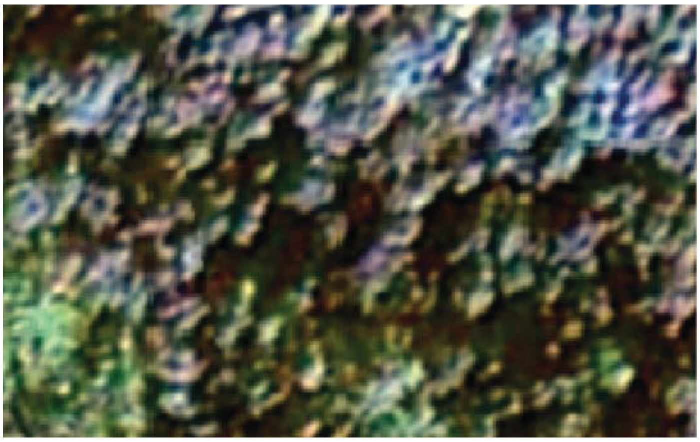

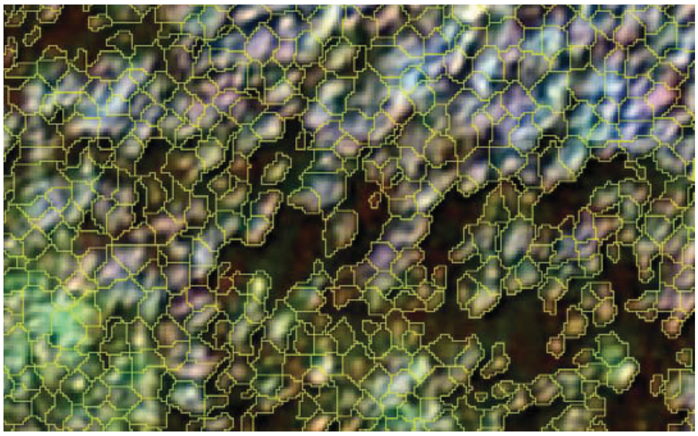

Figure 18: Image segmentation result

The total 369 trees were digitised as the reference to assess the accuracy of segmentation, classification result as well as the extracted height from the CHM. Accurate segments are the segments that have one to one matching with the corresponding reference crown. The one to one matching criteria were introduced in the Methodology chapter.

Out of 369 trees, there are 265 trees meet the one to one matching criteria. Thus, the segmentation accuracy in general is 71.9 % (28.1% error). It means 71.9 % of total reference crowns were matching to Region Growing crown delineation with 1:1: correspondence. The higher the percentage of 1:1 matching indicates higher accuracy.

In addition, the quality of segmentation outputs are defined in terms of under and over segmentation as well as goodness of fit (D). The goodness of fit (D) is the function of the degree of under and over segmentation. The obtained D value is 0.32. As the goodness of fit increases the degree of mismatch between the segmented and reference objects increases which indicates minimum accuracy. Over segmentation yields commission errors as one tree is segmented to more than one object for one reference tree. If there is no tree is identified for one reference tree exist, under segmentation or omission errors are made.

Table 9: The accuracy assessment result of segmentation

Class	**Under segmentatio n**	**Over segmentation**	**D**	**One to one matching crowns**	**Accuracy of segmentation S (%)**	**Error of segmentation S' (%)**
Shorea robusta	0.101	0.427	0.32	216/301	71,8%	28.2%
Other species	0.11	0.425	0.33	49/68	72,0%	28%
All trees	0.104	0.424	0.32	265/369	71.9%	28.1%

5.5. Canopy height model validation

Within each delineated crown, the maximum value derived from the CHM is assigned as the height of individual tree. The linear regression model was used to relate the LiDAR-derived heights with the field inventory data of the individual trees. The independent variable is LiDAR-derived height and dependent variable is the measured height. Of the 369 trees, one third was selected randomly to validate the LiDAR-derived height of individual tree. The obtained coefficient of determination is 0.72. The RMSE is 2.68 (m), RMSE in percentage is 17.9%.

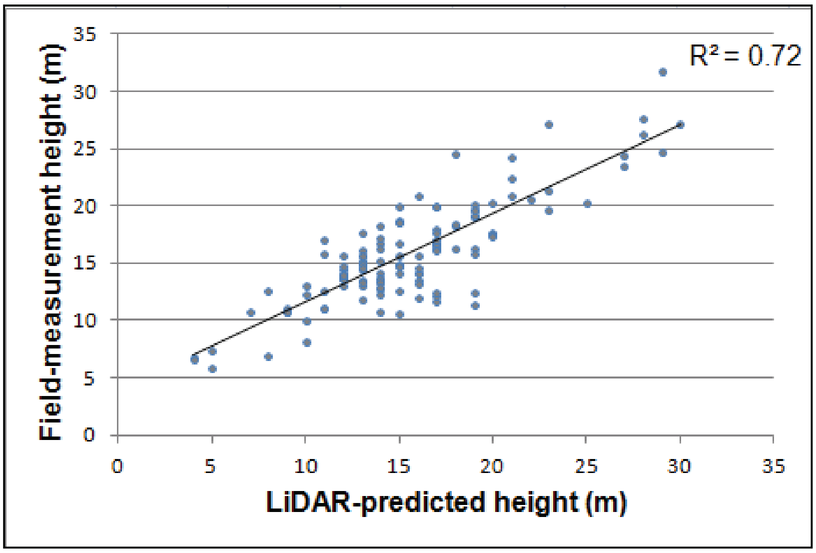

Figure 19: Predicted and field- measured height

5.6. Object-based image classification

The reference dataset of 369 trees was randomly divided into two parts, two third was used as training data, one third was used as validation data. The delineated crowns were used to classify into two classes: *Shorea robusta* and *Other species*.

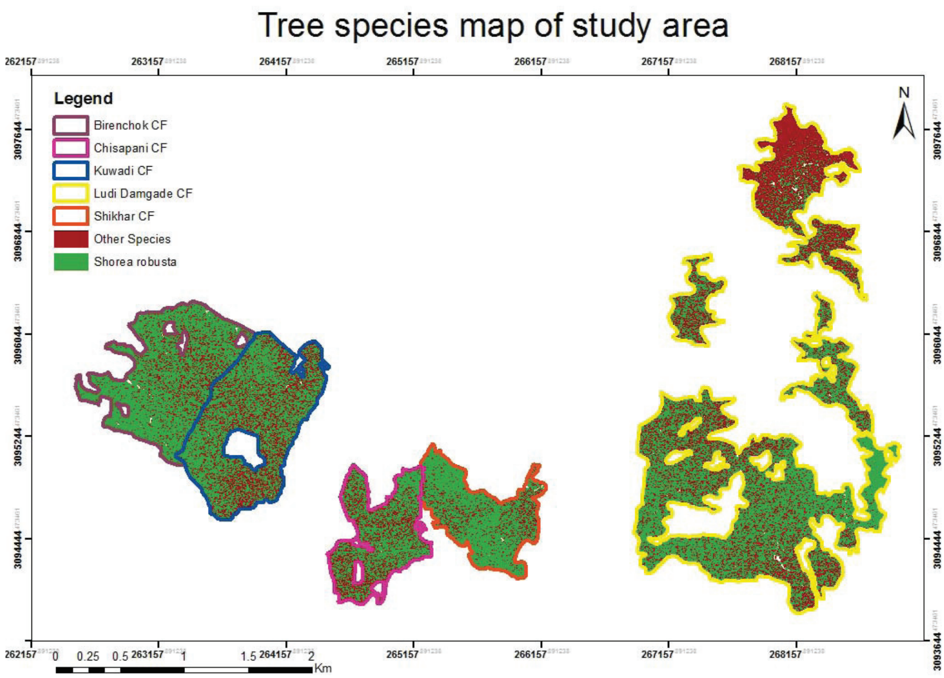

Figure 20: Map of tree species in the study area

The classification result was validated using 123 trees. Confusion matrix of errors and accuracies are shown in the following table:

Table 10: Confusion matrix of classification error

Class Name	**Reference Data**		**Classified totals**	**Error of commission (%)**	**User's accuracy (%)**
	Shorea robusta	Others			
Shorea robusta	78	3	81	3.7%	96.3%
Others	20	22	42	47.6%	52.4%
Totals	98	25	123		
Error of omission (%)	20.4%	12%			
Producer's accuracy (%)	79.6%	88%			
Overall Classification Accuracy = 81.30%					

Overall classification accuracy is 81.30% (19.7% error) and kappa is 0.4023. *Shorea robusta* was classified better compared to *Other species* with Producer's accuracy is 79.6% and Users accuracy is 96.3%.

5.7. Regression analysis

Out of a total of 369 trees, 73 *Shorea robusta* trees and 26 *Other species* trees was used for regression analysis. Firstly linear regression analysis was used to test whether CPA and LiDAR-derived height of individual crown could explain the amount of carbon stock of individual tree. The test was applied for the two classless: *Shorea robusta* and *Other species*. Analysing the result will help us to make sure that it makes sense to include both independent variables (CPA and Height) in multiple regression models.

Table 11: The relationship between CPA and Height with the carbon stock of *Shorea robusta*

Shorea robusta		
Regression Statistic	**CPA (segment)**	**Height (LiDAR)**
Multiple R	0.782579	0.820546
R Square	0.612429	0.673296
Adjusted R Square	0.606971	0.668695
Standard error	37.2344	34.18581
Observations	73	73
Coefficient		
Intercept	-115.411	-99.5807
Slope	11.18141	10.93337
P-value		
Intercept	4.29E-08	8.35E-09
Slope	2.91E-16	6.46E-19
One Way ANOVA test		
F	112.1924	146.3223
F significant	2.91E-16	6.46E-19

Table 12: The relationship between CPA and Height with the carbon stock of *Other species*

Other Species		
Regression Statistic	**CPA (segment)**	**Height (LiDAR)**
Multiple R	0.763434	0.731133
R Square	0.582832	0.534555
Adjusted R Square	0.567381	0.517316
Standard error	29.59039	31.2557
Observations	29	29
Coefficient		
Intercept	218.5738	8.381427
Slope	-5.90025	6.284426
P-value		
Intercept	8.72E-12	0.65129
Slope	1.46E-06	6.64E-06
One Way ANOVA test		
F	37.72208	31.009
F significant	1.46E-06	6.64E-06

It can be seen from the above two tables that, both CPA and height have a significant relationship with the amount of carbon of each individual tree. Therefore, it is significant to involve both CPA and height in the multiple regression analysis to estimate carbon. In the multiple regression model, the independent variables are CPA and height and the dependent variable is carbon. The carbon model was built for species class.

Table 13: Multiple regression analysis for *Shorea robusta* and *Other species*

Shorea robusta		***Other Species***	
Regression Statistic		**Regression Statistic**	
Multiple R	0.872763	Multiple R	0.82393
R Square	0.761716	R Square	0.678861
Adjusted R Square	0.754908	Adjusted R Square	0.654158
Standard error	29.40335	Standard error	26.45676
Observations	73	Observations	29
Coefficient		Coefficient	
Intercept	-139.75	Intercept	125.3983
Slope CPA	5.886757	Slope CPA	-3.85821
Slope Height	7.133373	Slope Height	3.500388
P-value		P-value	
Intercept	1.49E-13	Intercept	0.002566
Slope CPA	2.82E-06	Slope CPA	0.002087
Slope Height	6.05E-09	Slope Height	0.009776
One Way ANOVA test		One Way ANOVA test	
F	111.8833	F	27.48093
F significant	1.58E-22	F significant	3.86E-07

It is also needed to test the correlation of CPA and height to ensure that there are no relationship between CPA and height of the tree. The correlation between CPA and Height is calculated bases on the variance inflation factors (VIF):

$$VIF=1/(1-R^2)$$

Where R square is the coefficient of determination obtained from regression analysis of CPA and height. The rule is VIF >10 indicate that multi-collinearity may influence linear regression analysis. For *Shorea robusta* and *Other species*, the value of VIF is 4.1 and 3.0 respectively. Therefore, we can conclude that there is no relationship between CPA and tree height. The One way Analysis of Variance (ANOVA) test indicates the significant of the model. From the table 13, it can be clearly seen that explanation of carbon stock by segmented CPA and LiDAR derived height was statistically significant at 95% confidence level.

Model validation

A linear regression model was applied to validate the developed carbon predictive model above. Measured and predicted carbon stocks were plotted against each other and the regression co-efficient was calculated. The coefficient of regression for *Shorea robusta* is 0.68 and for *Other species* is 0.62. The RMSE is equal to 36% for *Shorea robusta* and 23.8% for *Other species*.

a. *Shorea robusta* b. *Other species*

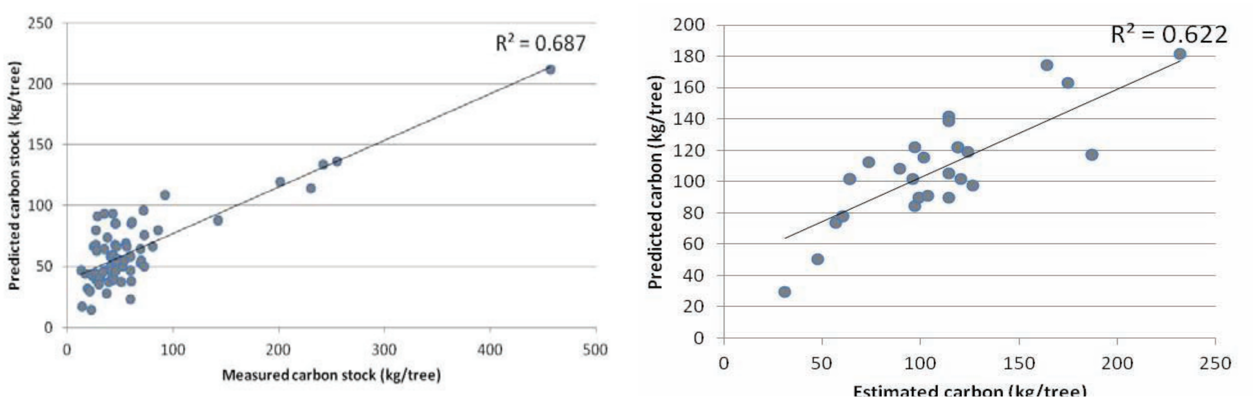

Figure 21: Scatter plot of measured carbon stock and predicted carbon stock

5.8. Monte Carlo Simulation implementation

5.8.1. Error estimated based on the error sources

The Monte Carlo Simulation process was applied separately for both classes *Shorea robusta* and *Other species*. The input table contains the number of tree used for *regression predictive model of carbon*. In order to operate the simulation process, the error of each parameter was estimated. The following table shows the range of error as the input for Monte Carlo Simulation:

Table 14: The magnitude of various errors used for Monte Carlo Simulation

Estimated error	**Value**	
	Shorea robusta	***Other species***
$E_{\text{C-field based}}$	2.1 (kg)	4.5 (kg)
$E_{\text{C-field based wrong}}$	4.3 (kg)	2.6 (kg)
$E_{\text{Height-well}}$	2.6 (m)	5.2 (m)
$E_{\text{Height-poor}}$	4.4 (m)	6.1 (m)
$E_{\text{CPA-well}}$	6.5 (m^2)	6.8 (m^2)
$E_{\text{CPA-poor}}$	12 (m^2)	11.6 (m^2)
	Other errors	
	Shorea robusta	***Other species***
Segmentation error	28.3%	28%
Image classification error	3.7%	47.6%
Standard error of allometric equation	0.95 (kg)	3.35(kg)

5.8.2. Output of Monte Carlo Simulation

The Monte Carlo Simulation process is aimed at generating different sets of input data by adding random error for each parameter. Each realization created one *regression predictive model of carbon*. After N realizations, N set of coefficient and intercept was obtained. From that, the carbon stock of the individual tree as well as the carbon stock of study area can be calculated and compared with the calculated value without error.

	A	B	C	D	E
1	No	Intercept	CPA' (Slope CPA)	Height' (Slope height)	
2	1	-100.59	2.04239	8.64721	
3	2	-102.109	2.07326	8.88042	
4	3	-104.518	1.72119	9.47454	
5	4	-83.417	2.21316	8.09666	
6	5	-94.3094	2.13456	8.39344	
7	6	-107.12	1.52386	9.60706	
8	7	-96.845	1.7907	8.8655	
9	8	-80.4461	2.91214	6.59391	
10	9	-87.2038	2.41918	7.72623	

Figure 22: An example of the output of Monte Carlo Simulation

5.8.3. Analysis result of Monte Carlo Simulation

Monte Carlo studies result in a large amount of data to be analysed (Hutchinson *et al.*, 1997). For this reason, two analyse approached were selected to analyse the results of Monte Carlo simulation process.

The variation of predicted carbon stock in the study area

From the set of simulated regression model (1000 model), 50 models were randomly selected for each class. Afterward, these models were used to calculate carbon stock for the total study area. The figure 23 shows the result of 50 simulation of carbon stock in the study area. The straight line shows the estimated carbon stock using the carbon predictive model without error propagation simulation. The zigzag line shows a distribution of possible values for carbon stock in the study area. The value of carbon stock in study area varies between 35ton/ha and 42.5 ton/ha.

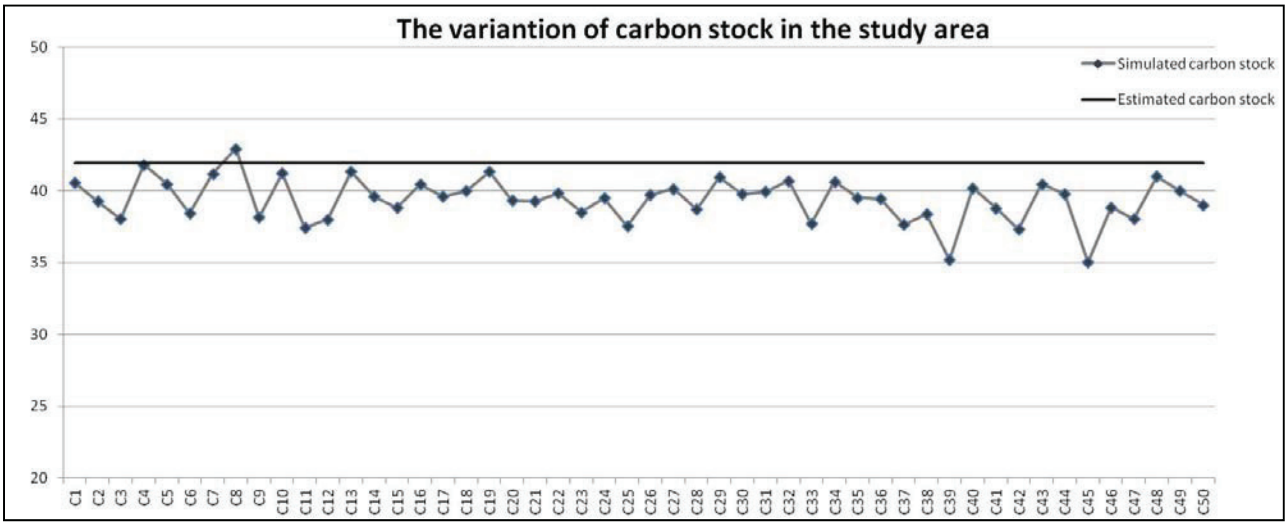

Figure 23: The variation of carbon stock in the study area

The variation of predicted carbon stock of individual tree

The variation of predicted carbon stock of individual tree can be extracted from the simulation results. The figure (24) and (25) are two example of the extracted information about predicted carbon stock variation. In almost all cases, the amount of carbon stock varies in the range 1 to 10 kg of carbon of individual tree. There are some extreme cases, in which, the variation of carbon stock is around 20 kg for small tree (DBH<20), and around 30 kg for bigger tree (DBH>20). These cases are corresponding to the scenario that the tree is wrongly classified.

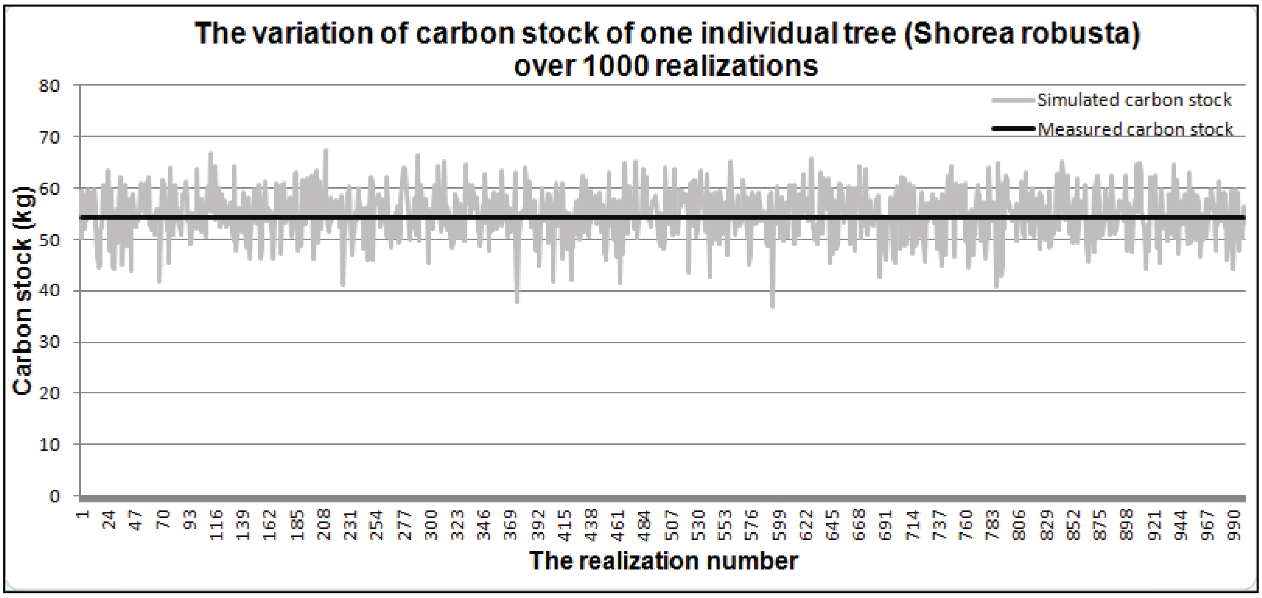

Figure 24: The variation of carbon stock of individual tree (*Shorea robusta*)

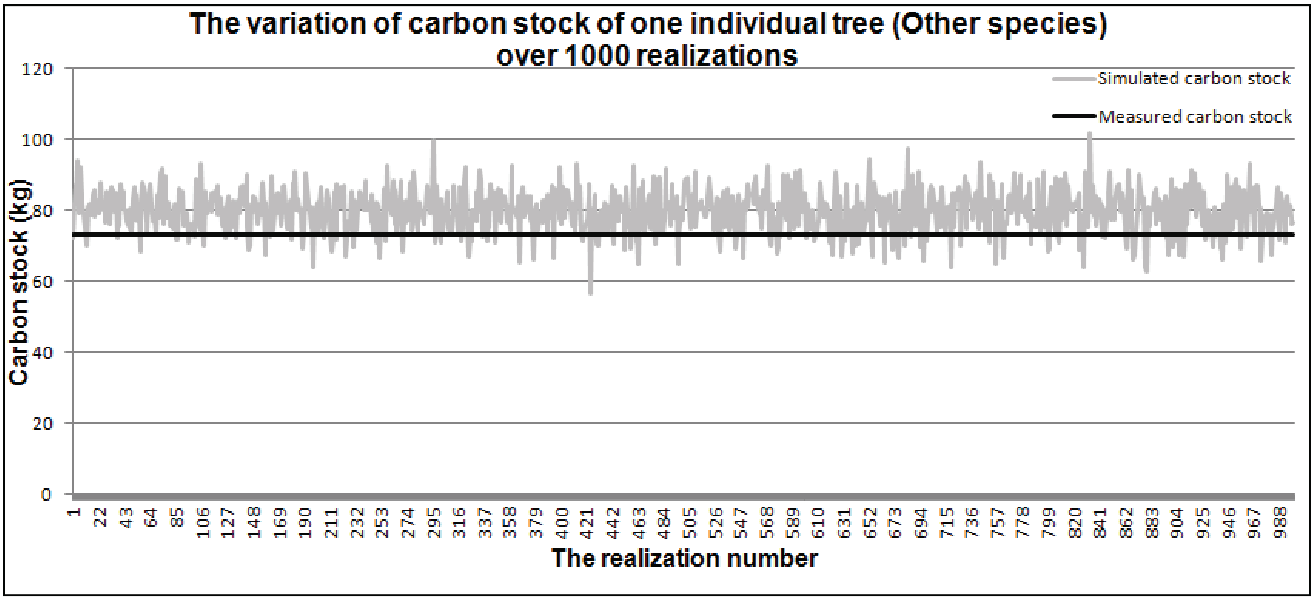

Figure 25: The variation of carbon stock of individual tree (*Other species*)

Monte Carlo Simulation validation

The results which are obtained from IDL programming language program were found to be similar to those from the Visual Basic program. The following figures show the comparable results from Visual Basic program IDL program.

a. Output of Visual Basic program (*Shores robusta*)

	A	B	C	D	E
1	No	Intercept	CPA' (Slope CPA)	Height' (Slope height)	
2	1	-100.59	2.04239	8.64721	
3	2	-102.109	2.07326	8.88042	
4	3	-104.518	1.72119	9.47454	
5	4	-83.417	2.21316	8.09666	
6	5	-94.3094	2.13456	8.39344	
7	6	-107.12	1.52386	9.60706	
8	7	-96.845	1.7907	8.8655	
9	8	-80.4461	2.91214	6.59391	
10	9	-87.2038	2.41918	7.72623	

b. Output of IDL program (*Shores robusta*)

	A	B	C	D
1	iter	c (intercept)	a (slope CPA)	b (Slope height)
2	1	-96.7284	1.50214	9.17318
3	2	-94.7018	3.32943	7.20121
4	3	-86.9876	2.3287	7.94018
5	4	-70.807	0.965949	8.27608
6	5	-100.351	2.61001	8.06492
7	6	-84.8132	1.53822	8.49573
8	7	-94.4579	2.935	7.47467
9	8	-92.3595	2.17242	8.20431
10	9	-94.0127	1.45823	9.0146

c. Output of Visual Basic program (*Other species*)

	A	B	C	D
1	No	Intercept	CPA' (Slope CPA)	Height' (Slope height)
2	1	81.74284602	-1.143685049	1.828171237
3	2	108.1824316	-1.482080624	0.406121388
4	3	81.13548535	-1.517092054	2.444317865
5	4	122.1150059	-2.443884885	1.211155189
6	5	60.84507379	-0.601465667	2.579485089
7	6	121.1788293	-2.162125243	0.711303909
8	7	81.67144761	-0.672956051	1.236723558
9	8	96.03234705	-1.806106976	1.499877305
10	9	57.71649917	-1.299935779	3.936479648
11	10	64.48561209	-1.074975787	2.609910556
12	11	35.82161312	-0.468202102	3.837296126
13	12	76.23270943	-1.504089829	2.751155467
14	13	70.03370279	-1.303610324	3.009027298
15	14	63.47073858	0.047699945	1.598450915
16	15	73.26055346	-0.86534895	1.855491096

d. Output of IDL program (*Other species*)

	A	B	C	D
1	iter	c (intercept)	a (slope CPA)	b (Slope height)
2	1	102.983	-2.26455	2.8351
3	2	86.9167	-2.06728	3.96884
4	3	102.077	-1.85922	2.87534
5	4	74.0827	-1.39821	3.42525
6	5	79.064	-1.70821	3.88462
7	6	68.9673	-1.80646	4.37277
8	7	104.563	-2.64037	3.47876
9	8	89.4177	-2.24026	3.77689
10	9	121.457	-2.36482	2.44456
11	10	104.307	-2.34782	3.21494
12	11	91.794	-1.97596	3.21494
13	12	104.224	-2.74149	3.51033
14	13	97.6442	-2.42419	3.38651
15	14	60.6598	-0.777999	3.95008
16	15	110.971	-2.40621	3.33119

Figure 26: Outputs of Visual Basic and IDL programs

From the results of Monte Carlo simulation obtained after using IDL program, the mean of simulated carbon stock from 100 realizations were calculated for one individual tree. This mean value was compared with the mean of simulated carbon stock from 100 realizations for the corresponding tree using the results obtained from Visual Basic model. The comparison was executed for both *Shorea robusta* and *Other species*. The results show the comparable resultsfrom Visual Basic program IDL program.

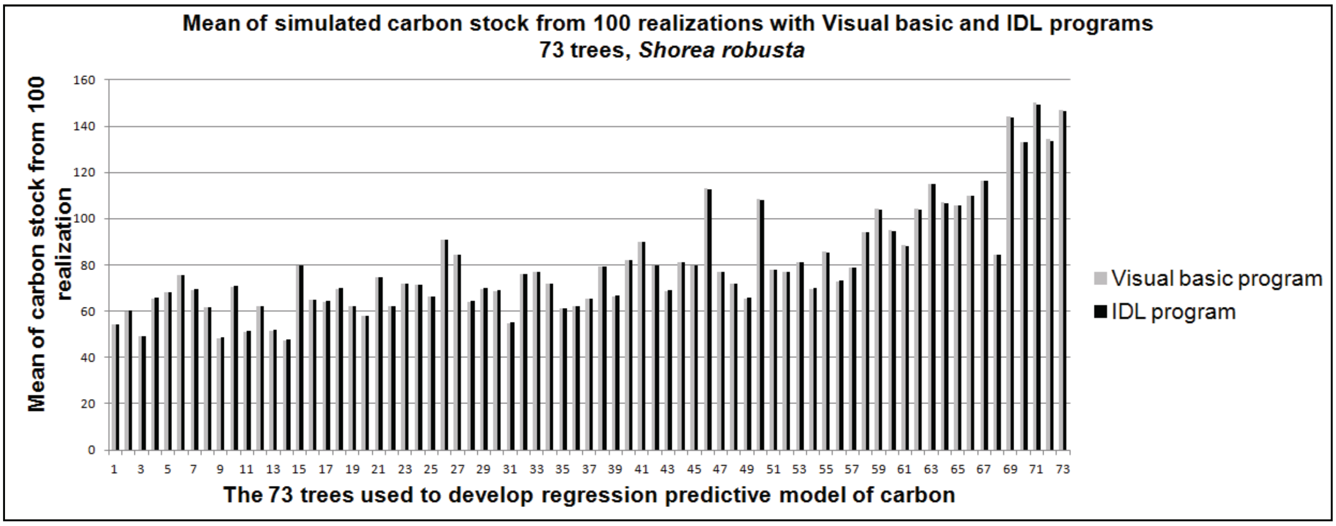

Figure 27: Validation of simulated carbon stock of 73 individual *Shorea robusta* - trees using the result of Visual basic and IDL program

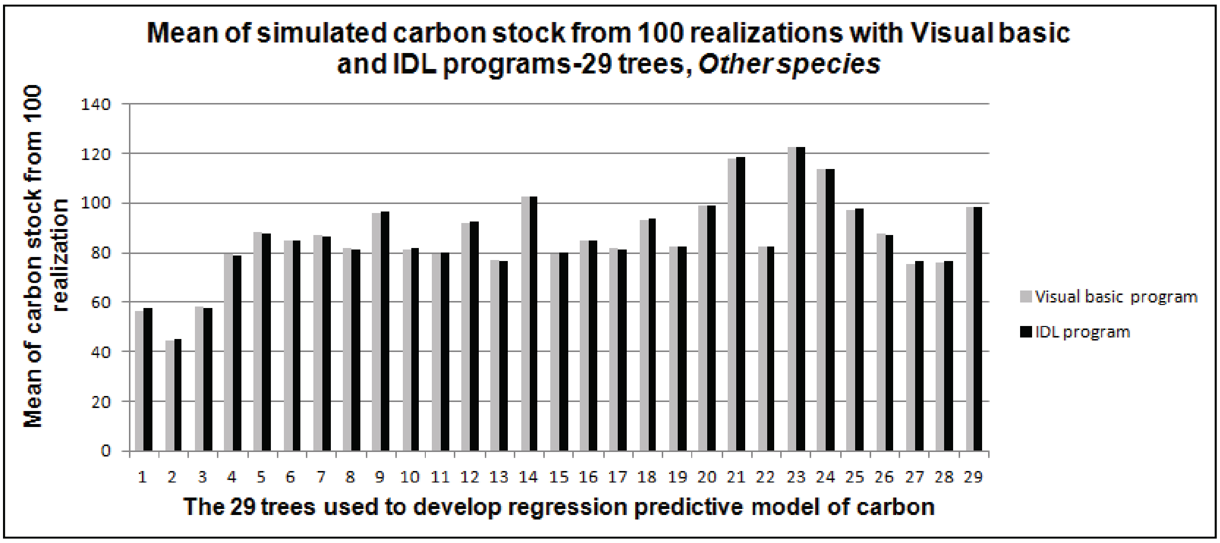

Figure 28: Validation of simulated carbon stock of 29 individual *Other species* -trees using the result of Visual basic and IDL program

6. DISCUSSION

6.1. Field based carbon estimation

The error of field-based carbon estimation for individual tree is primarily related to the allometric equation and the field measurement of DBH. In this research, the standard error of the allometric equation is considered in the error propagation process. However, the uncertainty of allometric equation selection could not be explored because the tree in study area does not have its own allometric equation. The allometric equation was selected based on the rainfall and the temperature of study area only whereas other information of tree age, soil type and stand structure also needed to be considered.

The error of DBH measurement propagates to carbon estimation through the allometric equation. Several researches have noticed the contribution of DBH measurement error in final biomass estimation. Chave *et al* (2004) demonstrated that the error of DBH measurement proportionally relates to the magnitude of DBH, for example, the tree with 30 cm DBH has a typical error of 0.27 cm. However, in the research of Chave *et al* (2004), the mean error of DBH measurement is not mentioned. Gonzalez *et al* (2010) assessed the DBH measurement error by repeated measures of a random sample of 169 trees (19cm<dbh<148cm) and determined the error of DBH measurement is 0.027. This 0.027 cm error of DBH measurement was used in our research.

In our research, the error of field based carbon estimation may cause 2.1 and 4.5 kg error in carbon estimation for *Shorea robusta* and *Other species*, respectively. In the research of Chave *et al* (2004), the error of AGB due to the error of DBH measurement error was found to be in the range between 0.235 to 0.547 kg in AGB estimation (or 0.03 to 0.25kg C). Chave *et al* (2004) also studied the effect of allometric equation selection separately and cited that an error of greater 20% on the AGB estimate due to the choice of allometric equation.

6.2. Tree crown delineation

The accuracy assessment of individual tree crown delineation was obtained by one to one matching of manually digitized reference polygons to automatic segments. One to one matching of the segements resulted in 71.9%. The uncertainties of tree crown delineation may due to the algorithm used to delineate the tree crown as well as the image quality.

The Region growing algorithm for individual tree delineation releases the satisfactory results in previous study (Broadbent *et al.*, 2008; Darius *et al.*, 2002). The accuracy of segmentation achieved in this study is almost exactly similar to the results of research of Bunting *et al* (2006) who obtained 72% well isolated trees. Tiede *et al.* also reported 72% accuracy of crown delineation of the tree in forest area Germany. Ke *et al.* (2011) obtained the accuracy of 70% while using region growing to delineate the tree crown for Norway spruce trees.

However, in dense forest area, the neighbouring trees might have shade and obscure the edges of their neighbours which results in darker image values at tree boundaries and leads to the identification of false seeds (local minima and local maxima) (Li *et al.*, 1992). The over-segmentation produced multiple segments overlapping with a single reference object. On the other hand, under-segmentation may produce larger segments which contain the reference (Ke et al., 2010). In our study, the number of tree over segmentation was found more than the tree under segmentation. Among the reference crowns, *Shorea robusta* has 81 over-segmented crowns and only 4 under- segmented crowns; *Other species* class poses 16 over segmented crowns and 3 under segmented crowns. The reason for these uncertainties may also be explained by the complex forest structure in the study area. We have observed the overlapping and intermingling situation in almost sampling plot.

The shadow is also the main factor causing uncertainties in crown delineation (Martinez Morales *et al.*, 2008). The shadow in the image is due to the affect of view angle, topography and sun elevation. The image for this study was acquired around 10a.m with view area within $\pm 22^0$ off-nadir with sun angle 45^0. The view of $\pm 22^0$ off-nadir may result in casting high shadows because the trees trend to lean away from the nadir. In addition, the study area is on the mountainous terrain, therefore, topographic distortions is observed negatively affect the image quality by causing more shadow effect. The poor spectral separability between different species is also one of reasons causing poor delineated crown. Additionally, there are a number of trees cannot delineated because of the weak signal.

The tree crown delineation accuracy indirectly affects the LiDAR derived height and classification accuracy. Ke *et al.* (2010) highlighted that better segmentation lead to higher classification accuracy. In addition, poor delineated crowns pose challenges when relating image-based crown delineation results to field measurement (Pouliot *et al.*, 2002).

6.3. LiDAR derived height

Each crown delineated from the Geo-Eye imagery is considered an individual tree. The height of one individual tree is the maximum pixel value of CHM which is inside the boundary of the tree crown. In general, the height derived from LiDAR data (point density of $0.8/m^2$) fitted quite well with the measured height from the field with the R^2 of 0.72. Compared to the research of Leckie *et al* (2003) in coniferous forest, the R^2 when fitting measured height and predicted height yields 0.84 with the LiDAR point density of $2/m^2$ for . With the same point density ($2/m^2$), St-Onge (2000) archived the R^2 of 0.90 for coniferous forest. Reitberger *et al* (2007) results indicate that the detection rate for coniferous trees is 61 % and for deciduous trees 44 %, respectively 7 % of the detected trees are false positives. There are a limited number of researches on the LiDAR derived height in the deciduous forest and tropical forest (Asner *et al.*, 2011). Drake *et al.*(2002) examined the relationship between corresponding LiDAR and field profile metrics and achieved R^2 of generally 0.83.

There are many reasons causing the error of LiDAR derived height. Firstly, the LiDAR point does not hit the top of the tree (St-Onge *et al.*, 2001), especially in dense forest like the study area, and leads to the inaccurate predicted height. In addition, the extracted tree height in this study also depends on the delineated crown from Geo-Eye imagery. If the crown is poor delineated, the top of tree A may be placed in the crown of tree B. The residual of DTM and DSM interpolation process is also one source of errors.

6.4. Error of CPA and height from well-delineted and poor-delineated segments

In our study, the crown delineation accuracy is the factor that mostly affects the accuracy of carbon estimation. The reason is that inaccurate delineated crown leads to the error of CPA and extracted height which are the independent variable in the carbon predictive model. The error magnitude of extracted CPA and height from poor delineated crowns is obviously larger than the error magnitude of well-delineated tree crowns. With the aim at uncertainty analysis, the delineated crown is necessary to separate in two sets, one is well-delineated and one is poor-delineated.

Lim *et al* (2003) highlighted that the CHM is generally underestimate the measure height, the height was underestimated by 2.1-3.7m. Næsset (1997) also found that the mean of the LiDAR canopy heights within each stand underestimated ground-based estimates by 4.1–5.5 m. In our study, the error of LiDAR-extracted height is mainly due to the under-estimation. The error of LiDAR-derived height of well delineated crowns (2.6 m for *Shorea robusta* and 5.2 m for *Other species*) is less than the error of poor delineated crowns (4.4 m for *Shorea robusta* and 6.1 for *Other species*). Leckie *et al* (2003) also indicated that the poor delineated crown produced poor height estimate. In his research, Leckie *et al* (2003) found the error of height estimate from poor isolated crown ranging from 3.5 to 10 m mean while the height estimate error of good match tree is within 0.6 to 2.0 m.

Song *et al.*(2010) started that the error from delineation of trees crown can affect the result of modelling DBH based on CPA. The error of CPA of well-delineated tree crown is 6.5 m^2 and 6.8 m^2 for *Shorea* *robusta* and *Other species*, respectively. Meanwhile, the error of CPA of poor-delineated tree crown is almost double 12 m^2 and 11.6 m^2 for *Shorea robusta* and *Other species*, respectively.

6.5. Object based image classification

The classification accuracy achieved in this study gives reasonable results, with a classification accuracy of 80 %. This result is comparable to the classification accuracy of 77 % obtain from the research of Erickson (2004) with less than 10 cm spatial resolution images. The user's accuracy obtained in this study for *Shorea robusta* was relatively high (96.3%) and the user's accuracy for *Other species* is rather low (only 52.4%). The overall Kappa is 0.53. We can consider this is a good result while comparing to the Kappa statistic range define by Landis, *et al.* (1977). Landis, *et al.* (1977) defined the agreement criteria for Kappa statistic as poor when $K<0.4$, good when $0.4 <K<0.7$ and excellent when $K>0.75$.

The reason for the high user's accuracy of *Shorea robusta* is that approximately 75% of the trees recognized in the field were *Shorea robusta*. In addition, in the *Other species* class, different species with variation in spectral characteristics had to be grouped together to form a single class which introduced confusion in the spectral response from this class. According to the field observation, *Other species* are all most understory trees (under the crown of *Shorea robusta*) therefore it leads to the difficulty of detecting them in the image. With the same trend, Voss *et al* (2008) using nearest neighbour classification acquired 57% accuracy while classifying the tree species and revealed the low accuracy is due to less number of samples given to the classifier. *Clark et al.* (2011) estimated the tropical forests plot-level mean height.

6.6. Model Development

Multiple regression analysis was used to develop the relationship between CPA, height and carbon stock of the individual tree. The regression analysis shows that tree height of *Shorea robusta* has stronger relationship with the carbon stock (R^2=0.67) compare to CPA. Meanwhile, for other species, the opposite is the case, the CPA (and not the height) of *Other species* is more strongly link to carbon stock.

The coefficient of determination obtained for *Shorea robusta* was 0.76 and 0.67 for *Other species*. The reason why *Other species* has lower coefficient of determination is that many different species are used the same allometric equation for this class. Different species each have their own characteristics, for example, *Schima wallichhii* is short but the crown is large mean- while *Castanopsis indica* is tall but the crown is medium in size.

Both CPA and height can be include in the multiple regression model because, CPA and height is tested and has no relationship. The reason is that the leaves of *Shorea robusta* are always collected to make traditional bow by the local people, there for many tree has the deformed crown.

6.7. Biomass and Carbon stock estimation

The results of this research show that the carbon stock of the study area was approximately 41 Mg Cha^{-1}. This result is comparable to the carbon stock estimated with the range of 34.30 – 97.86 $MgCha^{-1}$ in Nepal forest of Baral *et al.* (2009). Rachna (2011) also chose Ludhikhola watershed as the study area. However the research of Rachna (2011) focused on the carbon estimation Ludi damgade community, one of five community forests in our research, with the carbon estimate of $31MgCha^{-1}$.

6.8. Model development and Monte Carlo Simulation

The Monte Carlo Simulation was generated in order to assess the variation of carbon stock estimation when the whole source of uncertainty involves in the carbon estimation process. From the Monte Carlo simulation result, the error of different error source may cause the variation of carbon estimates in the study area varies between 1 and 7 Mg Cha-1. This result is comparable to the research of Chave *et al* (2004), who found that the error of carbon estimation may vary from 4.2 to 50 Mg Cha-1 based on the different sources of error. Samalca (2007) explored the integration of error in biomass estimate in Indonesia and indicated that the variation of biomass estimate is in between ± 29.7 Mg Cha^{-1} (equal to 13.95 Mg Cha^{-1} carbon).

In general, the bias of estimated carbon stock for individual tree may vary in the range of 0 to 20kg. The largest error occurred for carbon estimate for individual tree when the tree is wrongly classified. The medium error occurred for carbon estimate for individual tree when the tree is poor delineated. The error of field based carbon contributes least to the error of carbon stock estimate.

6.9. Limitations of the research

The limitations of the research are:

- Low density LiDAR data may lead to the lack of height information in some places where the LiDAR points are missing.
- No ground truth data with points of known elevation were collected to estimate the accuracy of DEM itself. The accuracy of DEM is therefore in the accuracy of estimating tree heights.
- The dissimilarities between LiDAR data and Geo-Eye imagery cause random error of co-registration. Although the co-registration was applied, there are still several places where the crown in Geo-Eye imagery does not match with the CHM.
- The affect of shadow and distortion in Geo-Eye imagery leads to the inaccuracy of CPA and LiDAR derived height.
- The eCognition software only allows delineation process on a small area (<250ha). Therefore it causes the difficulties to apply the developed crown delineation method in the large area.
- In the error propagation process, the error from the sampling design method and the allometric equation selection are not considered.
- The height measured in the field is considered the truth to estimate the range of predicted height. However, this measurement itself contains the error which is not considered in this study.
- Identifying the tree in the field is a key step in the carbon estimation for an individual tree. Due to the error of GPS and the personal ability of tree recognition, the tree may also be wrongly linked with the crown in the image. However, it is hard to assess this uncertainty.
- The Monte Carlo Simulation developed in this study can be applied for related researches; however, it is needed to re-analysed the sources of error as well as the magnitude of error as the input for the process.
- Like any methodology, Monte Carlo studies are not without disadvantages; their usefulness depends in large part on the realism of the conditions that are modeled. An inappropriate choice of model conditions will result in a lack of external validity for the study. In addition, Monte Carlo simulation is computationally intensive and not amenable to detailed analysis of error structure.

7. CONCLUSION AND RECOMMENDATIONS

The main objective of this study is to assess error propagation in carbon estimation using the combination of LiDAR data and VHR Geo-Eye imagery in five community forests of Ludhikhola watershed, Gorkha, Nepal. With respect to this, the following conclusions are drawn for each sub-objective.

7.1. Conclusions

Related to the sub-objective 1, **"Develop a predictive model of carbon using tree height derived from airborne LiDAR data and crown projection area (CPA) derived from high resolution satellite imagery"**

For each class (*Shorea robusta* and *Other species*), linear regression analysis was used to relate carbon stock of individual tree with CPA and height, one after other. The results of linear analysis show that, both CPA and height have relatively good relationships with the carbon stock of individual tree. Therefore, the multiple regression analysis was applied to use both CPA and height to explain carbon stock. The developed model then was called the *regression predictive model of carbon*. The multiple coefficient of regression obtained from regression predictive model of carbon for *Shorea robusta* is higher than the one of *Other species*, R^2= 0.76 and 0.68 respectively.

Related to research sub-objective 2, **"Analyse the sources of error causing the uncertainties in the carbon estimation process and assess the accuracy of each parameter, which takes part in the predictive model of carbon"**

The error in our study come from (i) field measurement of DBH, (ii) selection of the allometric equation, (iii) co-registration CHM and Geo-Eye imagery, (iv) CHM processing, (v) crown delineation processing; (vi) wrong link between measured tree and delineated crown and (vii) image classification. The first five sources lead to the error of field-based carbon stock (obtained from the allometric equation on DBH), the extracted CPA and derived height of individual trees. The magnitudes of error of these three parameters were shown in table 14. In addition, it can be seen that well delineated tree suffer from less error than poor delineated trees. Hence, the reference trees were divided into two sets to estimate the error magnitude for CPA, height and field based carbon. The segmentation accuracy is 72.9%. It means there is 28% of chance that a tree will be poor delineated, ultimately leading to a wrong link between measured tree and delineated crown. As for the contribution of object-based image classification error, the wrongly classified tree will use the wrong allometric equation to calculate field-based carbon. For example, if the *Shorea robusta* tree was classified as *Other species*, this tree will use allomtric equation of Other species to calculate field based carbon. The accuracy of image classification is 80% overall, with the error of 4% and 47.6% for *Shore robusta* and *Other species*, respectively.

Related to research sub-objective 3, **"Develop a method for assessing the propagation of error in carbon estimation"**

In general, the set of reference trees is randomly divided in two parts, one for model development and one for validation. This random selection will cause the error in carbon predictive model, and ultimately carbon estimation. Monte Carlo Simulation is applied for the one-to-one matching and truly classified trees which are considered to have less error. The main idea of simulation is generating different input by randomly adding error to the variables used for regression analysis, both independent variables (CPA, height) and the dependent variable (carbon – C) to see the variation in the output. The output of iteration can be link with simulated input in order to analyses the contribution of different error source.

Related to research sub-objective 4, **"Estimate the carbon stock in the study area and analyse the impact of error propagation in this carbon stock estimation"**

The carbon estimation from the developed model with the tree without error released 41 Mg Cha^{-1}. When the error is propagated, by mean of Monte Carlo simulation, we found that the error of carbon estimation can range from this value can range from ±1 and ±7 Mg Cha^{-1}.
This research indicated the utility of the combination of LiDAR data and VHR Geo-Eye imagery for forest carbon estimation accompanied with error propagation analyses. Monte Carlo simulation provides a robust method to assess the uncertainties due to error propagation. This method is purely based on statistical analysis and the complicated relationships between variable are not required to be defined.

7.2. Recommendations

- The combination of LiDAR data and VHR Geo-Eye imagery provides a good source of information which can be used for forest carbon stock estimation
- In order to increase the accuracy carbon estimation using the combination of LiDAR data and VHR Geo-Eye imagery, the foreseen uncertainties should be reduced by: (i) developing local level allometric equations for Nepal for better carbon stock estimation, (ii) finding a method to better integrate the CHM and Geo-Eye imagery in tree crown delineation process.
- Due to the limitation of time, this study only uses Monte Carlo Simulation to analyse the uncertainties of one input data set and one method. However, the research suggests that Monte Carlo Simulation can be used to compare the results of different methods and different datasets for carbon estimation.

LIST OF REFERENCES

Anderson, J. E., Plourde, L. C., Martin, M. E., Braswell, B. H., Smith, M.-L., Dubayah, R. O*., et al.* (2008). Integrating waveform lidar with hyperspectral imagery for inventory of a northern temperate forest. *Remote Sensing of Environment, 112*(4), 1856-1870.

Asner, G., Mascaro, J., Muller-Landau, H., Vieilledent, G., Vaudry, R., Rasamoelina, M*., et al.* (2011). A universal airborne LiDAR approach for tropical forest carbon mapping. *Oecologia*, 1-14.

Banskota, K., Karky, B.S. & Skutsch, M. (2007). *Reducing Carbon Emissions through Community-managed Forests in the Himalaya*. Kathmandu: ICIMOD.

Baral, J. S. (2011). *Mapping carbon stock using high resolution satellite images in sub - tropical forest of Nepal.* MSc thesis. University of Twente Faculty of Geo-Information and Earth Observation ITC, Enschede. Pages 60.

Baral, S. K., R, M., & S, R. (2009). Above-ground carbon stock assessment in different forest types of Nepal. *Banko Jankari, 19(2)*(10-14).

Basuki, T. M., van Laake, P. E., Skidmore, A. K., & Hussin, Y. A. (2009). Allometric equations for estimating the above-ground biomass in tropical lowland Dipterocarp forests. *Forest Ecology and Management, 257*(8), 1684-1694.

Bhattarai, K., Conway, D., & Yousef, M. (1999). Determinants of deforestation in Nepal's Central Development Region. *Journal of Environmental Management, 91*(2), 471-488.

Blackard, J. A., Finco, M. V., Helmer, E. H., Holden, G. R., Hoppus, M. L., Jacobs, D. M*., et al.* (2008). Mapping U.S. forest biomass using nationwide forest inventory data and moderate resolution information. *Remote Sensing of Environment, 112*(4), 1658-1677.

Bortolot, Z. J., & Wynne, R. H. (2005). Estimating forest biomass using small footprint LiDAR data: An individual tree-based approach that incorporates training data. *ISPRS Journal of Photogrammetry and Remote Sensing, 59*(6), 342-360.

Brandtberg, T., & Walter, F. (1998). Automated delineation of individual tree crowns in high spatial resolution aerial images by multiple-scale analysis. *Machine Vision and Applications, 11*(2), 64-73.

Broadbent, E. N., Asner, G. P., Keller, M., Knapp, D. E., Oliveira, P. J. C., & Silva, J. N. (2008). Forest fragmentation and edge effects from deforestation and selective logging in the Brazilian Amazon. *Biological Conservation, 141*(7), 1745-1757.

Brown, S. (2002). Measuring carbon in forests: current status and future challenges. *Environmental Pollution, 116*(3), 363-372.

Bunting, P., & Lucas, R. (2006). The delineation of tree crowns in Australian mixed species forests using hyperspectral Compact Airborne Spectrographic Imager (CASI) data. *Remote Sensing of Environment, 101*(2), 230-248.

Burnett, C., & Blaschke, T. (2003). A multi-scale segmentation/object relationship modelling methodology for landscape analysis. *Ecological Modelling, 168*(3), 233-249.

Chave, J., & ... (2004). Error propagation and scaling for tropical forest biomass estimates. *In: Philosophical Transactions: Biological Sciences, 359(2004)1443 : Tropical Forests andGlobal Atmospheric Change, pp. 409-420*.

Chopping, M., Schaaf, C. B., Zhao, F., Wang, Z., Nolin, A. W., Moisen, G. G*., et al.* (2010). Forest structure and aboveground biomass in the southwestern United States from MODIS and MISR. *Remote Sensing of Environment, In Press, Corrected Proof.*

Clark, M. L., Roberts, D. A., Ewel, J. J., & Clark, D. B. (2011). Estimation of tropical rain forest aboveground biomass with small-footprint lidar and hyperspectral sensors. *Remote Sensing of Environment, In Press, Corrected Proof.*

Clinton, N., Holt, A., Scarborough, J., Yan, L., & Gong, P. . (2010). Accuracy Assessment Measures for Object-based Image Segmentation Goodness. *American Society for Photogrammetry and Remote Sensing (ASPRS), 76(3)*, 289-299.

Dalponte, M., Bruzzone, L., & Gianelle, D. (2011). A System for the Estimation of Single-Tree Stem Diameter and Volume Using Multireturn LIDAR Data. *Geoscience and Remote Sensing, IEEE Transactions on, 49*(7), 2479-2490.

Darius, S., & Culvenor. (2002). TIDA: an algorithm for the delineation of tree crowns in high spatial resolution remotely sensed imagery. *Computers & Geosciences, 28*(1), 33-44.

Definines. (2009). eConigtion Developer 8, reference book. Munchen, Germany.

DOF. (2004). *Community Forestry Inventory Guidelines*. Kathmandu, Nepal: Community Forest Division, Department of Forests.

Dong, J., Kaufmann, R. K., Myneni, R. B., Tucker, C. J., Kauppi, P. E., Liski, J.*, et al.* (2003). Remote sensing estimates of boreal and temperate forest woody biomass: carbon pools, sources, and sinks. *Remote Sensing of Environment, 84*(3), 393-410.

Drake, J. B., Dubayah, R. O., Knox, R. G., Clark, D. B., & Blair, J. B. (2002). Sensitivity of large-footprint lidar to canopy structure and biomass in a neotropical rainforest. *Remote Sensing of Environment, 81*(2–3), 378-392.

ERDAS. (2011). HPF Resolution Merge Norcross, Georgia, USA.

Erickson, M. (2004). Species classification of individally segmented tree crowns in high-resolution areial images using radiometric and morphologic image measures. *Remote Sensing of Environment, 92(3-4)*, 469-477.

Erik, & Økland, T. (2002). Estimating tree height and tree crown properties using airborne scanning laser in a boreal nature reserve. *Remote Sensing of Environment, 79*(1), 105-115.

Erikson, M., & Olofsson, K. (2005). Comparison of three individual tree crown detection methods. *Machine Vision and Applications, 16*(4), 258-265.

Fang, J., Brown, S., Tang, Y., Nabuurs, G.-J., Wang, X., & Shen, H. (2006). Overestimated Biomass Carbon Pools of the Northern mid- and High Latitude Forests. *Climatic Change, 74*(1), 355-368.

Foody, G. M., Boyd, D. S., & Cutler, M. E. J. (2003). Predictive relations of tropical forest biomass from Landsat TM data and their transferability between regions. *Remote Sensing of Environment, 85*(4), 463-474.

Foody, G. M., Cutler, M. E., McMorrow, J., Pelz, D., Tangki, H., Boyd, D. S.*, et al.* (2001). Mapping the biomass of Bornean tropical rain forest from remotely sensed data. *Global Ecology and Biogeography, 10*(4), 379-387.

Frazer, G. W., Magnussen, S., Wulder, M. A., & Niemann, K. O. (2011). Simulated impact of sample plot size and co-registration error on the accuracy and uncertainty of LiDAR-derived estimates of forest stand biomass. *Remote Sensing of Environment, 115*(2), 636-649.

García, M., Riaño, D., Chuvieco, E., & Danson, F. M. (2010). Estimating biomass carbon stocks for a Mediterranean forest in central Spain using LiDAR height and intensity data. *Remote Sensing of Environment, 114*(4), 816-830.

García, R., Suárez, J. C., & Patenaude, G. (2007). Delineation of individual tree crowns for LiDAR tree and stand parameter estimation in Scottish woodlands

The European Information Society. 55-85.

Gibbs, H. K., Brown, S., Niles, J. O., & Foley, J. A. (2007). Monitoring and estimating tropical forest carbon stocks: making REDD a reality. *Environmental Research Letters, 2*(4).

Gill, S., Biging, G., & Murphy, E. (2000). Modeling conifer tree crown radius and estimating canopy cover. *Forest Ecology and Management 126*, 405-416.

Gonzalez, P., Asner, G. P., Battles, J. J., Lefsky, M. A., Waring, K. M., & Palace, M. (2010). Forest carbon densities and uncertainties from Lidar, QuickBird, and field measurements in California. *Remote Sensing of Environment, 114*(7), 1561-1575.

Haddon, J. F., & Boyce, J. F. (1990). Image segmentation by unifying region and boundary information. *Pattern Analysis and Machine Intelligence, IEEE Transactions on, 12*(10), 929-948.

Haness, S. J., Roberts, L. A., Warwick, J. J., & Cale, W. G. (1991). Testing the utility of first order uncertainty analysis. *Ecological Modelling, 58*(1-4), 1-23.

Harrell, P. A., Kasischke, E. S., Bourgeau-Chavez, L. L., Haney, E. M., & Christensen Jr, N. L. (1997). Evaluation of approaches to estimating aboveground biomass in Southern pine forests using SIR-C data. *Remote Sensing of Environment, 59*(2), 223-233.

Holmgren, J., & Persson, Å. (2004). Identifying species of individual trees using airborne laser scanner. *Remote Sensing of Environment, 90*(4), 415-423.

Huang, H., Gong, P., Cheng, X., Clinton, N., & Li, Z. (2009). Improving Measurement of Forest Structural Parameters by Co-Registering of High Resolution Aerial Imagery and Low Density LiDAR Data. *Sensors, 9*(3), 1541-1558.

Hutchinson, S. R., & Bandalos, D. L. (1997). A guide to Monte Carlo Simulation research for applied researchers. *Journal of Vocational Education Research, 22(4)*, 233-245.

ICIMOD. (2010). *Report on forest carbon stocks in Ludikhola, Kayyarkhola and Charnwati Watershed of Nepal*. Katmandu, Nepal.

IPCC. (2001). *Summary for Policymakers*. Cambridge, United Kingdom and New York, United State of America.

IPCC. (2003). *Good Practice Guidance for Land Use, Land-Use Change and Forestry*. Japan.

IPCC. (2006a). *2006 ICPP Guidelines for National Greenhouse Gas Inventories* (No. 4-88788-032-4): Institute for Global Environmental Strategies (IGES) for the IPCC.

IPCC. (2006b). *2006 ICPP Guidelines for National Greenhouse Gas Inventories* (No. 4-88788-032-4): Institute for Global Environmental Strategies (IGES) for the IPCC.

IPCC. (2007). *Good Practice Guidance for Land Use, Land-Use Change and Forestry*.

ITC. (2010). *GI science and earth observation : a process - based approach : also as e-book*. Enschede: University of Twente Faculty of Geo-Information and Earth Observation ITC.

James, L. A., Watson, D. G., & Hansen, W. F. (2007). Using LiDAR data to map gullies and headwater streams under forest canopy: South Carolina, USA. *CATENA, 71*(1), 132-144.

Jennings, S., Brown, N., & Sheil, D. (1999). Assessing forest canopies and understorey illumination: canopy closure, canopy cover and other measures. *Forestry, 72*(1), 59-74.

Jianping, F., Yau, D. K. Y., Elmagarmid, A. K., & Aref, W. G. (2001). Automatic image segmentation by integrating color-edge extraction and seeded region growing. *Image Processing, IEEE Transactions on, 10*(10), 1454-1466.

Jochem, A., Hollaus, M., Rutzinger, M., & Höfle, B. (2011). Estimation of Aboveground Biomass in Alpine Forests: A Semi-Empirical Approach Considering Canopy Transparency Derived from Airborne LiDAR Data. *Sensors, 11(1)*, 278-295.

Jochem , A., Holllaus, M., Rutzinger, M., Hofle, B., Shaudeuder, K., & Maier, B. (2009). Estimation of aboveground biomass using airborne LiDAR data

Ke, Y., & Quackenbush, L. J. (2011). A comparison of three methods for automatic tree crown detection and delineation from high spatial resolution imagery. *International Journal of Remote Sensing, 32*(13), 3625-3647.

Ke, Y., Quackenbush, L. J., & Im, J. (2010). Synergistic use of QuickBird multispectral imagery and LIDAR data for object-based forest species classification. *Remote Sensing of Environment, 114*(6), 1141-1154.

Kellner, J. R., Clark, D. B., & Hofton, M. A. (2009, 12 February 2009). Canopy height and ground elevation in a mixed-land-use lowland Neotropical rain forest landscape. *Ecological Archives* Retrieved 20 Jan, 2011, from http://esapubs.org/archive/ecol/E090/233/metadata.htm

Kim, S., Kwak, D., oLee, W., Son, Y., Bea, S., Kim, C.*, et al.* (2010). Estimation of carbon storage based on individual tree detection in Pinus densiflora stands using a fusion of aerial photography and LiDAR data. *SCIENCE CHINA Life Sciences, 53*(7), 885-897.

Krishna, B. K. C. (2011). Linking physical, economic and institutional constraints of land use change and forest conservation in the hills of Nepal. *Forest Policy and Economics, 13*(8), 603-613.

Kuo, W., & Uppuluri, V. R. R. (1983). A review of error propagation analysis in systems. *Microelectronics Reliability, 23*(2), 235-248.

Lamonaca, A., Corona, P., & Barbati, A. (2008). Exploring forest structural complexity by multi-scale segmentation of VHR imagery. *Remote Sensing of Environment, 112*(6), 2839-2849.

Landgrebe, P.-F. H. a. D. (1998). Lowpass Filter For Increasing Class Separability.

Landis, J. R., & Koch, G. G. (1977). The Measurement of Observer Agreement for Categorical Data. *Biometrics, 33*(1), 159-174.

Larocque, G. R., Bhatti, J. S., Boutin, R., & Chertov, O. (2008). Uncertainty analysis in carbon cycle models of forest ecosystems: Research needs and development of a theoretical framework to estimate error propagation. *Ecological Modelling, 219*(3-4), 400-412.

Leckie, D., Gougeon, F., Hill, D., Quinn, R., Armstrong, L., & Shreenan, R. . (2003). Combined high-density lidar and multispectral imagery for individual tree crown analysis. *Canadian Journal of Remote Sensing, 29(5)*, 633-649.

Leckie, D. G., Gougeon, F. A., Tinis, S., Nelson, T., Burnett, C. N., & Paradine, D. (2005). Automated tree recognition in old growth conifer stands with high resolution digital imagery. *Remote Sensing of Environment, 94*(3), 311-326.

Lefsky, M. A., Cohen, W. B., & Spies, T. A. (2001). An evaluation of alternate remote sensing products for forest inventory, monitoring, and mapping of Douglas-fir forests in western Oregon. *Canadian Journal of Forest Research, 31*(1), 78-87.

Li, X., & Strahler, A. H. (1992). Geometric-optical bidirectional reflectance modeling of the discrete crown vegetation canopy: effect of crown shape and mutual shadowing. *Geoscience and Remote Sensing, IEEE Transactions on, 30(2)*(276-292).

Lim, K., Paul Treitza, Michael Wulder, St-Ongec, B., & Floodd, M. (2003). LiDAR remote sensing of forest structure.

Lim, K. S., & Treitz, P. M. (2004). Estimation of above ground forest biomass from airborne discrete return laser scanner data using canopy-based quantile estimators. *Scandinavian Journal of Forest Research, 19*(6), 558-570.

Lo, E. (2005). Gaussian error prpagation applied to eclological and post-ice storm downed woody viomass/. *Ecological Monographs, 75*(4), 451-466.

Lu, D. (2006). The potential and challenge of remote sensing-based biomass estimation. *International Journal of Remote Sensing, 27*(7), 1297-1328.

Lu, D., Mausel, P., Brondízio, E., & Moran, E. (2004). Relationships between forest stand parameters and Landsat TM spectral responses in the Brazilian Amazon Basin. *Forest Ecology and Management, 198*(1-3), 149-167.

MacDicken, K. G. (1997). A Guide to Monitoring Carbon Storage in Forestry and Agroforestry Projects.

Martinez Morales, R., Miura, T., & Idol, T. (2008). An assessment of Hawaiian dry forest condition with fine resolution remote sensing. *Forest Ecology and Management, 255*(7), 2524-2532.

Maskey, V., Gebremedhin, T. G., & Dalton, T. J. (2006). Social and cultural determinants of collective management of community forest in Nepal. *Journal of Forest Economics, 11*(4), 261-274.

Means, J. E., Acker, S. A., Fltt, B. J., Renslow, M., Emerson, U., & and Hendrix, C. J. (2000). Predicting forest Stand Characteristics with Airborne Scanning Lidar

MOFSC. (2009). Ministry of Forests and Soil Conservation, Government of Nelpal/ REDD- Forestry and Climate change cell. Retrieved 28 May, 2011, from http://mofsc-redd.gov.np/introduction/

Monni, S., Peltoniemi, M., Palosuo, T., Lehtonen, A., Mäkipää, R., & Savolainen, I. (2007). Uncertainty of forest carbon stock changes – implications to the total uncertainty of GHG inventory of Finland. *Climatic Change, 81*(3), 391-413.

Morsdorf, F., Nichol, C., Malthus, T., & Woodhouse, I. H. (2009). Assessing forest structural and physiological information content of multi-spectral LiDAR waveforms by radiative transfer modelling. *Remote Sensing of Environment, 113*(10), 2152-2163.

Muukkonen, P., & Heiskanen, J. (2007). Biomass estimation over a large area based on standwise forest inventory data and ASTER and MODIS satellite data: A possibility to verify carbon inventories. *Remote Sensing of Environment, 107*(4), 617-624.

Næsset, E. (1997). Determination of mean tree height of forest stands using airborne laser scanner data. *ISPRS Journal of Photogrammetry and Remote Sensing, 52*(2), 49-56.

Næsset, E. (2002). Predicting forest stand characteristics with airborne scanning laser using a practical two-stage procedure and field data. *Remote Sensing of Environment, 80*(1), 88-99.

Næsset, E. (2004). Accuracy of forest inventory using airborne laser scanning: evaluating the first nordic full-scale operational project.

Næsset, E., & Gobakken, T. (2008). Estimation of above- and below-ground biomass across regions of the boreal forest zone using airborne laser. *Remote Sensing of Environment, 112*(6), 3079-3090.

Næsset, E., Gobakken, T., Holmgren, J., Hyyppä, H., Hyyppä, J., Maltamo, M.*, et al.* (2004). Laser scanning of forest resources: the nordic experience. *Scandinavian Journal of Forest Research, 19*(6), 482-499.

Nguyen, N. T. (2010). *Estimation and mapping of above ground biomass for the assessment and mapping of carbon stocks in tropical forest using SAR data : a case study in Afram headwaters forest, Ghana.* Unpublished MSc Thesis, MSc thesis. University of Twente Faculty of Geo-Information and Earth Observation ITC, Enschede. Pages 79.

Ni-Meister, W., Lee, S., Strahler, A. H., Woodcock, C. E., Schaaf, C., Yao, T.*, et al.* (2010). Assessing general relationships between aboveground biomass and vegetation structure parameters for improved carbon estimate from lidar remote sensing. *J. Geophys. Res., 115*, G00E11.

Nogués-Bravo, D., Araújo, M. B., Errea, M. P., & Martínez-Rica, J. P. (2006). Exposure of global mountain systems to climate warming during the 21st Century. *Global Environmental Change, 17*(3-4), 420-428.

Packalén, P., & Maltamo, M. (2006). Predicting the plot volume by tree species using airborne laser scanning and aerial photographs. *Forest Science, 52*(6), 611-622.

Parker, R. C., & Evans, D. L. (2009). LiDAR Forest Inventory with Single-Tree, Double-, and Single-Phase Procedures. *International Journal of Forestry Research, 2009*.

Patenaude, G., Milne, R., & Dawson, T. P. (2005). Synthesis of remote sensing approaches for forest carbon estimation: reporting to the Kyoto Protocol. *Environmental Science & Policy, 8*(2), 161-178.

Pavlidis, T., & Liow, Y. T. (1990). Integrating region growing and edge detection. *Pattern Analysis and Machine Intelligence, IEEE Transactions on, 12*(3), 225-233.

Persson, A., ., Johan, H., & Ulf, S. (2002). Detecting and Measuring Individual Trees using an Airborne Laser Scanner. *Photogrammetric Enginnering & Remote Sensing*, 68(9), 925-932

Platt, R. V., & Schoennagel, T. (2009). An object-oriented approach to assessing changes in tree cover in the Colorado Front Range 1938–1999. *Forest Ecology and Management, 258*(7), 1342-1349.

Popescu, S. C. (2007). Estimating biomass of individual pine trees using airborne lidar. *Biomass and Bioenergy, 31*(9), 646-655.

Popescu, S. C., Wynne, R. H., & Nelson, R. F. (2002). Estimating plot-level tree heights with lidar: local filtering with a canopy-height based variable window size. *Computers and Electronics in Agriculture, 37*(1-3), 71-95.

Popescu, S. C., Wynne, R. H., & Nelson, R. F. (2003). Measuring individual tree crown diameter with lidar and assessing its influence on estimating forest volume and biomass. *Canadian Journal of Remote Sensing, 29*(5), 564-577.

Popescu, S. C., Zhao, K., Neuenschwander, A., & Lin, C. (2011). Satellite lidar vs. small footprint airborne lidar: Comparing the accuracy of aboveground biomass estimates and forest structure metrics at footprint level. *Remote Sensing of Environment, In Press, Corrected Proof*.

Pouliot, D. A., King, D. J., Bell, F. W., & Pitt, D. G. (2002). Automated tree crown detection and delineation in high-resolution digital camera imagery of coniferous forest regeneration. *Remote Sensing of Environment, 82*(2–3), 322-334.

Rachna, S. (2011). Comparison of individual tree crown delineation method for carbon stock estimation using very high resolution satellite images. Unpublished MSc Thesis. University of Twente Faculty of Geo-Information and Earth Observation ITC,.

Rahman, M. Z. A., & Gorte, B. (2008). *Individual tree detection based on densities of high points of high resolution airborne LiDAR*. Paper presented at the GEOBIA 2008 - Pixels, Objects, Intelligence: GEOgraphic Object-Based Image Analysis for the 21St Century. Retrieved from http://www.isprs.org/proceedings/XXXVIII/4-C1/Sessions/Session12/6790_Rahman_Proc.pdf

Ranson, K. J., Sun, G., Weishampel, J. F., & Knox, R. G. (1997). Forest biomass from combined ecosystem and radar backscatter modeling. *Remote Sensing of Environment, 59*(1), 118-133.

Reitberger, J., Heurich, M., Krzystek , P., & Heyder, U. (2007). single tree detection in forest area wiht high densitt LiDAR data

Riitters, K., Wickham, J., O'Neill, R., Jones, B., & Smith, E. (2000). Global-scale patterns of forest fragmentation. *Conservation Ecology, 4 (2)*(3).

Saatchi, S., Marlier, M., Chazdon, R. L., Clark, D. B., & Russell, A. E. (2010). Impact of spatial variability of tropical forest structure on radar estimation of aboveground biomass. *Remote Sensing of Environment, In Press, Corrected Proof*.

Samalca, I. (2007). *Estimation of forest biomass and its error : a case in Kalimantan, Indonesia.* MSc thesis. ITC, Enschede. Pages.

Schade, B., & Wiesenthal, T. Biofuels: A model based assessment under uncertainty applying the Monte Carlo method. *Journal of Policy Modeling, 33*(1), 92-126.

Shah, S. K. (2011). *Modelling the relationship between tree canopy projection area and above ground carbon stock using high resolution geoeye satellite images*. MSc thesis. University of Twente Faculty of Geo-Information and Earth Observation ITC, Enschede. Pages.

Sherrill, K., Lefsky, M., Battles, J., Waring, K., & Gonzalez, P. (2006). An Error Propagation Analysis of Estimates of Aboveground Biomass Estimates From Lidar Remote Sensing. Retrieved 23-Aug, 2011, from http://adsabs.harvard.edu/abs/2006AGUFM.B43D..07S

Shi, W., Fisher, P. F., & Goodchild, M. F. (2002). *Spatial data quality*. London: Taylor & Francis.

Shimano, K. (1997). Analysis of the relationship between DBH and crown projection area using a new model. *Journal of Forest Research, 2*(4), 237-242.

Soares, M. L. G., & Schaeffer-Novelli, Y. (2005). Above-ground biomass of mangrove species. I. Analysis of models. *Estuarine, Coastal and Shelf Science, 65*(1-2), 1-18.

Sohn, G., & Dowman, I. (2007). Data fusion of high-resolution satellite imagery and LiDAR data for automatic building extraction. *ISPRS Journal of Photogrammetry and Remote Sensing, 62*(1), 43-63.

Song, C., Dickinson, M. B., Su, L., Zhang, S., & Yaussey, D. (2010). Estimating average tree crown size using spatial information from Ikonos and QuickBird images: Across-sensor and across-site comparisons. *Remote Sensing of Environment, 114*(5), 1099-1107.

St-Onge, B. (2000). *Estimating individual tree heights of the boreal forest using airborne laser altimetry and digital videography*. Paper presented at the Workshop of ISPRS WG III/2 & III/5 : Mapping surface structure and topography by airborne and spaceborne lasers.

St-Onge, B., Hu, Y., & Vega, C. (2008). Mapping the height and above-ground biomass of a mixed forest using lidar and stereo Ikonos images. *International Journal of Remote Sensing, 29*(5), 1277-1294.

St-Onge, B. A., & Achaichia, N. (2001). Measuring forest canopy height using a combination of LiDAR and aerial photograhpy data *International Archives of Photogrammetry and Remote Sensing 34*(3/W4), 131-137.

Suárez, J. C., Ontiveros, C., Smith, S., & Snape, S. (2005). Use of airborne LiDAR and aerial photography in the estimation of individual tree heights in forestry. *Computers & Geosciences, 31*(2), 253-262.

Takahashi, T., Awaya, Y., Hirata, Y., Furuya, N., Sakai, T., & Sakai, A. (2010). Stand volume estimation by combining low laser-sampling density LiDAR data with QuickBird panchromatic imagery in closed-canopy Japanese cedar (Cryptomeria japonica) plantations. *International Journal of Remote Sensing, 31*(5), 1281-1301.

Timo, K. (1991). Relationships between crown projected area and components of above-ground biomass in Norway spruce trees in even-aged stands: Empirical results and their interpretation. *Forest Ecology and Management, 40*(3–4), 243-260.

Tsendbazar, N. E. (2011). *Object based image analysis of geo - eye VHR data to model above ground carbon stock in Himalayan mid - hill forests, Nepal.* MSc thesis. University of Twente Faculty of Geo-Information and Earth Observation ITC, Enschede. Pages 63.

UNFCCC. (2005). Kyoto Protocol. Retrieved 26 May, 2011, from http://unfccc.int/kyoto_protocol/items/2830.php

Voss, M., & Sugumaran. (2008). Seasonal Effect on Tree Species Classification in an Urban Environment Using Hyperspectral Data, LiDAR, and an Object- Oriented Approach. *Sensors, 8(5)*, 3020-3036.

Watson, C. (2009). Forest carbon accounting: Overview and Principle. Retrieved 26 May 2011: http://www.undp.org/climatechange/carbon-finance/Docs/Forest%20Carbon%20Accounting%20-%20Overview%20&%20Principles.pdf

Weir, M. J. C. (1999). *Ensuring and maintaining data quality in geographical information systems for forest land management.* PhD thesis. University of London, Birkbeck College, London. Pages 320.

Weir, M. J. C. (2002). Monte Carlo simulation of long-term spatial error propagation in forestry databases. *Spatial data quality*, 294-303.

Wulder, M., White, J., Stinson, G., Hilker, T., Kurz, W., Coops, N.*, et al.* (2010). Implications of differing input data sources and approaches upon forest carbon stock estimation. *Environmental Monitoring and Assessment, 166*(1), 543-561.

Y. Nakai, F. Hosoi, & Omasa, K. (2009). Estimating carbon stocks of coniferous woody canopy trees using airborne LiDAR and passive optical sensor.

Yu, X., Hyyppä, J., Holopainen, M., & Vastaranta, M. (2010). Comparison of Area-Based and Individual Tree-Based Methods for Predicting Plot-Level Forest Attributes. *Remote Sensing, 2*(6), 1481-1495.

Yu, X., Hyyppä, J., Hyyppä, H., Maltamo, M. M., , & (2004). Effect of flight altitude on tree height estimation using Airborne Laser Scanning *ISPRS Journal of Photogrammetry and Remote Sensing, 36-8/W2*.

Zavorin, I., & Le Moigne, J. (2005). Use of multiresolution wavelet feature pyramids for automatic registration of multisensor imagery. *Image Processing, IEEE Transactions on, 14*(6), 770-782.

Zhao, K., Popescu, S., & Nelson, R. (2009). Lidar remote sensing of forest biomass: A scale-invariant estimation approach using airborne lasers. *Remote Sensing of Environment, 113*(1), 182-196.

Zhengrong, L., Hayward, R., Jinglan, Z., & Yuee, L. (2008, 1-3 Dec. 2008). *Individual Tree Crown Delineation Techniques for Vegetation Management in Power Line Corridor*. Paper presented at the Computing: Techniques and Applications, 2008. DICTA '08.Digital Image.

Zimble, D. A., Evans, D. L., Carlson, G. C., Parker, R. C., Grado, S. C., & Gerard, P. D. (2003). Characterizing vertical forest structure using small-footprint airborne LiDAR. *Remote Sensing of Environment, 87*(2–3), 171-182.

APPENDICES

Appendix 1: Data collected form

Data Collection Format

Name of Recorder: Date:

Stratum ID: Sample Plot ID:

Bearing from the road		Bearing for the 1st tree from the center of the plot		Plot center	
X		X		X	
Y		Y		Y	
Angle		Angle			

Slope:

Plot radius: Aspect: E Altitude: Crown density (%):

S.N	Species	Scientific name	DBH(cm)	CD (m)	Ht (m)	Intermingled	Remarks
1							
2							
3							
4							
5							
6							
7							
8							
9							
10							
11							
12							
13							
14							
15							
16							
17							
18							
19							
20							
21							
22							
23							
24							

APPENDICES

Appendix 2: Map of the sample plot used for tree identification in the field

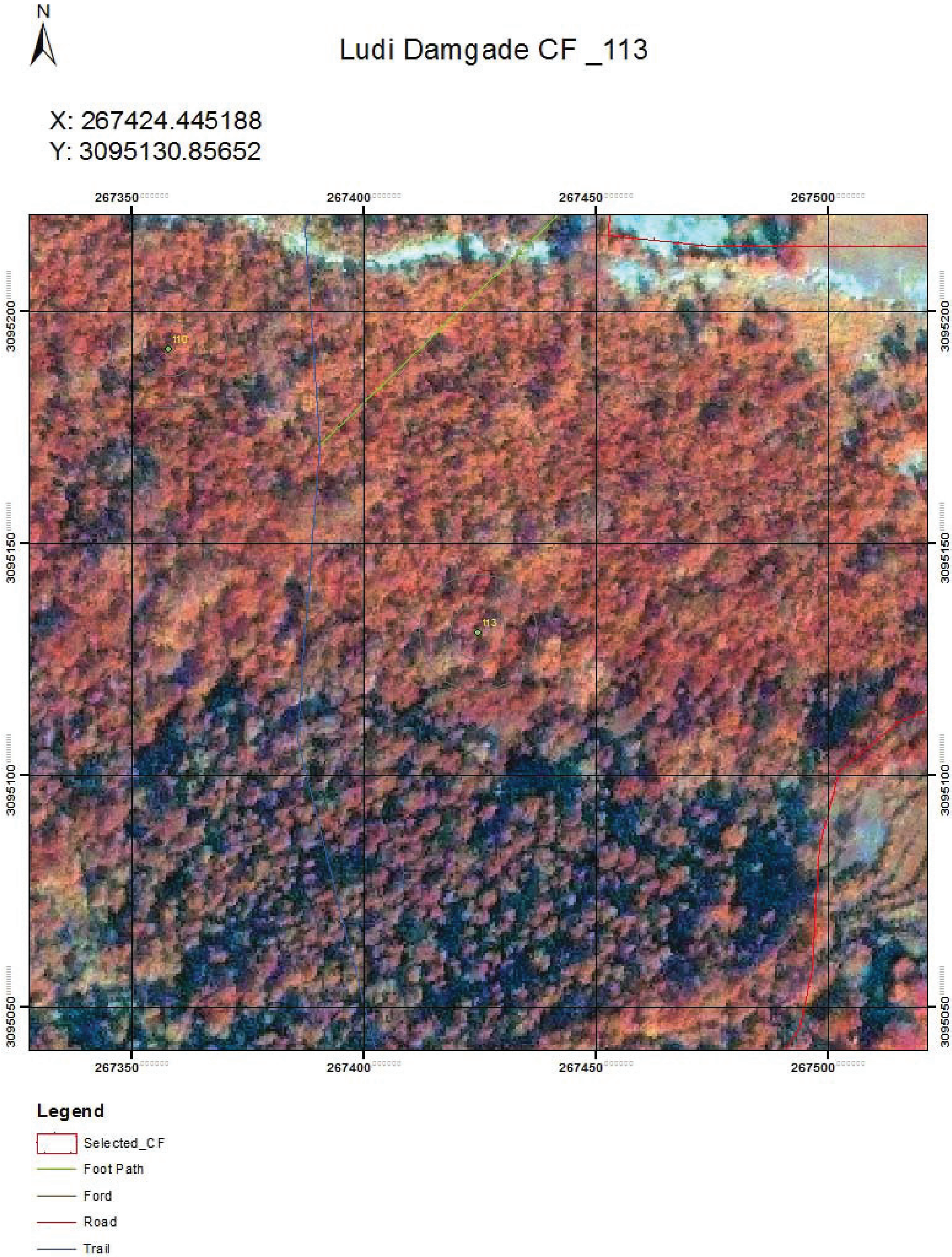

APPENDICES

Appendix 3: Region growing rule set for crown delineation

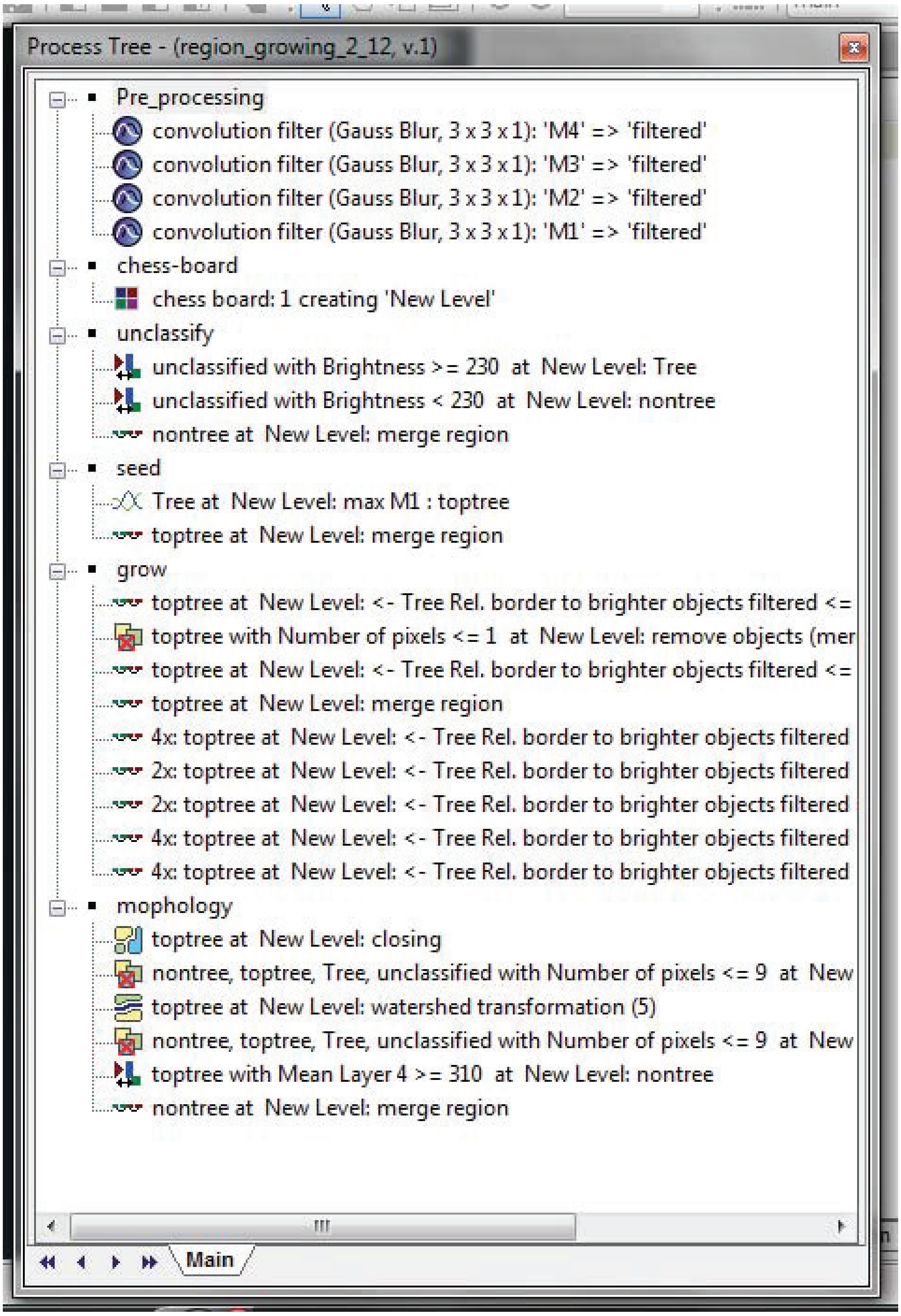

APPENDICES

Appendix 4: Co-registration process

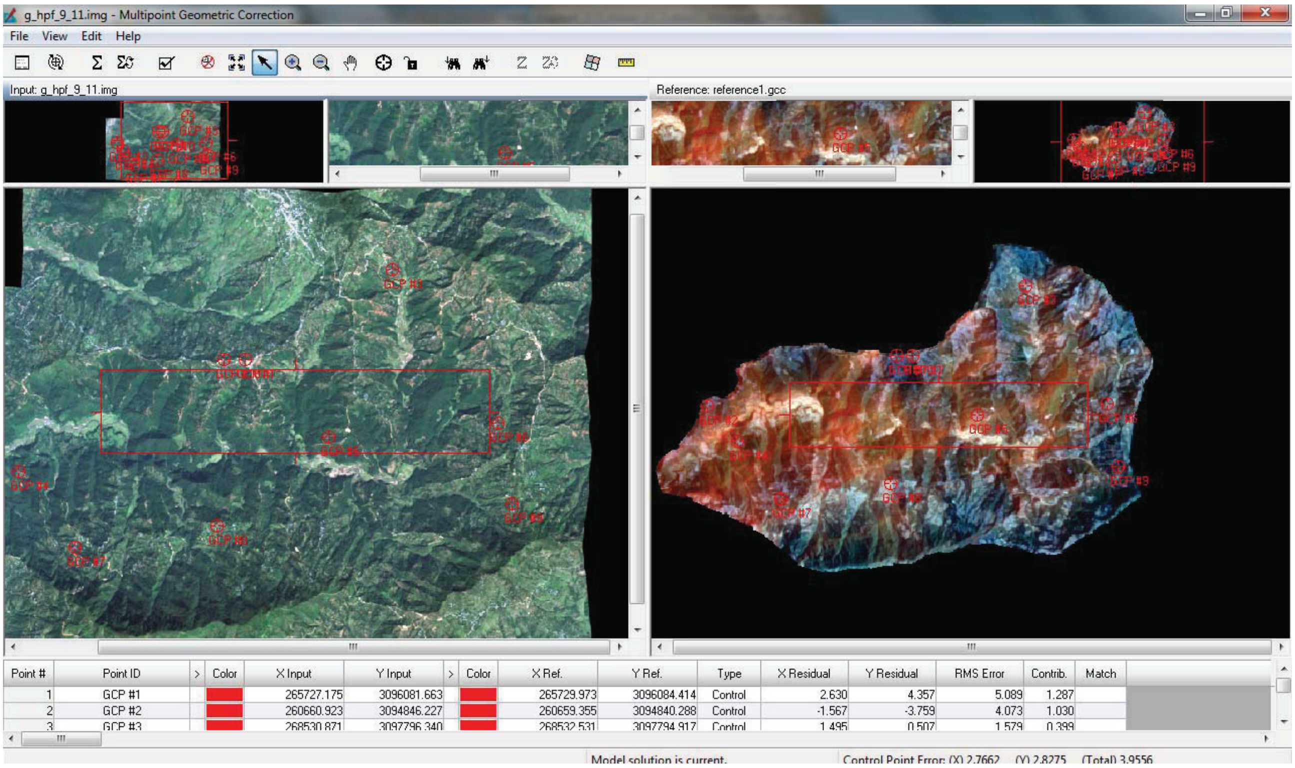

APPENDICES

Appendix 5: Slope correction table

Slope correction table

Plot size 500 m^2

Slope%	Radius(m)	Slope%	Radius(m)	Slope%	Radius(m)
0	12.62				
1	12.62	36	13.01	71	13.97
2	12.62	37	13.03	72	14.00
3	12.62	38	13.05	73	14.04
4	12.62	39	13.07	74	14.07
5	12.62	40	13.09	75	14.10
6	12.63	41	13.12	76	14.14
7	12.63	42	13.14	77	14.17
8	12.64	43	13.16	78	14.21
9	12.64	44	13.19	79	14.24
10	12.65	45	13.21	80	14.28
11	12.65	46	13.24	81	14.31
12	12.66	47	13.26	82	14.35
13	12.67	48	13.29	83	14.38
14	12.68	49	13.31	84	14.42
15	12.69	50	13.34	85	14.45
16	12.70	51	13.37	86	14.49
17	12.71	52	13.39	87	14.52
18	12.72	53	13.42	88	14.56
19	12.73	54	13.45	89	14.60
20	12.74	55	13.48	90	14.63
21	12.75	56	13.51	91	14.67
22	12.77	57	13.53	92	14.71
23	12.78	58	13.56	93	14.74
24	12.79	59	13.59	94	14.78
25	12.81	60	13.62	95	14.82
26	12.82	61	13.65	96	14.85
27	12.84	62	13.68	97	14.89
28	12.86	63	13.72	98	14.93
29	12.87	64	13.75	99	14.97
30	12.89	65	13.78	100	15.00
31	12.91	66	13.81	101	15.04
32	12.93	67	13.84	102	15.08
33	12.95	68	13.87	103	15.12
34	12.97	69	13.91	104	15.15
35	12.99	70	13.94	105	15.19

APPENDICES

Appendix 6: Details of LIDAR data acquisition

Customer	**Forest Resource Assessment in Nepal, Ministry of Forests and Soil Conservation**
Date Flown	20110316 / 20110328 / 20110401 / 20110402
Times of collection (UTC)	02:45 – 08:20 / 03:46 – 05:00 / 04:01 – 05:45 / 03:31 – 05:30
Date Processed	20110530
Projection	UTM
Datum	WGS84
Files included	ASPRS LAS v. 1.2 - 3002 nos.(IC01.las to IV300.las)
Aerial Platform	Helicopter (9N-AIW)
Flying altitude	2200 m AGL
Flying speed	80 knots
Sensor pulse rate	52.9 khz
Sensor Scan speed	20.4 lines/second
Nominal outgoing pulse density @ground level	Average: 0.8 points per square meter
Scan FOW half-angle	20 degrees
Swath @ ground level	1601.47 m
Point spacing	max 1.88 m across, max 2.02 m down
Beam footprint @ ground level	50 cm
Gap file name	No gaps
Tile index file name	tileindex_Block_icomod.dgn

APPENDICES

Appendix 7: Field-work pictures